



**NATURAL RADIOACTIVITY LEVELS IN ROCKS AND SAND FROM
TYAA RIVER IN MWINGI, KITUI COUNTY**

MUTHAMA MATSITSI

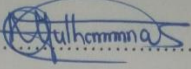
I64/KIT/20647/2015

**A THESIS SUBMITTED IN PARTIAL FULFILLMENT OF THE
REQUIREMENTS FOR THE DEGREE OF MASTER OF SCIENCE IN
PHYSICS OF SOUTH EASTERN KENYA UNIVERSITY**

FEBRUARY 2020

DECLARATION

I understand that plagiarism is an offense and I, therefore, declare that this thesis is my original work and has not been presented to any other institution for an award.

Signature:  Date: 14/02/2020

Muthama Matsitsi

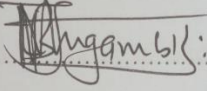
Department of Physical Sciences,

South Eastern Kenya University.

I64/KIT/20647/2015

SUPERVISORS DECLARATION

This thesis has been submitted for examination with our approval as University Supervisors.

Signature:  Date: 19/02/2020

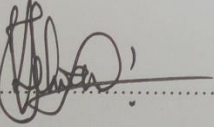
Dr. Mugambi J. Linturi

Department of Physical Sciences,

South Eastern Kenya University,

P.O Box 170,

Kitui, Kenya.

Signature:  Date: 17/02/2020

Dr. Jeremiah M. Kebwaro

Department of Physical Sciences,

Karatina University,

P.O Box 1957,

Karatina, Kenya.

ACKNOWLEDGEMENT

I am sincerely grateful to my supervisors Dr. Linturi J. Mugambi and Dr. Jeremiah M. Kebwaro for their unceasing effort, time and energy they have put in guiding me to come up with the research topic, proposal development, corrections and useful suggestions accorded to me throughout the research and the entire work. I greatly benefited from their prowess and vast experience in radiation detection, measurement, and scientific data analysis.

My sincere appreciation to Shadrack Kyalo Muli, a workmate in the Humanities department who stood with me particularly during sorting and placement of different rocks into their Precambrian origin, may God bless him abundantly. Much appreciation to my family members for their financial support and encouragement during the entire period of study. Thanks to members of St. Peter's Nzambani Secondary whom I established rapport with during the entire span of my research; their encouragement during difficult times is highly appreciated, God bless you.

Special thanks to Ministry of Mining and Petroleum, the Republic of Kenya for allowing me use their Laboratory during pre-counting stages, Institute of Nuclear Science and Technology of the University of Nairobi for allowing me to use their gamma-ray spectrometer for my sample analysis, it cannot go unmentioned that their welcoming nature and generosity of ideas made my stay at their laboratory comfortable particularly by inducting me to the software (Maestro Ortec) used for the data acquisition and analysis, they were readily available for my consultation Leonard Kiragu and Simon Bartilol to be specific.

I wish to thank dearly the Kenya DAAD Scholars Association (KDSA) for granting me an opportunity to present my preliminary findings in an international conference on science, technology, and innovation for sustainable development in dryland environments held at UMMA University in Kajiado County from 21st-23rd Nov 2018.

Above all, I thank the almighty God for His grace, providence, mercies, strength, love, and kindness which is better than life. *“The Lord will fulfill his purpose for me; your steadfast love endures forever. Do not forsake the work of your hands”.*

(Psalms 138:8).

DEDICATION

To my beloved wife Gladys M., my dotting daughter Emily Ndinda and dear mum Mary Ndinda.

TABLE OF CONTENTS

DECLARATION	Error! Bookmark not defined.
ACKNOWLEDGEMENT	ii
DEDICATION	iv
TABLE OF CONTENTS	v
LIST OF TABLES	x
LIST OF FIGURES	xi
LIST OF APPENDICES	xiii
ABBREVIATIONS AND ACRONYMS	xiv
ABSTRACT	xv
CHAPTER ONE	1
INTRODUCTION	1
1.1 Background of the Study	1
1.2 Statement of the Research Problem	4
1.3 Objectives of the Study	5
1.3.1 Main Objective	5
1.3.2 Specific Objectives	5
1.4 Research questions	5
1.5 Justification of the Study	5
1.6 Scope of the Study	6
CHAPTER TWO	8
THEORETICAL BACKGROUND	8
2.1 Introduction	8
2.2 Types of Radiations	8
2.2.1 Gamma Rays	8

2.2.2 Alpha Particles	9
2.2.3 Beta Particles	10
2.3 Radiation Interaction with Matter	10
2.3.1 Compton Scattering	11
2.3.2 Photoelectric Absorption	13
2.3.3 Pair Production.....	14
2.4 Biological Aspects of Ionizing Radiation	15
2.5 Health Effects from Ionizing Radiation	16
2.5.1 Chromosomal Aberrations and Genetic Mutation	17
2.6 Radiation Field Quantities and Radiation Dosimetry	17
2.6.1 Particle Fluence.....	18
2.6.2 Energy Fluence	18
2.6.3 Kerma.....	18
2.6.4 Absorbed Dose, D.....	18
2.6.5 Equivalent Dose (H)	19
2.7 Radiation Measurement Techniques, Challenges, and Advancements.....	19
2.8 Theoretical Aspects of Gamma-ray Spectrometry.....	20
2.9 Working Principle of the HPGe Gamma-ray Spectrometer.....	24
2.10 Transient Equilibrium	25
2.11 Non-equilibrium.....	25
2.12 Secular Equilibrium	26
CHAPTER THREE	27
LITERATURE REVIEW	27
3.1 Background Information.....	27
3.2 Radiometric Surveys around the Globe	27

3.3 Radiological Surveys in Kenya.....	30
3.4 Radiation-Related Anomalies and Cancer Incidences	34
CHAPTER FOUR.....	35
MATERIALS AND METHODS	35
4.1. Geology of the Study Area	35
4.2 Materials and Equipment Used in the Study.....	37
4.3 Sampling and Sample Collection.....	38
4.3.1 Sampling	38
4.3.2 Collection of Sand Samples	38
4.3.3 Collection of Rock Samples.....	39
4.4 Sample Preparation	39
4.5 Gamma-ray Spectrometry	40
4.6 Pre-requisites before Sample Counting.....	41
4.6.1 Energy Calibration of HPGe Spectroscopy	41
4.6.7 Detector Counting Efficiency (ϵ).....	42
4.6.8 Detector Resolution	43
4.7 Specifications of the Gamma-ray Spectrometer	43
4.8 Samples Analysis.....	44
4.8.1 Activity Concentration in Bqkg^{-1}	44
4.8.2 Radium Equivalent (Ra_{eq})	45
4.8.3 Estimation of Absorbed Dose (D).....	45
4.8.4 Annual Effective Dose Rate (AEDR)	46
4.8.5 External Hazard Index (H_{ex})	46
4.8.6 Internal Hazard Index (H_{in})	47

CHAPTER FIVE	47
RESULTS AND DISCUSSIONS	47
5.1 Introduction.....	47
5.2 Preliminary Analysis.....	48
5.2.1 Energy Calibration	48
5.2.2 Detector Counting Efficiency	49
5.2.3 Detector Energy Resolution	50
5.2.4 Background Spectrum.....	51
5.3 Sample Dosimetric Analysis.....	56
5.3.1 Activity Concentration from the Representative Sand Samples	56
5.3.2 Activity Concentration of ^{238}U , ^{232}Th , and ^{40}K in Rock Samples	59
5.3.3 Absorbed Dose Rate in Sand and Rocks sampled during the Rainy Season	60
5.3.4 Annual Effective Dose Rate (AEDR)	61
5.3.5 Radiation Hazard Indices	64
5.4 Seasonal Effect on Natural Radiation Level of ^{238}U , ^{232}Th , and ^{40}K	68
5.4.1 Activity Concentration of ^{238}U , ^{232}Th , and ^{40}K in Sand for the Two Seasons.....	68
5.4.2 Absorbed Dose Rate	69
5.4.3 Radiological Hazard Indices	71
5.5 Statistical Evaluation	73
5.5.1 Descriptive Statistics for Activity Concentration of ^{238}U , ^{232}Th , and ^{40}K in Sand and Rocks Sampled	73
5.5.2 Correlational Analysis	74
5.5.3 Comparison of the Findings of the Current Study with Data from Similar Studies ...	75
CHAPTER SIX	77
CONCLUSIONS AND RECOMMENDATIONS	77
6.1 Conclusion	77

6.2 Recommendation	79
REFERENCES	80
APPENDIX 1	89
APPENDIX 2	90
APPENDIX 3	91
APPENDIX 4	92
APPENDIX 5	95
APPENDIX 6	96
APPENDIX 7	97
APPENDIX 8	98
APPENDIX 9	100
APPENDIX 10	102

LIST OF TABLES

Table 1.1:	Parameters, their corresponding SI units, and world's recommended threshold	3
Table 2.1:	Quantities and their respective units used in radiation dosimetry	19
Table 4.1:	Technical specifications for the gamma-ray spectrometer used	44
Table 5.1:	The polynomial and fit parameters used to convert channel numbers to energies during energy calibration	49
Table 5.2:	The Gaussian fit and fit parameters used to calculate detector resolution	52
Table 5.3:	Activity concentration of ^{238}U , ^{232}Th and ^{40}K in sand sampled Rainy season	56
Table 5.4:	Activity concentration of ^{238}U , ^{232}Th , and ^{40}K in sand sampled dry season	59
Table 5.5:	Annual effective dose rates in rock and sand samples collected from Tyaa river course during rainy season	62
Table 5.6:	Radium equivalent for the rocks and sand samples collected upper and lower stream during the rainy and dry season	65
Table 5.7:	Absorbed dose rate in rocks and sand sampled from the lower during the rainy and dry season	70
Table 5.8:	Mean values for radiological parameters for the sand and rock samples subjected for analysis for the two seasons	73
Table 5.9:	Descriptive statistics for activity concentration in sand and rock samples used for this work	74
Table 5.10:	Comparison of mean activity concentration of ^{226}Ra , ^{232}Th , and ^{40}K in sand reported by this work and other similar studies	75
Table 5.11:	Comparison of mean activity concentration of ^{226}Ra , ^{232}Th , and ^{40}K in rocks reported by this work and other similar studies.	76

LIST OF FIGURES

Figure 1.1:	Annual percentages of radiation doses from anthropogenic and primordial sources	3
Figure 2.1:	The beta decay scheme of $^{60}_{27}\text{Co}$ to excited $^{60}_{28}\text{Ni}$. The nickel emits gamma-rays in succession to attain the ground state	9
Figure 2.2:	Energy attenuation curve for the alpha particle in air medium	10
Figure 2.3:	Gamma ray-photon intensity attenuation as it traverses a matter	11
Figure 2.4:	Compton scattering of a photon by an electron assumed to be at rest	12
Figure 2.5:	Photoelectric emission due to the absorption of electromagnetic radiation	13
Figure 2.6:	Pair production effected by high energy photon	14
Figure 2.7:	Direct and indirect actions of electromagnetic radiation on matter	16
Figure 2.8:	Vertical dipstick cryostat used for storing LN ₂ used to cool HPGe crystal	23
Figure 2.9:	Physical components of HPGe gamma-ray spectrometer block	24
Figure 2.10:	A sketch showing interaction mechanisms within the practical detector volume	25
Figure 4.1:	Map showing sampled points along a section of Tyaa River in Mwingi Kitui County	37
Figure 4.2:	A sketch of the sampling method used along the sampled length of Tyaa River from Nairobi-Mwingi-Garissa highway	39
Figure 5.1:	A plot of energy calibration of the HPGe detector done using standard sources	49
Figure 5.2:	Detector efficiency response at different gamma-ray energies calculated from standard sources	50
Figure 5.3:	^{137}Cs spectral peak at 661.5 keV with Gaussian fit used to derive fit parameters used to determine energy resolution for this study	51

Figure 5.4:	Background spectrum collected for 30,000 s using de-ionized water in the same counting geometry	53
Figure 5.5:	A typical gamma-ray spectrum from sand samples collected upstream along the course of Tyaa River during rainy season	54
Figure 5.6:	A typical gamma-ray spectrum analyzed from Granitoid Gneisses rock collected from (0°56'21.5 S, 38°02'34.8 E) during dry season	55
Figure 5.7:	A typical gamma-ray spectrum from a sand sample acquired for 30,000 seconds before and after background subtraction	55
Figure 5.8:	Comparisons of activity concentration of ^{238}U , ^{232}Th and ^{40}K for the sand samples collected lower stream	58
Figure 5.9:	Comparisons of absorbed dose for sand samples collected lower and upper stream during rainy season	60
Figure 5.10:	A pie chart showing the annual effective dose rate for rock samples collected upper stream during dry season	61
Figure 5.11:	Comparison of indoor annual effective dose rate for sand and rock samples collected lower stream during rainy season	63
Figure 5.12:	Comparison of annual effective dose rate for rock and sand samples collected upper stream during the dry season	66
Figure 5.13:	Scatter plot showing internal hazard indices for the rock and sand samples collected upper stream during rainy season	67
Figure 5.14:	A bar graph showing the concentration of ^{226}Ra in sand samples collected during the rainy and dry seasons	69
Figure 5.15:	Evaluation of seasonal effect using sand samples collected lower stream during rainy and dry seasons	71
Figure 5.16:	Comparison of radium equivalent for sand samples collected lower stream	72
Figure 5.17:	A scatter plot showing a correlation between radium equivalents of sand and rocks	74

LIST OF APPENDICES

APPENDIX 1	90
APPENDIX 2	91
APPENDIX 3	92
APPENDIX 4	93
APPENDIX 5	95
APPENDIX 6	96
APPENDIX 7	97
APPENDIX 8	98
APPENDIX 9	100
APPENDIX 10	102

ABBREVIATIONS AND ACRONYMS

AED	Annual Effective Dose
ADR	Annual Dose Rate
BDL	Below Detection Limit
Bqkg ⁻¹	Becquerel per kilogram
EC	European Commission
EPA	Environment Protection Agency (UPA)
HiBRA	High Background Radiation Area
H _{ex}	External hazard index
IAEA	International Atomic Energy Agency
ICRP	International Commission on Radiation Protection
KRPB	Kenya Radiation Protection Board
MCA	Multi Channel Analyzer
mSvy ⁻¹	milli Sievert per year
NCRP	National Commission on Radiation Protection
nGyh ⁻¹	nano Gray per hour
NORM	Naturally Occurring Radioactive Materials
NRPB	National Radiation Protection Board
RBE	Relative Biological Effectiveness
ROI	Region of Interest
TENORM	Technologically Enhanced Naturally Occurring Radioactive Materials
UNSCEAR	United Nations Scientific Committee on Effects of Atomic Radiations
WHO	World Health Organization

ABSTRACT

The variability of background radiation from primordial radionuclides has led to the exposure of human beings to radiation doses of different ranges. Prompt or delayed harmful effects as a result of radiation exposure have been reported in areas with enhanced levels of radioactivity. The residents of Kitui County near Tyaa River and the surrounding regions heavily mine sand and rocks from its riverine for construction purposes despite the scanty information on the potential harm in case the latter has elevated levels of radioisotopes. Conducting a radiometric survey was therefore imperative as the area neighbors Machakos and Thika regions whose bedrock comprises of granites and silic rocks whose mineral accessories is similar to those found in Uranium-Thorium rich rocks. A total of 56 samples of raw building materials (sand and rocks) each weighing 500 g were randomly sampled along the riverine during the consecutive rainy and dry seasons and prepared for analysis. The ^{238}U (^{226}Ra), ^{232}Th and ^{40}K radionuclides present in geological samples were identified and quantified from spectra recorded using HPGe gamma-ray spectrometry. The spectral analysis reports an overall mean activity concentration of ^{226}Ra , ^{232}Th , and ^{40}K of 33 ± 1.7 Bq/Kg for ^{226}Ra , 55 ± 2.8 Bq/Kg for ^{232}Th , and 812 ± 40 Bq/Kg for ^{40}K in sand samples which surpasses the world's average of 35 Bq/Kg, 30 Bq/Kg and 400 Bq/Kg respectively. A similar analysis of rock samples reveals a mean of 21 ± 2.5 BqK g^{-1} , 49 ± 2.5 BqK g^{-1} and 782 ± 39 BqK g^{-1} for ^{226}Ra , ^{232}Th and ^{40}K respectively. The average corresponding dose rates and radiological hazard indices were within the safety limits recommended in ICRP reports. The higher activity concentration of ^{226}Ra , ^{232}Th , and ^{40}K was reported for samples collected during the dry season and as such the seasonal changes had a significant effect on the natural levels of radioactivity in sediments from this river.

CHAPTER ONE

INTRODUCTION

1.1 Background of the Study

Living organisms around the globe have been constantly exposed to radiation doses of different ranges present in all the geological formations like soils, air, water masses and rocks (UNSCEAR 2000). The significant radiation doses to which the human biota is continually exposed is due to inescapable ionizing emissions from decay chains of radionuclides existing naturally in all mediums including in our bodies (Halime *et al.*, 2016). Ionizing radiations are both useful and harmful to human life and the environment in case of over exposure. Some beneficial applications of ionizing radiation in our daily encounters include diagnostic and radiation-based therapeutic procedures like radiotherapy useful in the treatment of cancer. In agriculture, tritium and phosphorus are some of radioactive elements used as tracers to monitor the mineral salts uptake by plants. In nuclear power plants, radioactive materials are used as fuel for electric power generation and in nuclear industries, the concept of energy accompanying radioactive decay has been relied upon to make powerful weapons (UNSCEAR 2008).

Generally, the human activities that lead to radioactive emission are said to be anthropogenic and exposure to ionizing radiation from such sources can be regulated. However, the exposure of human beings to radiation from natural sources is unavoidable. The level of background radiations from terrestrial radionuclides varies from one location to another depending on the geological composition of soils which in turn depends on the nature of the parent rock (Varley, 1998). Some places like Ramsar city in Iran, Kerala and Tamilnadu states in India, and Mrima hill in Kenya have reported high levels of natural background radiations (Kebwaro 2011).

The inadvertent human interaction with materials containing high levels of radioactive contaminants either through the settlement in High Background Radiation Area (HiBRA), or dwelling in houses erected with raw materials drawn from backgrounds

with elevated levels of radionuclides has reported harmful health effects over time. Some undesirable biological effects emanating from human exposure to radiations in excess of the threshold levels include skin burns, Myeloid leukemia, modification or death of the biological cells in case the radiation dose severity is high (UNSCEAR, 2000).

To avert the life-threatening effects of ionizing radiation, several radiometric surveys have been carried out all over the world using different detectors and the findings published widely. Regulatory bodies like International Commission on Radiological Protection (ICRP), National Commission for Radiation Protection (NCRP) and Kenya Radiation Protection Board (KRPB) among others use findings from such surveys to map HiBRA and assess their potential radiological impact so as to advise the government and the public on measures to minimize the exposure from such materials. The regulatory measures could be through restricting the use of such contaminated materials or advising locals to migrate to safer grounds in case radiological parameters exceeds the permissible thresholds (ICRP,1992). Annual effective dose, radium equivalent, external and internal hazard indices are among the quantities relied upon in determining the radiological safety of materials human population interacts with. Table (1.1) shows the world’s agreed safety levels for some radiological parameters.

Table 1.1: Parameters, their corresponding SI units, and world’s recommended threshold

Parameter	SI unit	Recommended value	Body
Radium equivalent	Bq/Kg	370	UNSCEAR, 1988
Absorbed dose rate	Gy/h	60 nGy/h	UNSCEAR, 2010
Annual effective dose	Sv/y	1	ICRP, 1990
Hazard indices		1	ICRP, 2005

The existing data banks on radiometric surveys show that, though humans receive radiation doses of varying ranges from different sources, the radon gas and its accompanying short-lived decay products contribute the largest percentage of the mean

absorbed dose, followed by radiation doses from raw building materials (UNSCEAR 2000).

Figure 1.1 shows different sources contributing to the average radiation dose. ^{222}Ra has a short half-life of 3.82 days and thus its deleterious decay products accumulate fast.

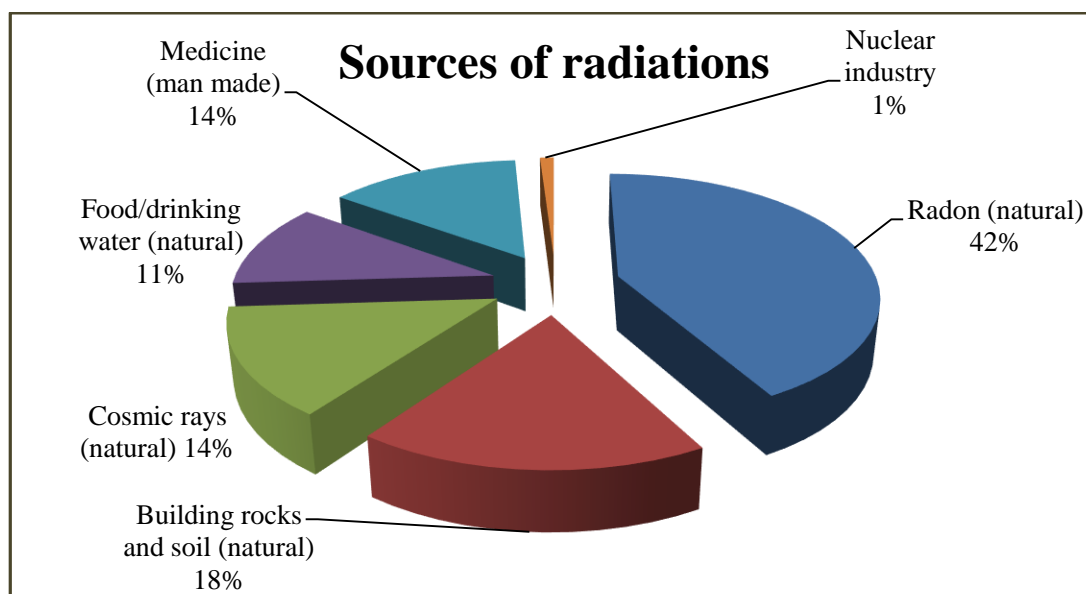


Figure 1.1: Annual percentages of radiation doses from anthropogenic and primordial sources (UNSCEAR, 2000).

Figure (1.1) shows that building material (rocks and soils) which has been evaluated in this work contributes significant radiation dose to human beings. Building materials are usually drawn from a variety of rocks with different concentrations of radionuclides. Lithological studies in various regions of the world reveal that the three classes of rocks i.e sedimentary, igneous and metamorphic reports the concentration of ^{238}U , ^{232}Th , and ^{40}K from at least trace to levels exceeding 370 Bq/Kg but some consistent trends have been established like, felsic igneous rocks generally have higher levels of radionuclides than sedimentary rocks (Bastos, 2009).

Kitui County where the current research has been done lies within the Central Eastern part of the Mozambique Belt Segment (CEMBS) and constitutes the Eastern part (Nyamai *et al.*, 2003). Earlier studies revealed that the region is dominated by gneiss, pelitic and semi-pelitic schists, and migmatites but with time evolution, the area currently shows abundance in lithological units of Anorthositic, Granitoid, Gabbroic to Ultramafic intrusions and some traces of Andesitic volcanoes (Dodson, 1953).

Some sampled rocks during this survey include Quartzite (metamorphic rock), Granitoid Gneiss (metamorphic rock), Conglomerate (sedimentary rock) and Limestone (sedimentary rock) (see Appendix 7). Generally, metamorphic rocks are the dominant rock species especially around the area studied. Earlier radiometric surveys on sand and similar rocks have been carried out in various parts of Kitui County; Limestone deposits in Kitui South (Mulwa *et al.*,2012), Coal deposits in Mui basin in Mwingi (Ochieng *et al.*,2016) and sands from Tiva and Mita-Syano rivers (Koech *et al.*,2017).

Kitui County is underlied by the three classes of rocks and there is a possibility that the mineral accessories present in sand and soils of this region are similar to the minerals of the prevailing parent rocks. The rocks and sand from Tyaa river are constantly mined for construction purposes. There is however limited information on the levels of natural radioactivity of these geological materials and hence there is a potential harm to the population in case of elevated radiation levels.

This research, therefore, sought to provide data on the natural radioactivity levels (^{238}U , ^{232}Th , and ^{40}K) in sand and rocks using representative samples from Tyaa River in Mwingi, Kitui County. High-resolution gamma-ray spectrometry was adopted for qualitative and quantitative measurements during the rainy season (November 2017 - January 2018) and the dry season (February - March 2018). The findings were further analyzed to establish whether seasonal variation in hydration levels had a significant effect on the natural radioactivity levels in sand and rocks sampled from Tyaa River by collecting samples for the consecutive rainy and dry seasons. Correlational analyses were done to establish the relationship between the trend in levels of terrestrial radionuclides in sand and rocks.

1.2 Statement of the Research Problem

As human beings undertake economic activities along the riverine like mining (sand and rocks), irrigation on river banks and use of water for a variety of domestic demands, they directly or indirectly interact with the river or sediments from the river like for the case of building materials. It is potentially risky to collect and use raw stone-based building materials without background radioactivity tests, as research shows they contribute over 18% of the total radiation doses received by the human population.

Areas known for elevated ambient radiations have some particular geological composition like the presence of Granitic, Silic, Shale and Phosphate rocks which have reflected consistent trends of high natural radioactivity. Rocks of similar mineral constituents are present along the course of the studied river. This factor coupled with proper knowledge of the probable deleterious effects as a result of human interaction with ionizing radiations of high energy formed a strong basis for this research.

1.3 Objectives of the Study

1.3.1 Main Objective

To determine the natural radioactivity levels in rocks and sand from Tyaa River, Mwingi Kitui County.

1.3.2 Specific Objectives

- i. To determine the radiological parameters of ^{238}U , ^{232}Th , and ^{40}K in the representative rock and sand samples.
- ii. To determine the seasonal effect on natural radioactivity levels of the rocks and sand.
- iii. To determine the correlation between the radioactivity levels of rocks and that of sand samples.

1.4 Research Questions

- i. What is the level of the radiological parameters of ^{238}U , ^{232}Th , and ^{40}K in rocks and sand from Tyaa River?
- ii. What is the seasonal effect on the natural radioactivity levels of rock and sand in Tyaa River?
- iii. What is the correlation between the radioactivity levels in rock and sand of the area of study?

1.5 Justification of the Study

The human population can never escape from exposure to radiation since gamma radiations from cosmic rays and primordial radionuclides in the earth's crust exist in all ranges from trace to elevated radiation levels. It is therefore wise to be cautious

whenever the geology of the region matches the geology of the regions with high background radiations as the geology majorly determines the levels of radioactivity in the area.

Among the many major rivers in Kitui County like Tiva River, Mwewe, Semea, Thua and others, Tyaa river was chosen because of the following reasons; the river flows through the neighborhood of Tharaka and Thika regions whose geology reports elevated levels of terrestrial radionuclides and similar geology prevails in the studied region.

The current study was imperative since no available data on the background radioactivity in this area and particularly on this river despite the potential harm in case the levels of radioactivity surpass the safety thresholds.

High Purity Germanium detector was used for spectrometric analysis due to its high resolution. The accurate data on the levels of background radiations enabled the precise evaluation of the external gamma irradiation from ^{40}K and internal exposures from radon and thoron gases from ^{226}Ra and ^{232}Th which may accumulate to alarming levels in enclosed dwellings from floors, soils beneath the floors, walls, and ceilings, basically the building materials in case they have enhanced levels of natural radionuclides. (UNSCEAR, 2000).

The findings of this research will provide data on the natural radioactivity levels of ^{238}U , ^{232}Th and ^{40}K in the sand and rocks from Tyaa River which will be useful for advisory and regulation by the relevant bodies like KRPB, ICRP, NRPB, and NEMA. The findings of this research will also form a background radiometric survey for subsequent scholars in the same field.

1.6 Scope of the Study

The present research experimentally estimated the radiation levels from terrestrial radionuclides in sands and rocks employing high-resolution spectroscopy meant to provide requisite radiological baseline information and to measure the dose rates from the natural radioisotopes. The data was further analyzed to examine whether the levels

of radioactivity in rocks and sands are varying with seasons. Correlation analyses were done to determine the relationship in trends of radioactivity in sands and rocks. Comparison of the trends of radioactivity from the Mwingi - Garissa highway upstream and lower stream was done too.

The study covered a stretch of a maximum of 1 kilometer on each side of Tyaa Bridge across Nairobi-Mwingi-Garissa Highway because this stretch is the epicenter of sand and rock mining favored by the good transport network. The study focused on analyses of samples for the specific activity levels of ^{226}Ra , ^{232}Th , and ^{40}K . To determine the safety of the rocks and sand from this river when used as a building material, dose rates and radiological hazard indices were evaluated from the specific activity concentrations of ^{226}Ra , ^{232}Th , and ^{40}K using the relevant mathematical equations and the corresponding conversion factors suggested in various reports. The data from this research was compared with findings from similar studies available in the literature. The study was conducted during the rain and dry seasons.

CHAPTER TWO

THEORETICAL BACKGROUND

2.1 Introduction

This chapter discusses the theoretical concepts governing radioactivity and radioactive emissions, their interaction mechanisms with living and non-living matter, effects of the interaction of ionizing radiations with biomatter, dosimetric quantities useful in the measurement of radiation doses and their experimental techniques, Structural and operational principles of the High Purity Germanium gamma-ray spectrometer.

2.2 Types of Radiations

2.2.1 Gamma Rays

Gamma rays are electromagnetic radiations whose energy is given by $E=h\nu$. Gamma rays have no mass thus, high penetrating power. Gamma rays easily pass through matter spreading their energy over larger depth which may result to less damage per interaction thus characterized as low “Linear Energy Transfer” (LET).

Gamma-ray photons carry no electrical charge; therefore, they ionize matter indirectly by first causing photoelectric absorption, Compton scattering or through pair production. The reported biological damaging energy range of gamma rays is (3 to 10) MeV as observed in the gamma-ray window.

Gamma rays of energy > 10 MeV are less harmful because the body becomes transparent to them and may pass without interaction. Gamma-rays accompanies beta decay as most beta decays leaves daughter radio nuclides excited. The excited atom attains their ground state by emission of gamma photon (s) as shown in Figure 2.1 (Knipp, 1936).

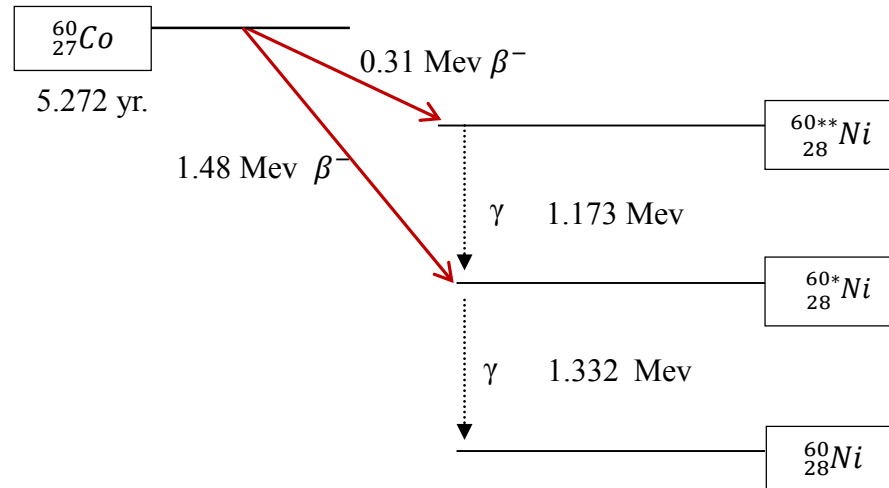


Figure 2.1: Decay scheme of $^{60}_{27}\text{Co}$. The transition is beta decay to an excited state of $^{60}_{28}\text{Ni}$. The resulting $^{60}_{28}\text{Ni}$ emits gamma-rays in succession to attain the ground state.**

2.2.2 Alpha Particles

These are heavily charged particles equivalent to the helium nucleus. Alpha decay leads to a decrease in mass number by 4 and atomic number by 2 units. Alpha particles interact primarily through coulomb forces which causes ionization and excitation of matter leading to their energy loss over depth along their track as explained by the Bragg curve shown in Figure 2.2 (Gilmore, 2008).

Alpha particles are classified as high LET and interact with matter by depositing energy over smaller volume due to their massive nature causing more damage to fewer cells. Due the massive nature of alpha particles as compared to electrons, they travel in straight trajectories as they traverse the living tissue as shown in Figure 2.2 (Furusawa, 2014). Appendix 9 (b) shows $4n+2$ decay series with most transitions involving alpha decay

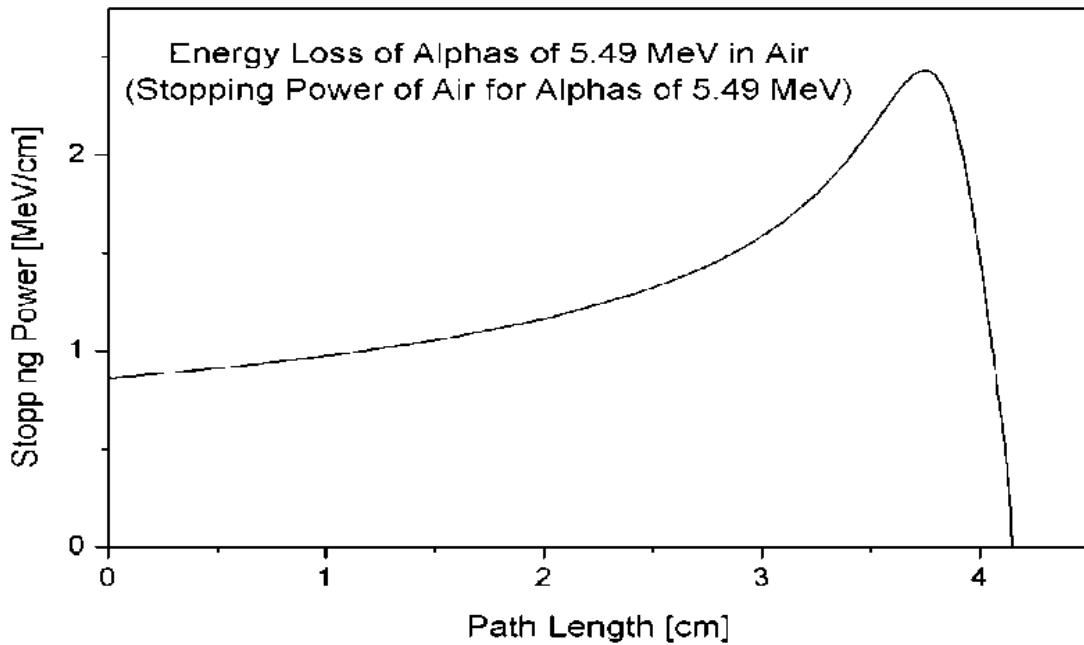


Figure 2.2 Energy attenuation curve of alpha particle in the air (Gilmore, 2008; Halliday, 1987)

2.2.3 Beta Particles

Beta particles are also known as beta rays and are produced through electron or positron decays. Beta particles are much lighter as compared to alpha particles and have a single negative charge. They penetrate absorbing material following a zigzag trajectory. They cause less damage to living cells compared to alpha particles. The transition of ^{212}Pb to ^{212}Bi in ^{232}Th series gives significant exposure to radiation doses from Thoron gas because of the short half-life of ^{212}Pb (Krane, 1988). Appendix 9 (c) shows the decay progression of 4n series with some decay transitions involving beta decay.

2.3 Radiation Interaction with Matter

A gamma-ray photon interacts with matter through the following mechanisms; pair production, photoelectric absorption, and Compton scattering. Whenever gamma-ray photon interacts with matter, at least one of the three things may happen to the photon; the intensity of radiation beam may be attenuated, the photon may undergo total absorption or may be scattered by matter (Knoll, 2010).

Other interaction mechanisms of less significance in gamma-ray spectroscopy include coherent scattering and photonuclear reaction. Coherent scattering involves re-emission

of gamma-ray of the same energy but different direction thus no energy transfer to the detector. Photonuclear reaction requires energy above 5 MeV for it to take place and may not take place for most practical gamma-ray measurements for geological samples (Gilmore, 2008). The intensity (I) of the photon beam is a function of depth (x) of penetration in the matter and is given by the exponential absorption law stated in Equation 2.1 (Gilmore, 2011).

$$I = I_0 e^{-\mu x} \dots\dots\dots (2.1)$$

Where; I is the remaining beam intensity, I_0 is the initial radiation intensity, x is the depth of radiation penetration in the absorbing material, μ is the linear attenuation coefficient which is the probability per unit length that the photon will be removed from the beam (Knoll, 2010).

As the photon traverses the matter, the interactions along its path leads to the partial or total transfer of photon energy to electron energy.

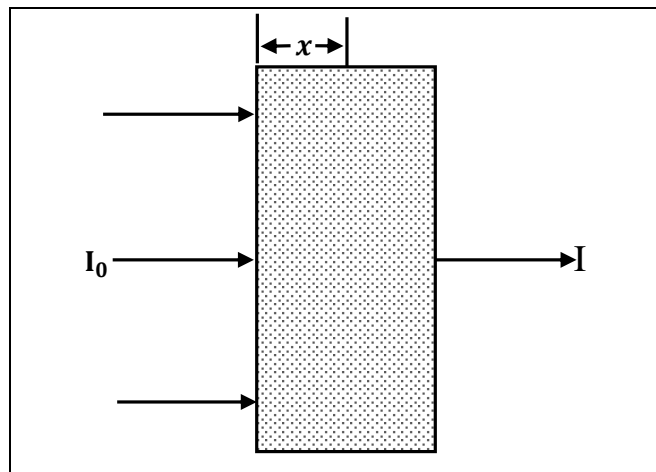


Figure 2.3: Attenuation of gamma-ray photon intensity as it traverses matter

The three interaction mechanisms which are useful in practical gamma ray spectrometry are discussed in details in the paragraphs below.

2.3.1 Compton Scattering

Is the interaction mechanism which takes place between the incident gamma-ray photon and a loosely bound electron probably outside the K, L and M orbits. The electron is

assumed to be stationary in the absorbing material. Assuming the incoming gamma ray photon has energy given by; $E = hv$ and momentum $P = \frac{hv}{c}$ being deflected through an angle θ , with respect to its original direction. If the photon partially transfers the energy to the recoil electron (assumed to be at rest initially) with initial momentum $P_e = 0$ and the rest mass energy given by $E_0 = m_0c^2$. Upon the interaction, the scattered gamma-ray has momentum whose magnitude is given by $P' = \frac{hv'}{c}$ and reduced energy of $E' = hv'$. The recoil electron scattered at an angle ϕ has momentum $p_e' = \frac{1}{c}\sqrt{E_e^2 - E_0^2}$ and energy $E_e = mc^2$ which varies from zero to a large fraction of the incident energy of photon because all scattering angles are possible (James, 2014). Equation 2.2 gives the relationship between the energy transferred and the scattering angle for any given Compton interaction and the expression takes care of both the momentum and energy conservation

$$hv' = \frac{hv}{1 + \frac{hv}{m_0c^2}(1 - \cos \theta)} \dots\dots\dots (2.2)$$

Where; m_0c^2 is the electron rest mass energy given as 511 keV. When $\theta \cong 0$, The recoil electron gains no energy, the scattered photon retains all its initial energy. When $\theta = \pi$, the incident gamma ray is backscattered and recoil electron moves along the direction of incidence (Rittersdorf, 2007)

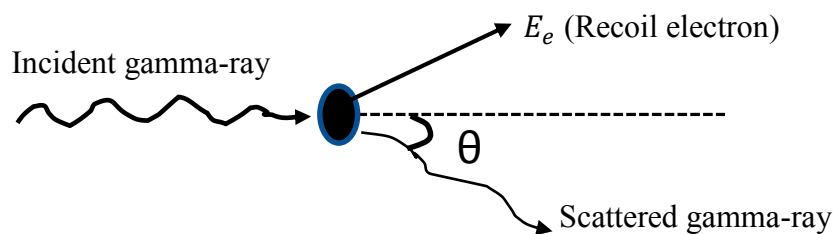


Figure 2.4: Compton scattering of an incident photon by an electron assumed to be stationary.

2.3.2 Photoelectric Absorption

In photoelectric absorption, the incident photon interacts with an electron in one of the bound shells of an atom. The photon is completely absorbed leading to the liberation of an electron from the tightly bound shells (K-shell) for high energy photons with kinetic energy given by equation 2.3. The excited atom recovers its equilibrium in two ways; the vacancy left by the photoelectron is filled by an electron from higher energy shell falling into it emitting characteristic x-ray through a process known as x-ray fluorescence (Figure 2.5 a). The emitted characteristic x-ray may also cause photoelectric absorption. The other possible way in which the atom may recover its equilibrium is by redistributing the excitation energy among the remaining electrons which may lead to the release of another electron, through a process known as Auger cascade (Figure 2.5 b).

The liberated photoelectron possesses kinetic energy equal to the difference between the incident photon energy minus the photoelectron binding energy in its original shell (Gilmore 1988).

$$E_e = h\nu - E_b \dots\dots\dots (2.3)$$

Where E_b is the photoelectron's binding energy in its original shell, $h\nu$ is the incident gamma-ray energy. The ejected electrons from the surface of the absorber pass through the surrounding matter as shown in Figure (2.4)

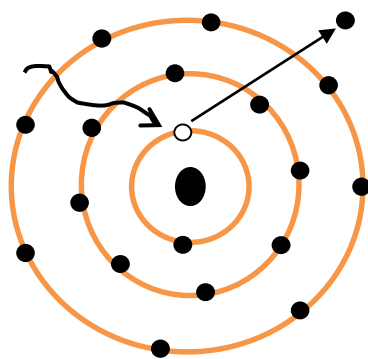


Fig 2.5a

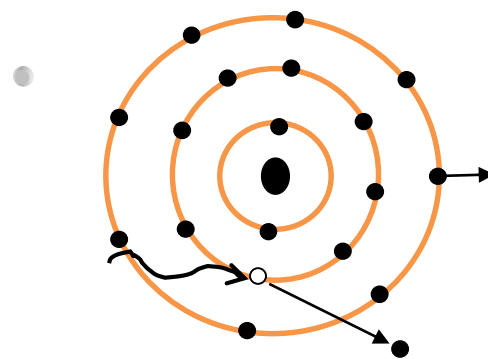


Fig 2.5b

Figure 2.5: Photoelectric emission of electrons by photo-absorption of electromagnetic radiations.

2.3.3 Pair Production

Pair production is the direct conversion of the pulse of electromagnetic energy (photon) to matter producing, an electron and a positron within the vicinity of the nucleus so as to conserve momentum. For it to occur the incident gamma-ray energy must exceed the twice rest mass-energy of the electron of 1022 keV (Hall, 2011). The gamma-ray photon disappears within the intense electric field of nucleus and electron-positron pair results (IAEA, 2005). The energy above 1.02 MeV of incident energy $h\nu$ i.e. $h\nu - 2m_e c^2$ is converted into motion of the electron-positron pair. The equation 2.4 below shows how the discrete quantum energy is shared between the latter

$$h\nu = 2m_e c^2 + E_{kin}^+ + E_{kin}^- \dots\dots\dots (2.4)$$

Where; $m_e c^2$ - is the rest mass energy of the electron and if a particle of mass m_o is converted to energy, that is the amount of energy which will be released. According to Einstein's theory; $E = mc^2$ so it is possible to convert mass to energy and vice versa.

It is worth noting that the positron and electron formed loses energy while creating electron-hole pairs in the detector medium and when the positron slows to thermal or close to thermal energies, it will annihilate with one of the electron in the medium releasing the duo annihilation photons of energy 511 keV each. The Figure 2.5 is a sketch showing pair production interaction mechanism and the resulting positron annihilation (Gruppen, 1996)

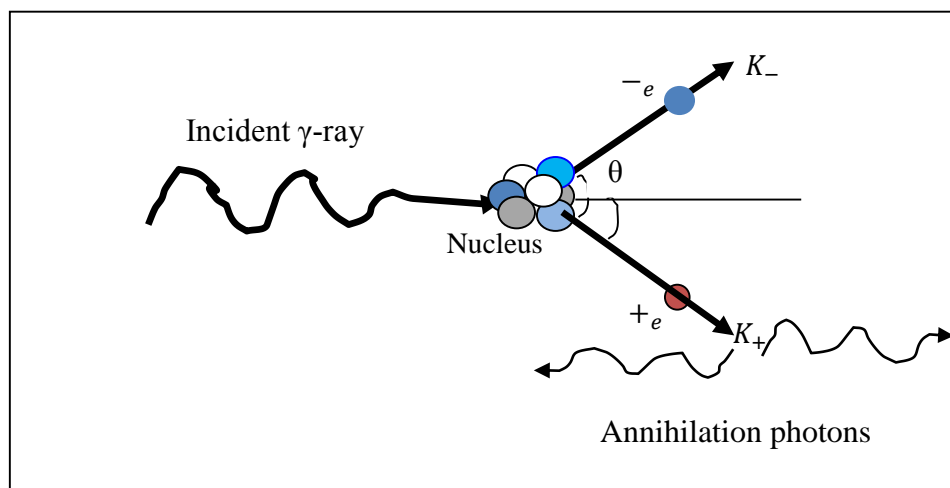


Figure 2.6: Pair production effected by high energy photon.

2.4 Biological Aspects of Ionizing Radiation

Radiation interaction with living matter is slightly different from non-living matter. Radiations have been placed into two categories depending on their nature of interaction with matter. Directly ionizing radiations are also known as particulate radiations e.g. alpha particles; protons, beta particles, and neutrons and are said to have high Linear Energy Transfer (LET) because of their large masses and charge, they ionize the cells directly.

When particulate radiation interacts with biomatter, it may hit DNA strand directly leading to imperfections referred to as nicks which may lead to change in molecular structure. Sometimes the damaged cells are repaired perfectly and in case the damage is severe the cell dies. In the case of imperfections during the repair of somatic cells, the resulting flaws may be replicated to further cells which may later lead to some forms of cancer. If the cell modified deals with the transmission of hereditary codes to descendants of the individual exposed, then there is a likelihood of occurrence of hereditary disorders (UNSCEAR, 2000).

High energy radiations like gamma rays and X-rays are referred to as indirectly ionizing radiations. Due to low linear energy transfer of gamma rays, they interact with water molecules which make over 70% of the cell producing free radicals a process known as water radiolysis. The free radicals Hydroxyl (HO.) and Alkoxy (RO₂.) have unpaired electrons in the structure which reacts with DNA molecules to cause molecular structural anomalies (Desouky *et al.*, 2015). Most radiation based deleterious effects in the cell are as a result of indirect action interaction mechanism of ionizing radiation due to high water composition in the cell (Saha, 2013).

The biological effects of ionizing radiation on the living cells depend on; the amount, type and rate of absorption of ionizing radiation, the number and type of cells affected (WHO, 2014), The greater the energy of ionizing radiation, and the higher the frequency of organ exposure, the more the likelihood of occurrence of health risks if the dose is high.

However, each type of ionizing radiation has its own characteristics. Figure 2.6 shows the direct and indirect actions of high energy radiation.

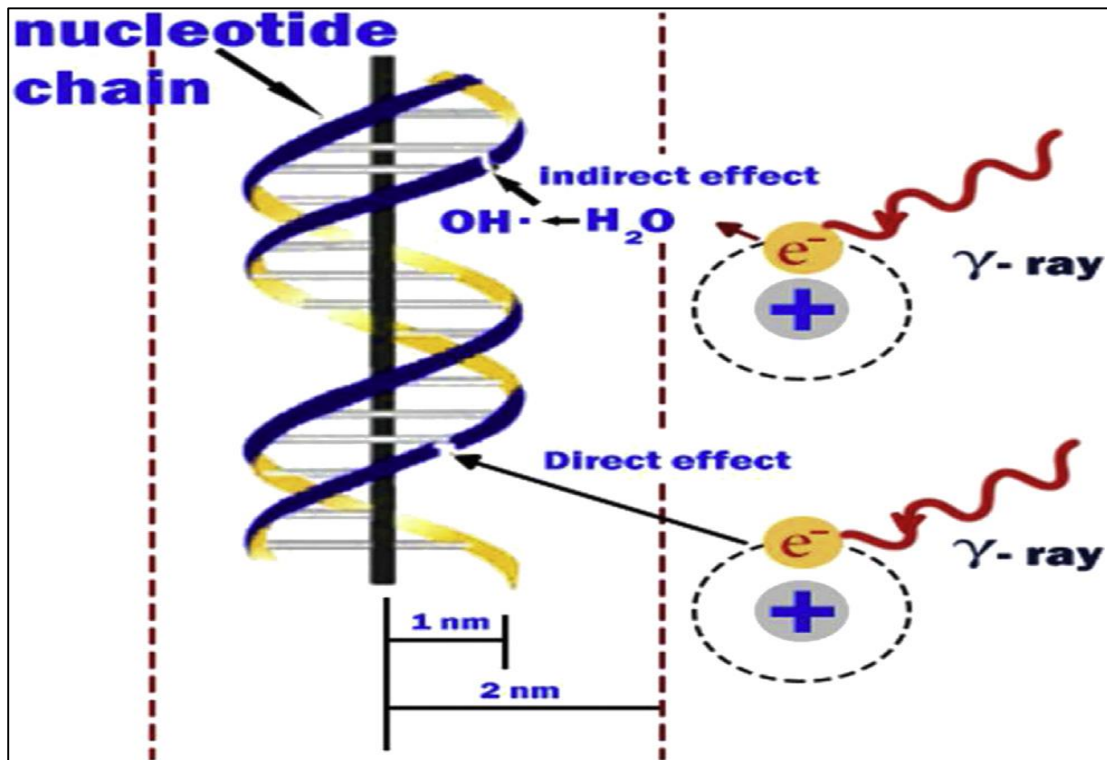


Fig.2.7. Direct and indirect actions of a gamma-ray photon (Hall, 2011).

2.5 Health Effects from Ionizing Radiation

Cases of health hazards have been reported in areas where the total cosmic radiation and emissions from primordial radioisotopes in water, air, soil, and foods have led to chronic internal and external exposure to the population (UNSCEAR 2017). Areas which cumulatively receive high radiation doses from such sources are known as High Natural Background Radiation Area (HiBRA).

The primary radiogenic elements naturally present in the crust of the earth that contribute significantly to human population exposure include; ⁴⁰K, ²³⁸U, and ²³²Th, and their radioactive decay daughters whose half-life is short e.g. ²²²Ra, and ²²⁰Th. The following paragraph 2.5.1 summarizes reported cases following the damaging nature of ionizing radiations are discussed below.

2.5.1 Chromosomal Aberrations and Genetic Mutation

A chromosome is a heritable material with unique properties found in the nucleus of the living cell. Organisms belonging to different species have a different number of chromosomes but the number remains 23 pairs within the cells of the same organism. During cell division, chromosomes ensure that the DNA replication and distribution in newly formed gamete cells is accurate (Jain *et al.*, 2017).

Chromosomal aberration refers to an anomaly in gamete cell caused by re-arrangement, incomplete, or presence of an extra portion of chromosomal DNA segments. The resulting chromosomal alterations result in genetic inconsistency or disorders like Triple X syndrome, chronic myeloid leukemia among other disorders. Anomalies in chromosomes are associated with birth defects, failures in gametogenesis, fertilization, deformities in live-born infants and mental retardations (Susman *et al.*, 2012). To avert the harmful effects of ionizing radiation like chromosomal aberrations which are greatly associated with exposures to ionizing radiation from natural radionuclides, the analysis of chromosomal structures and number were done in HiBRA, a study referred to as cytogenetic analysis. (Jain *et al.*, 2017).

Due to the delicate crucial role of accurate transmission of genetic materials played by chromosomes, there is need to protect them from alterations which may result from; ionizing radiations like X-rays, ultraviolet rays or gamma rays from artificial sources or natural sources. Free radicals in a biological system may cause DNA damage, replication error during the DNA synthesis phase (S-phase) as a result of normal cellular or environmental factors and chemical sources among other sources (Abhishek *et al.*, 2017).

2.6 Radiation Field Quantities and Radiation Dosimetry

These are quantities required to measure the absorbed dose of ionizing radiation within a medium while radiation dosimetry involves the measurement, calculation, and assessment of ionizing radiation dose absorbed by the human body using various techniques. The radiation dose received by the human population can be conveyed internally or externally. To assess the impact of exposure to radiations of low or high LET in biological systems, absorbed doses (D) and Equivalent dose (H) are estimated.

2.6.1 Particle Fluence

This is a measure of number dN of particles incident on a sphere of cross-sectional area dA and is given by equation 2.5 (IAEA, 2005)

$$\Phi = \frac{dN}{dA} \dots\dots\dots (2.5)$$

Where; dN is the number of particles incident on a sphere of cross sectional dA . It is measured in m^{-2} .

2.6.2 Energy Fluence

Energy fluence ψ is defined as the energy dE incident on a sphere of cross-sectional area dA .i.e.

$$\psi = \frac{dE}{dA} \dots\dots\dots (2.6)$$

In the case of the fluence Φ of particles all of energy E , the energy fluence $\psi = \Phi E$. It is measured in J/m^2

2.6.3 Kerma

Kerma is an acronym for "kinetic energy released per unit mass". Kerma is defined as the sum of the initial kinetic energies of all the charged particles liberated by uncharged ionizing radiation measured in gray (Gy)

$$K = \frac{d\bar{E}_{tr}}{dm} \dots\dots\dots (2.7)$$

Where; $d\bar{E}_{tr}$ is the mean kinetic energy transferred to charged particles from uncharged particles in mass dm of a given material. Total Kerma K_{total} can be split into two parts; collisional Kerma (K_{coll}) and radiative Kerma(K_{rad})

$$K_{total} = K_{coll} + K_{rad} \dots\dots\dots (2.8)$$

2.6.4 Absorbed Dose, D

It is a basic physical quantity used in clinical, radiation biology and radiological protection. It defines the amount of energy absorbed per unit mass of the tissue and is measured in Gray (Gy) (ICRP, 2007). At a given absorbed dose, the actual value of energy imparted in a cell is given by the product of the frequency of energy deposition events and the value of energy deposited in each event (ICRP, 2005).

A unit of energy expressed in Gray is equivalent to one Joule of radiation absorbed per unit kilogram of tissue (Mudd, 2008).

2.6.5 Equivalent Dose (H)

It is defined as the measure of biological effects of radiation on human tissue and it is estimated from the absorbed dose using respective conversion factors for various organs. The SI unit of equivalent dose is the Sievert (Sv), but the traditional unit of equivalent dose is rem. The conversion of rem to Sievert is done using the relation that 1 Sv = 100 rem.

$$H = D \times WR \dots\dots\dots (2.9)$$

Where; WR is the radiation weighting factor. Values of WR are based upon the Relative Biological Effectiveness (RBE) of various radiations for stochastic effects, especially compared with the effects of γ -rays at low doses (ICRP, 2005). Table 2.1 gives a summary of quantities conventionally used in radiation protection.

Table 2.1: Quantities and their units used in radiation dosimetry (Krane, 1987)

Parameter	Quantity	Traditional units	Si Unit
Activity	Decay rate	Curie (Ci)	Becquerel (Bq)
Exposure (X)	Ionisation in air	Roentgen (R)	Coulomb/Kilogram(C/Kg)
Absorbed dose	Energy absorption	Rad	Gray (Gy)
Equivalent dose	Biological effectiveness	Rem	Sievert (Sv)

2.7 Radiation Measurement Techniques, Challenges, and Advancements

Gamma-ray spectrometry is an analytical procedure that allows the identification and quantification of gamma-emitting radioisotopes in a variety of matrices (Reguigui *et al.*, 2006). With no much sample preparation, gamma-ray spectrometry allows the simultaneous detection of several gamma-emitting radionuclides in the sample by giving a spectrum of gamma energies.

The intensity of each energy peak is proportional to the activity of the radionuclide and its position on the horizontal axis gives an idea of its energy which is used to identify radionuclides present in the sample from the radionuclide library (Reguigui *et al.*, 2006). Radiation detection and measurement rely on transfer of photon energy (complete or partial) to the detector volume through the interaction mechanisms discussed in Chapter 2.3.

The operational and structural design of HPGe detectors are still a challenge as far as the detection efficiency, energy resolution and dead time losses are concerned. The detection efficiency of HPGe increases with the size of the Germanium crystal. The cost of manufacturing large crystal is high and this limits the detector size. Other factors which affect the efficiency include source-detector geometry and the detector casing material as it attenuates the photon energy falling on the entrance window.

To maintain the high resolution of the energy peaks and avoid ambiguity during the qualitative analysis of the spectrum, the detector crystal is maintained at 77 K. Cooling the detector crystal also minimizes the electronic noises resulting from thermal generation of electrons. To achieve this, the Dewar which stores the coolant usually liquid Nitrogen at -196 °C is refilled after a maximum of two weeks and for large number of samples is very costly.

To cater for dead time losses, several models have been developed; paralyzable (extended model) and non-paralyzable (non-extended model). In the paralyzable model, the events that occur during the dead time are not recorded as counts and are assumed to extend the dead time by starting from the last arrival time. In the non-extended model, the events that occur during the dead time are not counted and thus no effect on the output of the detector in this model no extension of the dead time by another period following the lost events.

2.8 Theoretical Aspects of Gamma-ray Spectrometry

Gamma-ray spectrometer combines hardware and software to actualize its operations. Spectroscopy in radiation measurements is a non-destructive technique relied upon in identification and quantification of natural radionuclides like ^{235}U , ^{238}U , ^{232}Th and ^{40}K present in rocks and sands and other sediments.

Other useful detectors used to assess radiation levels from decay cascades include Thallium doped Sodium Iodide NaI(Tl) detector, Thermo Luminescent Dosimeters (TLDs), in situ gamma-ray spectrometer and Ludlum pressurized ion chamber. In HPGe detectors, the ionizing radiation from primordial radionuclides interacts with germanium crystal through any of the three major processes; Compton scattering, photoelectric absorption, and pair production converting photon energy to charges (Knoll 2010).

The photoelectric effect is most preferred in detectors because it leads to full absorption of the energy of the incident photon which gives better detector response. A variety of software is installed in the PC coupled to the detector electronics. Genie series from Canberra has been popular in NaI (Tl) detectors. Germanium detectors use Maestro Ortec software to process signals to spectrum. This research used High Purity Germanium detector gamma-ray spectrometer because it was readily available and has an advantage of high resolution and precision in the measurement of the energy of gamma rays from decays, nuclear cascades and transition (Szymanska *et al.*, 2008).

Gamma-ray spectroscopy gives detailed energy information of gamma-emitting radionuclides from the samples under test and can measure the isotopic composition of the sample in a single measurement.

However, energy and efficiency calibration are pre-requisites before each measurement in HPGe detectors. Other disadvantages of HPGe are; the detector cannot count a large or heterogeneous sample, the bulkiness of the spectrometer makes it unsuitable for in-situ measurements. The physical parts of the gamma-ray spectrometer system and their respective functions are discussed in the paragraphs below.

Passive lead shield; the HPGe crystal is shielded from interactions with cosmic rays or emissions from unintended radionuclides in the walls, ceilings, floors or from soils and rocks beneath the floor within the detector site which may influence the quantitative aspect of the data from the sample under measurement. The lead shield is a 10cm thick cylinder with a fixed bottom and a movable cover.

Lead metal is preferred due to its high density thus high absorption power of the gamma rays (Reguigui, 2006).

Germanium crystal is made from pure semiconductor material, a group four element with a band gap of 0.7 eV which ensure high resolution of the detector when the crystal is maintained at 77 K. The modern manufacturing technology of HPGe crystal allows purity concentration of as low as 10^{10} atoms/cm². At this purity level, a depletion width of 10 mm is achievable with a reverse bias of less than 1000 V. The depletion depth (d) is a function of bias voltage, V (Rittersdorf, 2007).

$$d = \left(\frac{\epsilon V}{eN} \right)^{1/2} \dots\dots\dots (2.10)$$

The crystal is a semiconductor diode with a P-I-N structure. The intrinsic (I) region is very sensitive to ionizing radiation, particularly gamma rays and X-rays. The diode is maintained in reverse bias to make sure that it conducts only when the interaction occurs, the applied electric field extends across the depletion region

High voltage power supply- the detector power unit can supply up to 5000 V which is the maximum operational voltage for some detectors and their electronics.

The typical operational voltage for HPGe detector used for this work was about 1000 V. The bias voltage is usually maintained high to widen the depletion layer and increase the efficiency of the detector.

Preamplifier- is a circuit that collects the charge pulse created within the detector and converts it to voltage pulse after the gamma photon interacts with the germanium crystal. It also provides a match between the high impedance of the detector and the low impedance of coaxial cables to the amplifier, which may be located at great distances from the preamplifier.

An amplifier increases the signal level for further processing. The height of the voltage pulse is intensified and carefully manipulated to minimize the problems of baseline shifts, electronic noise pulses riding on the tails of preceding pulses. The amplifier improves the signal-to-noise ratio by filtering high- and low-frequency noises .The amplifier is usually linear to maintain the proportion between the radiation energy and pulse height (Knoll, 2010).

Analog to Digital Converter (ADC) forms the heart of the gamma spectrometer. It converts the analog information from the pulse trains to a digital format for computer

storage and processing. As the pulses arrive over time, the MCA collects them in memory with respect to pulse height. Series of memory locations corresponding to ADC channels contain pulses not necessarily similar and identical in height).

Multi-Channel Analyzer (MCA) houses control logic, Analog-to-Digital Converter (ADC), memory and display. It collects and displays in real time the sorted pulses in all voltage ranges at once. The most common type of multi-channel analyzer of greatest interest to nuclear spectroscopists is Pulse-Height Analysis (PHA). In MCA the voltage or the pulse height is proportional to the particle or photon energy. The pulse height analyzer for this work was a nucleus PCA-8000 with 8192 channels.

The detector cooling system consists of large cryostat filled with cryogenic liquid commonly used is liquid Nitrogen at -196°C (77 K). The detector crystal is maintained at this temperature to minimize thermal leakage current which lowers the detector resolution.

The crystal is encapsulated in a vacuum chamber to ensure that its surfaces are always dry. Figure 2.8 shows vertical dipstick cryostat.

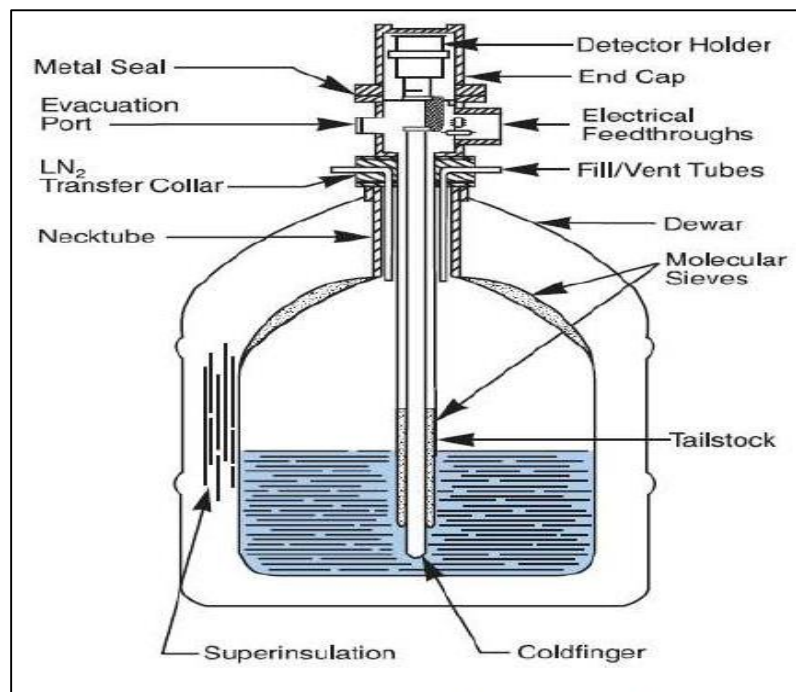


Figure 2.8: Vertical dipstick cryostat (Reguigui *et al.*, 2006).

A variety of softwares are available for use in Gamma spectrometers. Canberra Genie 2000 series has been popular in detectors like NaI(Tl). The MCA of gamma-ray spectrometer used for this work had pre-installed Maestro Multichannel Analyzer Emulation Software. The software was instrumental for; calibration of the MCA, generation, display, and storage of the final gamma-ray spectrum.

Other application software like MS-Excel was used for the quantitative analysis and spectral decomposition. OriginPro was useful for all the statistical graphing and data fitting. Figure 2.9 shows the hardware components of the gamma spectrometer block.

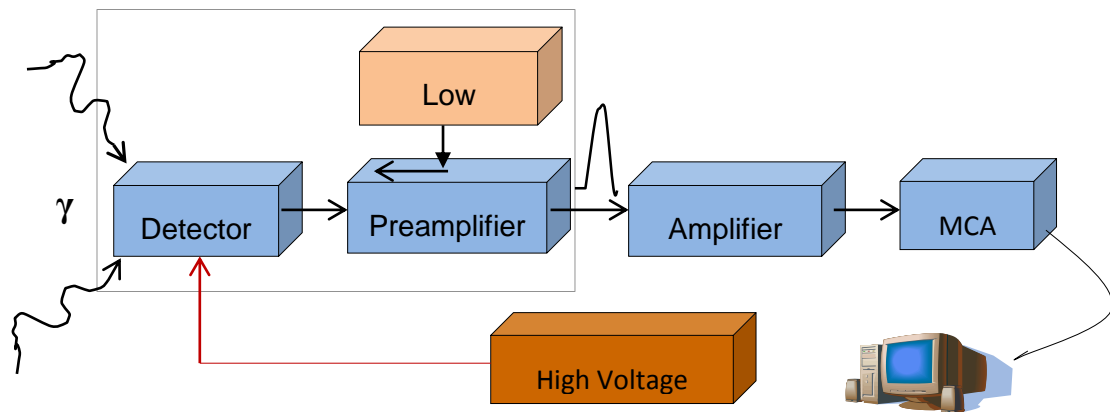


Figure 2.9: Physical components of HPGe gamma-ray spectrometer.

2.9 Working Principle of the HPGe Gamma-ray Spectrometer

The incident photon from geological or non-geological source interacts with detector crystal through photoelectric absorption, Compton scattering or pair production and a burst of charge carriers (electrons and holes) results whose number is proportional to the incoming photon energy deposited in the detector. Since the ionization takes place within the applied electric field, the applied bias voltage sweeps charges from crystal to the negative and positive electrodes and the resulting current forms a voltage signal pulse (integral charge sensitive preamplifier converts the charge to voltage pulse), whose height is increased by a preamplifier then the amplifier intensifies and shapes it. Analog to Digital Converter converts the Pulse intensity is into a digit which is sent to MCA for further processing. The photoelectron absorption gives detector better response due to total absorption of the photon energy.

Figure 2.10 shows a summary of possible interaction mechanisms in the detector crystal of the Gamma-ray spectrometer during its operation.

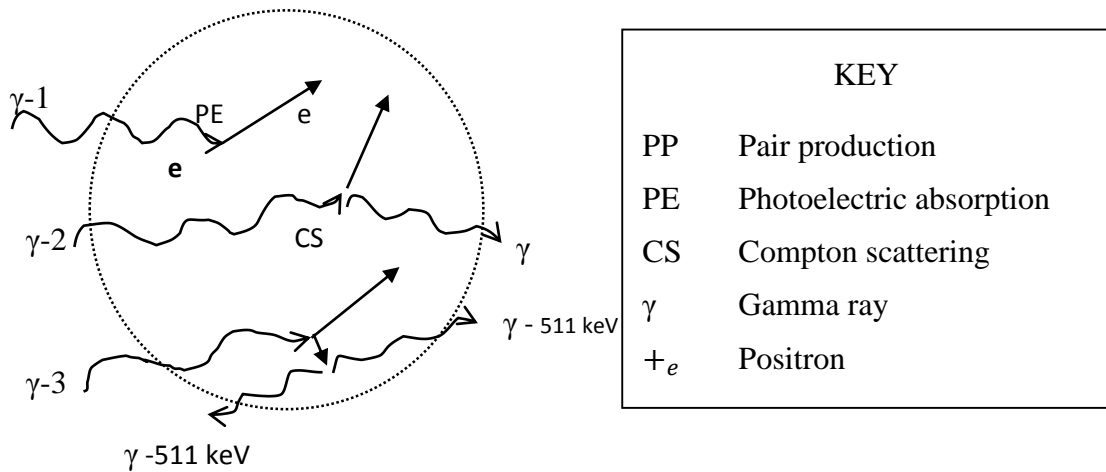


Figure 2.10: A sketch showing interaction mechanisms within the practical detector volume.

2.10 Transient Equilibrium

This type of equilibrium occurs when the time elapsing for the half the parent radionuclides to decay is long compared to the daughter half-life. This means if a sample is sealed and left undisturbed then the activity of the daughter nucleus build from zero to a maximum value and decays apparently at the same rate as the parent nuclei (Gilmore, 2008).

An example of this equilibrium occurs in thorium series for transition of ^{212}Pb to ^{212}Bi whose half-lives are ($t_{1/2} = 10.64$ hours) and ($t_{1/2} = 60.55$ minutes) respectively. Since $\lambda_p < \lambda_d$ or $(t_{1/2})_d < (t_{1/2})_p$. The total activity in the sample is the sum of the parent's and daughter's activities. When the daughter radionuclide undergoes transformation at the same rate as it is being formed, and its total activity then decays at the same rate (at $t = \infty$) as the original parent nuclide, the two species of decaying nuclei are termed to be in transient equilibrium.

2.11 Non-equilibrium

This equilibria occurs when the $t_{1/2}$ of daughter radionuclide is greater compared that of the parent and thus the activity of the parent vanishes leaving behind the daughter nuclide (Gilmore, 2008).

The following conditions must hold; $\lambda_d < \lambda_p$ Or $(t_{1/2})_p < (t_{1/2})_d$. Such condition occurs in transmutation of ^{218}Po ($t_{1/2} = 3.10$ minutes) to ^{214}Pb ($t_{1/2} = 26.8$ minutes)

2.12 Secular Equilibrium

Under secular equilibrium the decay rate of the parent radionuclide is equal to that of daughter radioisotopes. This is only possible if $(t_{1/2})_p \gg (t_{1/2})_d$ such that there is no significant decay during the time interval of interest. If the samples are left undisturbed for a quite some time, the rate of decay of parent radioisotope and hence the production rate of the daughter radionuclide becomes constant.

Under secular equilibrium, each member of the decay chain has the same activity due to the fact that the quantity of the daughter radionuclides builds up until the number of its atoms decaying per unit time becomes equal to the number being produced per unit time. In this case, the activity of the daughter radionuclide can be determined using the activity of the parent radionuclide.

By taking N_D and N_P to be the initial number of atoms of a daughter and parent radionuclide with the corresponding activities A_D and A_P respectively. This type of equilibrium can be explained in details using the decay laws (Gilmore 2008).

$$\frac{dN_D}{dt} = \lambda_P N_P - \lambda_D N_D \dots\dots\dots (2.11)$$

Where λ_P and λ_D are decay constants of the daughter and the parent respectively and can be calculated from half-life using the expression.

CHAPTER THREE

LITERATURE REVIEW

3.1 Background Information

The activity levels, dose rates (absorbed dose and annual effective dose) and hazard indices from different studies related to this work have been reported in this chapter. The corresponding gaps have been identified and the respective recommendations for each radiometric survey have been outlined. The chapter further discusses some radiation-related anomalies reported in High Background Radiation Area (HiBRA) round the globe.

3.2 Radiometric Surveys around the Globe

Studies on the radioactivity levels have been done around the globe reporting a range of radioactivity levels from trace to elevated levels in different geological formations. The variation in levels of natural radioactivity has been attributed to various factors like geological, geographical location, ecological and chemical factors. Most areas the past studies have explored are those with high potential of human occupancy regardless of whether they are temporal or permanent including prime sites which attract human interaction due to their high economic value like; mining sites, tourist attraction centers like sandy beaches, rivers and rocky sites which in case of elevated radiations from primordial radionuclides will lead to the exposure of the population to background radiation doses. Proper knowledge and documentation of radioactivity levels and their spread in different terrestrial sources in environmental media helps in the evaluation of possible health effects due to exposure. The published data on natural radiation levels is useful in monitoring fluctuations in radiation levels which helps to easily detect contamination from artificial sources or changes in radionuclides concentration as river rejuvenation takes place with a view of ensuring the safety of the human population in such environments or interacting with materials from such environments. (Senthilkumar *et al.*, 2010; Kurnaz *et al.*, 2011).

A detailed radiological study in high background radiation areas of Ramsar northern coastal city in Iran reports activity concentration of ^{238}U , ^{232}Th , and ^{40}K varying from Below Detection Limit (BDL) to 86400, 187, and 1350 Bq/Kg respectively which is higher than the world's averages of 35 BqKg⁻¹ for ^{226}Ra , 30 BqKg⁻¹ for ^{232}Th and 400 BqKg⁻¹ of ^{40}K (UNSCEAR 2000). The state reported annual dose rate of 260 mSv/y which is the highest annual dose reported (Ghiassi-Nejad *et al.*, 2002). This was attributed to high radium in deposits from hot springs. Travertine deposits contributed highly to thorium concentration (Sohrabi, 1990).

Radiation hazard indices for 7 samples out of 35 samples analyzed were more than a unit for samples from Talesh-Mahalleh, Abasiah, and Khak-Sefid. Since ^{226}Ra had a mean activity concentration of 144.8 BqKg⁻¹ which is four times the global average of 35 BqKg⁻¹, the area was termed to be a High Background Natural Radiation Area (HiBRA) and use of building materials from these areas was restricted. The indoor and outdoor external measurements in these regions reported a mean of 0.70 in normal radiation areas and mean of 6.00 in High Background Radiation Area (Bavarnegin, 2013).

Evaluation of the radiation hazard from ^{238}U , ^{232}Th , and ^{40}K radioisotopes was done by evaluating natural radioactivity levels in sand from Tamilnadu beach on the North East of India using NaI (TI). The findings from this research report the range of activity concentration from 15- 524 BqKg⁻¹ for ^{40}K , 13 – 3576 BqKg⁻¹ for ^{232}Th and BDL to 254 BqKg⁻¹ for ^{238}U which exceeds the world's reported ranges (Lakshmi, 2005). The mean radium equivalent reported from the entire beach sand was 1081.86 BqKg⁻¹ which surpass the recommended limit of 370 Bq/Kg (UNSCEAR, 2000). Except four locations, the radium equivalent for the rest of the samples exceeded the admissible value of 370 BqKg⁻¹ (Beretka, 1985). The average absorbed dose rate reported was 504.75 nGyh⁻¹ which is 8 times the world's average of 60 nGyh⁻¹ which was attributed to Monazite deposits. AEDR had a mean of 0.621 mSvy⁻¹. External hazard indices ranged between 0.54 and 11.408 with a mean of 2.91 which is twice the recommended limit of 1 mSvy⁻¹ (ICRP, 1992). The research concluded that the beach had enhanced natural radioactivity and posed significant radiological threat to people interacting with it.

The analyses of natural radioactivity levels of ^{226}Ra , ^{232}Th and ^{40}K in the sandy beaches of Quarapari state of Brazil reports the activity concentration varying from (6.0 to 4100) BqKg^{-1} , (6.0 to 3600) BqKg^{-1} , (20 to 57,000) BqKg^{-1} , (17 to 47,500 BqKg^{-1}) and (73 to 3000 BqKg^{-1}) for ^{226}Ra , ^{214}Pb , ^{232}Th , ^{212}Pb and ^{40}K . The level of thorium (^{232}Th) and potassium (^{40}K) species in Areia Preta was above the mean of corresponding global levels. The findings show that the absorbed dose rate ranged from (18 to 37,500) nGyh^{-1} which was above the documented global mean estimates of 60 nGy/h from primordial radiation and the world's range of (10 to 200) nGyh^{-1} . The largest contributor of annual dose rate in Areia Preta was ^{232}Th which is 94.7% while ^{226}Ra contributed 5%. The contribution due to ^{40}K was negligible. ^{232}Th in Areia Preta beach was higher than in other beaches of the world and other regions on the coast of Brazil (Vasconcelos *et al.*, 2013).

A radiogenic survey in Kerala State in India shows that the residents receive an average external dose rate of about 4.5 mGyh^{-1} from gamma-rays and about 2.4 mSv effective doses from internal exposures. In certain locations on the coast, the radiation levels were as high as 70 mSy^{-1} . There were relatively low concentrations of radon of 215 Bq/m^3 and an indoor thoron concentration of 92 Bq/m^3 (Eappen *et al.*, 2004).

Yangjiang in China reports a high level of ambient radiation from radionuclides notably ^{232}Th and ^{238}U in the surface soils and building materials. The reported mean annual effective dose was 6.4 mSv and an external dose range of 1-3 mSv (average 2.1 mSv) and an internal dose of 4.3 mSv which was thrice that of control areas (Sohrabi, 1998).

The contributions from the activities of ^{226}Ra , ^{232}Th and ^{40}K in different lithological units (rocks) was evaluated in Egypt using NaI(Tl) spectrometry. Different rocks presented varying ranges of activity concentration with a maximum ^{226}Ra concentration of 99 Bq/kg^{-1} in Gneiss, 134 Bq/kg^{-1} in Granite and 3382 Bq/kg^{-1} in Basalt rocks, and maximum ^{232}Th concentration of 211.6, 170.5 and 2344 Bq kg^{-1} in Gneiss, Granite and Basalt rocks respectively. The activity concentration of ^{40}K was 106 Bq kg^{-1} , 106 Bq kg^{-1} and 755 Bq kg^{-1}) in Gneiss, Granite and Basalt rock respectively.

Other types of rocks studied were Siltstone and Sandstone. Overall, the Granite rocks had the highest concentration of natural radionuclides, while Sandstone reported lower levels of natural radionuclides. The activity concentration was converted to other

dosimetric quantities to establish the potential deleterious effects due to use the various rocks for construction purposes. The radiogenic survey however, documented no significant possible harm as the radiation indices were below the recommended levels by ICRP reports (Shaban *et al.*, 2011).

In southern Nigeria, a radiogenic survey of rocks was done using gamma-ray scintillation spectrometry reported dose rate and AEDR ranging from 0.012 to 0.042 μGyh^{-1} and 0.06 to 0.21 mSvy^{-1} respectively, both below the world's average.

The level of activity concentration varied with the type of rock with granitic rocks reporting the highest activity concentration of ^{40}K of $(882\pm 298 \text{ Bgkg}^{-1})$ which was attributed to high silica content and fairly high activity concentration of ^{232}Th and ^{238}U of $131\pm 43 \text{ Bgkg}^{-1}$ and $129\pm 38 \text{ Bgkg}^{-1}$ respectively. Ferrogeneisis Shale rocks had the least activity concentration of ^{232}Th and ^{238}U radionuclides because of iron content where their level is always minimal. Despite the variation of the activity concentration with the mineral composition of different rocks, there was potential harm due to the use of such rocks as building material (Joshua *et al.*, 2009).

3.3 Radiological Surveys in Kenya

In Kenya, studies to determine the natural radioactivity levels and various radiological parameters have been done using different detectors and empirical models. Different ranges and mean indices of various dosimetric quantities have been reported. The possible potential harm to human population and environment emanating from radiation exposure has been adequately documented in the following paragraphs.

Odumo *et al* (2009) conducted both radiological survey and elemental flux analysis in four gold mines of Migori district in southern Nyanza, Kenya. Geological samples of different formations including ore, water, sediments, and dust were subjected to liquid scintillation gamma-ray spectrometer and ED-XRF. The mean activity concentration of ^{226}Ra , ^{232}Th , and ^{40}K was 25 Bq/kg, 41 Bq/kg and 100 Bq/kg respectively. Absorbed dose rate lied between (16 - 178.11) nGy/h while effective dose rate ranged between (0.7 - 4.2) $\mu\text{Sv/y}$. The activity concentration and annual effective doses were below the world's average.

Absorbed dose rate 1 meter above the ground averaged 42.11 nGyh^{-1} . The study revealed that, the radioactivity in sediments was below the global average. Further research was recommended to confirm the exact levels of Titanium, Copper, and Arsenic with a view of exploiting them if they have economic viability. Further study on the effect of seasonal changes on radioactivity levels in dust, ore sediments and water was recommended. Wearing safety clothing and mask while mining site and minimizing the time spent around the site was suggested too.

A radiometric assessment of Migori gold belt complex in western Kenya by Ouko (2015) reports a mean activity concentration in rock samples of $(69 \pm 11.29) \text{ Bqkg}^{-1}$ for ^{238}U , $(70 \pm 18.77) \text{ Bqkg}^{-1}$ for ^{232}Th and $(1012 \pm 22.81) \text{ Bqkg}^{-1}$ for ^{40}K . Different rock types subjected to analysis had activity concentration exceeding the global averages. Granite rock which is an igneous rock registered high content of potassium. The findings further showed a high abundance of natural radioactive elements in Granite rocks compared to other types of rocks. The average radium equivalent reported was below the recommended maximum values of 370 Bq/Kg^{-1} . The survey recommended numerical modeling to avail data on vertical variation in activity concentration along the soil profile. Extension of radiometric survey to crops and waters from various sources and indoor exposure from huts erected on Migori gold complex was recommended. (Ouko *et al.*, 2015).

Kebwaro *et al* (2011) reports high levels of natural background radiations from ^{238}U , ^{232}Th , and ^{40}K in Mrima Hill, South Coast of Kenya. Elevated levels of primordial radionuclides were attributed to the abundance of minerals such as Monazites and Carbonatites. The activity concentration of ^{238}U , ^{232}Th , and ^{40}K in soil samples determined using NaI (TI) detector reported average activity concentrations of 207.0 ± 11.3 , 500.7 ± 20.0 and $805.4 \pm 20.0 \text{ Bqkg}^{-1}$ for ^{238}U , ^{232}Th and ^{40}K respectively. Mean absorbed dose rate in the air was $(440.7 \pm 16.8) \text{ nGyh}^{-1}$ with a range of 253.8 ± 2.5 to $733.1 \pm 3.4 \text{ nGyh}^{-1}$ while AEDR estimate was $1.11 \pm 0.01 \text{ mSvy}^{-1}$. The mean value of $(440.7 \pm 16.8) \text{ nGyh}^{-1}$ is over 6 times the global average of 60 nGy/h (UNSCEAR, 2000). An epidemiological study was recommended in the area since ionizing radiations are carcinogenic. Earlier studies around Mrima hill area reports high background radiations with an annual dose of 106 mSvy^{-1} (Patel, 1991).

A radiometric survey by Kinyua *et al* (2011) shows the level of radionuclides in quarries in Kisii district was done ranged from 38.6 to 271.7 Bqkg⁻¹ for ²³²Th, 43.1 to 360 Bqkg⁻¹ for ²²⁶Ra, and 307 to 1780 Bqkg⁻¹ for ⁴⁰K. The mean absorbed dose rate for 1 meter above the ground for the 5 main quarries studied was found to be 541.4 nGyh⁻¹ while the average total absorbed dose rate inside the quarries was 177.6 nGyh⁻¹.

The dose rate below the earth surface was about 3 times the world's average of 60 nGyh⁻¹. The external and internal hazard indices were 1.27 and 1.03 respectively which slightly exceeded the permissible limits (ICRP, 1991). Therefore, based on radiation hazard indices, the soapstone from such quarries were not safe for exploration.

Otwoma *et al* (2013) analyzed representative rock and soil samples from the Homa mountain area in South Western, Kenya. The mean activity concentration of ⁴⁰K, ²²⁶Ra, and ²³²Th were 915.6, 195.3 and 409.5 Bq/kg respectively which surpassed the world's average of 400, 35 and 30 Bq/kg respectively. The mean absorbed dose rate in the air was 493.3 nGy/h which was higher than the world's estimate of 24 – 160 nGy/h from global terrestrial radiation. The individual radionuclide concentration compared with global levels were as follows; ²²⁶Ra reported activity concentration of 193.3 Bq/kg which is 5.58 times the global mean value of 30 Bq/kg, ²³²Th averaged 409.5 Bq/kg which is 13.65 times of 30 Bq/kg and ⁴⁰K reported a mean activity concentration of 915.6 Bq/kg which is twice the world's average of 400 Bq/kg (UNSCEAR, 2000). The average annual effective dose equivalent (AEDE) in Homa Mountain at 1 m above the ground was 0.47 mSv/y. Absorbed dose rate for all the samples except one exceeded the world's average level of 0.07 mSv/y. Based on the findings, the Homa mountain area qualified to be termed as High Background Radiation Area.

Achola (2012) estimated natural radioactivity in HiBRA of Lambwe east south western Kenya by analyzing 16 rock and 5 soil samples using gamma-ray spectrometry.

The mean activity concentration in rock and sand samples were as follows: 179 Bq/kg for ²³⁸U, 1397 Bq/kg for ²³²Th and 509 Bq/kg ⁴⁰K. The absorbed dose rate varied between 0.7 - 6.0 µGy/h with a mean of 2.3 µGy/h.

The overall mean of the measured absorbed dose rates was 2300 nGy/h which is approximately 40 times the world's population-weighted mean of 60 nGy/h. The

Annual Effective Dose calculated assuming an outdoor occupancy factor of 0.4 ranged between 1.7 – 14.7 mSv/y with a mean (+SD) of 5.7 +3.4 mSv/y which is higher than the annual global average effective external exposure of 460 μ Sv/y from terrestrial gamma rays.

This led to the conclusion that the study area had enhanced levels of natural background radiation which could be due to mainly ^{232}Th in carbonatite rocks. The relevant government bodies recommended for further work to scrutinize personal dosimetry, indoor exposure levels, and epidemiological studies to investigate the radiological implication of the enhanced levels of radiation on the local populations (Achola *et al.*, 2012).

Bendibbie *et al* (2013) carried out both elemental and radiometric survey to evaluate the activity concentration, annual effective dose equivalent, and radiation hazard indices using limestone samples from deposits in Kitui south. The activity concentration of ^{232}Th in all the samples was below the detection limit. The activity concentrations of ^{226}Ra had a mean value of 47.4 Bqkg⁻¹ and ^{40}K averaged 142.6 BqKg⁻¹. Generally, ^{226}Ra was found to be highest in Mwanyani with an average of 47.4 Bqkg⁻¹ and potassium activity concentration was highest in samples from Ndulukuni with a range between 56.1 Bqkg⁻¹ and 664.72 Bqkg⁻¹. Activity concentration ^{226}Ra , ^{232}Th , and ^{40}K were however below the global average of 35 Bqkg⁻¹, 30 Bqkg⁻¹ and 400 Bqkg⁻¹ respectively (UNSCEAR, 2000). Average Ra_{eq} was highest at Mwanyani with 58.38 Bqkg⁻¹ but still below the recommended level of 370 Bqkg⁻¹ which produces a radiation dose of 1.5 mGy/h (ICRP, 1991). All the radiation hazard indices were below the recommended limits of <1. Based on the findings from this study, limestone from Kitui South deposits does not pose significant risk to the population interacting with it as a result of radiation exposure (internal or external). Thus, the limestone deposit was declared safe for exploration, processing and consumption purposes.

The findings from this research are in agreement with literature as limestone is sedimentary rock and is associated with low levels of terrestrial radionuclides.

Though studies have been done in Kitui County to establish the levels of natural radiation and exposure levels (external and internal) from raw building materials, water, sediments, surface soil, and rocks, there is a need for more researches to increase the

geographical representativeness since radionuclides levels vary with environment. With plenty of data on levels and spread, human will be aware of their immediate natural environment with regard to the radiation levels and minimizing their harmful effects becomes possible. This research strives to avail data on natural radioactivity levels in Tyaa river of Mwingi using representative sand and rock samples. This area study area has been chosen because it is in the neighborhood of counties with carbonatite, shale, phosphate and silic rocks which have been reported in HBRA (Tzortzis, 2003).

3.4 Radiation-Related Anomalies and Cancer Incidences

The studies on the human population on areas with enhanced background radiation show prompt or delayed cellular alterations due to constant exposure to ionizing radiations from terrestrial radionuclides primarily ^{238}U , ^{232}Th , and ^{40}K . Similar studies in normal background radiation areas used for control purposes report minimal or no cases of such modifications.

The findings from a survey investigating the appearance and the number of chromosome in the nucleus of a eukaryotic cell conducted in HiBRA of Mumbai in India reports both structural and numerical anomalies with high-frequency of chromosomal aberrations attributed to utero radiation exposure (Jaikrishan, 1999). The cytogenetic survey investigating the number and structure of the chromosome is known as Karyotype. Cells in mitotic metaphase are preferred for such studies because chromosomes at this stage are clearly identifiable and their characteristics are distinct. A total of 1,267,788 cells from newborns in mitotic metaphases from newborns were subjected for a study where 964,390 of total cells were from High Background Radiation Areas whose (dose was greater than 1.5 mSv h^{-1}), and 303,393 cells were from low-background radiation areas ($<1.5 \text{ mSv h}^{-1}$) used as control areas (Ramachandran, 2013). A total of 162 (5.94%) cases of Karyotype anomalies were reported; 95 and 67 from HBRA and low-background radiation respectively. The findings show a positive correlation between radiation dose and chromosomal anomalies (UNSCEAR, 2017).

An assessment of the effects of elevated radiations from high natural background areas was carried out using blood samples from female adults at the Regional Cancer Centre

in Kerala. The findings report an average of 13 ± 6.8 chromosomal aberrations in lymphocytes per 1000 cells from adults who had received an estimated average cumulative dose of (187 ± 157) mSv. Similar studies from a normal background area of Kerala used as control area with a cumulative dose of average 15.6 mSv (SD=2.4 mSv), reports an average chromosomal aberration of 0.76 ± 0.77 per 1000 cells (UNSCEAR, 2017).

Cohort baseline survey done in Karunagappally reports a total of 1349 cases of cancer from 69,958 individuals subjected to statistical surveys. Three forms of cancer; lung, oropharyngeal, and breast cancer dominated with 189, 220, and 125 cases, respectively, however, 30 cases of leukemia (a form of cancer) was also too reported (Akiba et al., 2009).

Related surveys done in HiBRA of Yangjiang China to examine cancer deaths reports most forms of cancer associated with radiation exposure caused high mortality to local farmers. Cases of thyroid and skin cancer were also reported. A track of radiation-related health effects between 1979 and 1998 for 736,942 residents of Guangdong Province in China shows that they were at exposure risk and reported 956 cancer deaths out a total of 6,005 deaths including 15 deaths from leukemia (Tao *et al.*, 2012).

In Kenya, cancer has been rated as 3rd killer disease nationally by Kenyan Journal of cancer policy 2016. This journal ascertains that 28,000 cancer deaths which represent 7% of total annual deaths occur each year and 40,000 new cancer cases emerge annually (GOK, 2016). Other forms of cancer whose cause is pegged to radiation exposure include thyroid, lungs, leukemia and breast cancer (UNSCEAR, 2000).

CHAPTER FOUR

MATERIALS AND METHODS

4.1. Geology of the Study Area

Kitui County lies within the Central Eastern part of the Mozambique Belt Segment (CEMBS) and constitutes the eastern part (Nyamai *et al.*, 2003). The earlier studies

show that the region was dominated by Gneiss, Pelitic and semi-Pelitic Schists, and Migmatites but with time evolution, the area currently shows abundance in lithological units of Anorthositic, Granitoid, Gabbroic to ultramafic intrusions and some traces of Andesitic volcanoes (Dodson, 1953). The three classes of rocks are present within Kitui County, but high dominance of metamorphic rocks has been reported within the area studied. The following are some of the sampled rocks from the length of the river under radiogenic survey; Quartzite (metamorphic rock), Granitoid Gneiss (metamorphic rock), Conglomerate (sedimentary rock) and Limestone (sedimentary rock). The residents of the two locations (Kyanika and Kavuvwani) within the area under study are majorly subsistence mixed farmers; however, those near the river banks plant vegetables for commercial purposes. Residents bordering the river make bricks for commercial purposes. The bricks are used for the construction of homesteads and rental houses in Mwingi town and surrounding areas.

The present study was carried out in Mwingi Central district where river Tyaa is approximately 800 meters from Mwingi town CBD. Mwingi town is approximately 144 kilometers east of Nairobi and 97.6 kilometers east of Kitui town, the headquarters of Kitui County. The sampled area globally lies between latitude 0°55'0" S and 1°5'0" S and longitude 38°0'0" E and 38°15'0" E. The sampled length lies between Attitude 203 m -1378 m above sea level.

The area is relatively rocky along the river banks with some huge basement rocks within the river floor. The sand from the riverine is clean, coarse-grained free from organic contaminants and this could be one of the reasons the river attracts a lot of sand harvesters.

The entire stretch of the river studied is 2 km across Nairobi-Mwingi- Garissa highway. The highway properly networks the river with Mwingi town, Nguutani areas, Kithyoko areas, Kitui town, Kiambu, and Tharaka Nithi Counties. Due to the good road network, the sand and rock harvesting takes place throughout the year leading to their extensive use in the construction sector. Use of building materials (rocks and sand) with elevated levels of radionuclides may expose occupants of such dwellings to radiation and their associated radiological hazards. To ensure potentially harmful health effects due to the use of sand and rocks from this river as building materials are insignificant, the research

was carried out to establish the levels of primordial radionuclides in sediments from this mine. Figure 4.1 below shows a map of the study area. The points marked in black were sampled for sand and rocks for the consecutive rainy and dry seasons.

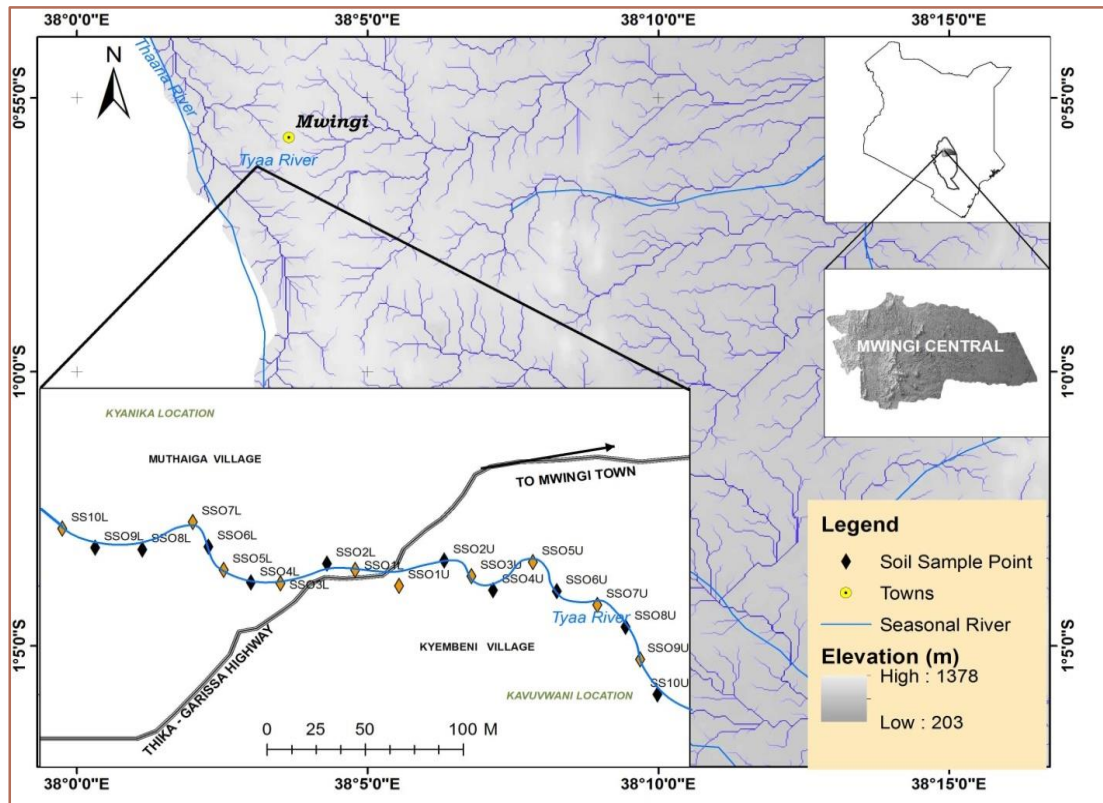


Figure 4.1: A map showing the sampled profile of the River Tyaa, Mwingi Kitui County. The points in black show areas sampled for both seasons. The points in brick yellow were sampled during rainy season only.

4.2 Materials and Equipment Used in the Study

The following are materials used during sampling, data collection and analysis; A mobile phone with GPS application, A 50 m long surveyor's tape measure, fifty six 500 ml plastic bottles, labeling stickers, marker pens and a metallic bucket for packing all the samples, a mallet hammer, 1 mm mesh sieve, digital weighing balance, fifty six standard 300 ml plastic bottles, aluminum foil and packing tape, IAEA certified reference samples (RG-series), a multi-nuclide source (Standard Reference Material), high resolution gamma-ray spectrometer and PC with necessary software. Maestro software was used for the acquisition of spectrum used during Multi-Channel Analyzer

(MCA) energy calibration, detector resolution determination, spectral decomposition, and analysis. Microsoft Excel and OriginPro were used for further statistical analysis.

4.3 Sampling and Sample Collection

4.3.1 Sampling

Systematic random sampling technique was used within the sampled length of approximately one kilometer on each side of Tyaa River Bridge from Mwingi-Garissa Highway. A total of 26 rock and 30 sand samples were collected and sufficient to represent fully the heavily mined length of the River for both rainy and dry seasons.

Starting from Tyaa River Bridge across Nairobi-Mwingi-Garissa upstream, a zigzag line was drawn such that the distance between two sharp turns was 50 meters where sand and rock samples were collected as shown in Figure 4.2. The same procedure was repeated on the other side of the bridge. The inter-sampling distance between two rock samples varied depending on the consistency of rocks. The co-ordinates of the global location for each sampled point was determined using a Global Positioning System (GPS) of the Mobile phone.

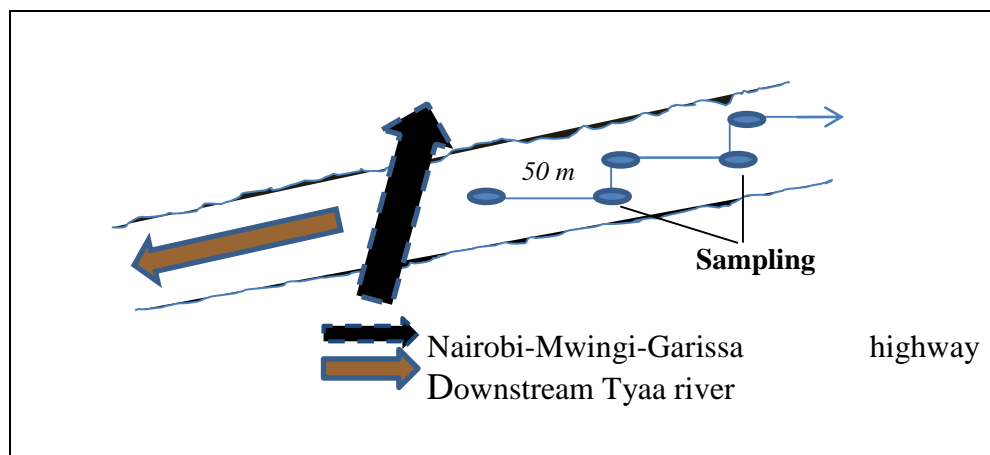


Figure 4.2: A sketch of the sampled length of Tyaa River from Nairobi- Mwingi-Garissa highway.

4.3.2 Collection of Sand Samples

Sand samples were collected using 500 ml plastic bottles up to a maximum depth of 0.5 m which is the common mining depth of sand along Tyaa River and from the center of

1 *m* radius circle to improve the representativeness of the samples. Top debris which contained vegetation was first stripped. The sand within 1 *m* radius circle for each GPS located the point was uniformly mixed up to a depth of 20 *cm* from which a homogeneous sand sample weighing 500 *g* was collected and provisionally packed tightly into a clean waterproof plastic bottles and marked individually with an identity tag, name, date of preparation, net weight, and GPS of the point of collection to avoid cross-contamination; Sand Sample number one was coded SS1-L- meaning sand sample number 1-lower stream, sample number 2 was coded SS2-L- meaning sand sample number 2-lower stream and the rest followed the same sequence using 50 meters as the inter-sample distance (Figure 4.2). Sand sampled upstream had their codes serialized; SS1-U for sand sample 1-upstream, SS2-U meaning sand sample 2-upstream, etc.

4.3.3 Collection of Rock Samples

The rock samples were pried from the basement rock within a stretch of 1 *km* on both sides of the bridge where most of the mining takes place due to efficient and convenient means of transport due to Mwingi - Garissa Highway.

Rock samples were packed into clean 500 *ml* plastic bottles and each package was clearly labeled individually with identification number, name, and date of preparation, net weight, and GPS of point of collection for example; rock samples were coded RS1-L meaning rock sample number 1-lower stream, RS2-L meaning rock sample number 2-lower stream and the rest followed the same order. The inter-sampling stretch for rocks varied depending with the consistency of their availability along the riverine. Using rock properties, samples of rocks collected were sorted and placed into their respective categories in accordance to their size of mineral grains, luster, color, texture and hardness before they were prepared for counting.

4.4 Sample Preparation

A total of 40 different environmental sand and rocks samples from river bed or banks for some rock samples were prepared for counting during the rainy season. The various samples were independently air dried to constant weight for at least about 12 hours in a dry environment.

The samples were ground separately to microscale for homogeneity by pulverizer at the Ministry of Mining and Petroleum, Nairobi. Drying samples drive out all the moisture content to enable activity concentration for various radionuclides of interest (^{226}Ra , ^{238}U and ^{40}K) present in the sample to be calculated direct (Benke, 1999).

A mass from each bulk sample approximately equal to the mass of reference sample was packed tightly into 300 ml standard plastic bottles and the caps lined with aluminum foil and packing tape to ensure that ^{238}U , ^{232}Th , and their short-lived decay daughters particularly radon and thoron does not leak. The latter was then kept for 4 weeks before counting so as to allow the reaching of secular equilibrium between ^{226}Ra and ^{220}Th , and their daughters (Mohanty *et al.*, 2004).

4.5 Gamma-ray Spectrometry

Assuming the tightly packed environmental samples had attained secular equilibrium after a minimum of 28 days, the samples were subjected to gamma-ray spectrometer. Prior to counting any geological sample, Standard Reference Material (SRM) was run for a roughly 400 seconds to calibrate the MCA.

Certified reference samples (RG-series) supplied by IAEA were run weekly before counting the geological samples to help monitor and determine the detector counting efficiency. Each sample at a time was placed symmetrically on top of the detector and counted for a live time of 30,000 s. The spectra for all the samples collected during the rainy season were obtained and stored.

The gamma-ray emission rate from background sources at the laboratory site was determined from spectral data acquired using de-ionized water for a counting live time equal to that used for environmental samples under study of 30,000 s and using standard plastic container similar to the one which held rock and sand samples, under identical measurement conditions and geometry. The background intensity was later subtracted from the gross intensity for each sample to get the net emission rate due to each radioisotope of interest present in the sample. The measured gamma-ray energy is characteristic and corresponds to a specific type of element and its isotope, while the count corresponds to the abundance of the radionuclide source present in the counted sample. The ^{226}Ra which is a member of the ^{238}U decay chain was estimated from γ -

peak of ^{214}Pb and ^{214}Bi . The ^{232}Th radionuclide was estimated from γ -peak of ^{212}Pb and ^{228}Ac , and ^{40}K was estimated from its standard 1461 keV γ –peak of itself.

The same procedure was repeated using samples collected during the dry season. The HPGe was preferred due to its advantage of high resolution over scintillators, can simultaneously detect multiple radionuclides, requires little sample preparation and has the ability to record data for both qualitative and quantitative analysis. The HPGe was also readily available at the time the research was being done. Despite the good energy resolution of HPGe, it is less efficient compared to the NaI (Tl) detector. Its detection efficiency decreases exponentially with energy increase and can only detect efficiently the radionuclides with lower energies (Hossain *et al.*, 2012). This effect was however minimized by determining the detection efficiency regularly using the standard sample which was useful during quantitative analysis.

4.6 Pre-requisites before Sample Counting.

4.6.1 Energy Calibration of HPGe Spectroscopy

Energy calibration is necessary for this detector as it helps to convert channel numbers to energies which is relied upon during identification of radioisotopes of interest in the sample. The pre-installed radionuclides library (Maestro software) has several radionuclides against their energies and therefore, proper knowledge of channel energy leads to knowledge of the corresponding radionuclide (Gilmore, 2008). A high activity multi-nuclide sample with Americium-241, Caesium-137 and Cobalt-60 mixture supplied by IAEA was run roughly for 400 seconds and the spectrum was recorded using the Ortec software. Despite the availability, this standard source was preferred because the peaks of interest from it are well spread and resolved and again the energy range of this source (^{241}Am -59.5 keV to ^{60}Co -1332 keV) covers the energy range of radionuclides the (^{212}Pb at 238 keV to ^{40}K at 1460 keV).

The spectrum from standard source acquired was to ensure that each channel of MCA matches particular energy through calibration; a second-order polynomial fit was done to convert all channels to energy. (Mansour *et al.*, 2016).

4.6.7 Detector Counting Efficiency (ϵ)

Detector counting efficiency is necessary for quantitative analysis. Counting efficiency is the probability that an emitted gamma ray will interact with the detector crystal and produce count (Reguigui, 2006). There are various types of efficiencies; absolute efficiency, intrinsic efficiency, relative efficiency, and full-energy-peak also termed photo-peak efficiency.

The efficiency of a detector depends on majorly three factors: Detector size - efficiency of the detector is proportional to its size detector. Big size detector provides a larger volume for gamma-ray interaction and absorption. The detector - source geometry - the number of ionizing radiations detected depends on how close the source is to the detector. The more the source is proximal to the detector, the higher the detection efficiency.

Marinelli beakers offers good source-detector geometry of the sample. Detector casing material- the material placed at the entrance window should be thin to minimize energy attenuation of incident gamma-ray.

Knowledge of detection efficiency (ϵ), makes the calculation of the activity of sample (A) under consideration easy, from the number of particles detected (N). The photopeak efficiency for detecting ^{238}U , ^{232}Th and ^{40}K were calculated from Certified Reference Materials (CRM) RG-series as RGK-1, RGU-1, and RGTh-1 traceable by the International Atomic Energy Agency (IAEA). The equation 4.1 below was used in the calculation of the photopeak efficiency.

$$\eta = \frac{N_p}{A \cdot P_{\gamma} \cdot t} \dots \dots \dots (4.1)$$

Where; η is the detection efficiency (photopeak) at particular gamma-ray energy E_{γ} . N_p -is the net gamma ray count at the full energy peak, A - represents the activity of the standard source in Bq and for this study was 4,940 Bq/Kg, 3,250 Bq/Kg and 14,000 Bq/Kg for ^{238}U , ^{232}Th and ^{40}K respectively. P_{γ} - is the standard gamma decay probabilities given by International Atomic Energy Agency (IAEA, 2007), as 0.3534, 0.4516, 0.4316, 0.258 and 0.1066 for ^{214}Pb at 351 keV, ^{214}Bi at 609 keV, ^{212}Pb at 238

keV, ^{228}Ac at 911 keV and ^{40}K at 1460 keV respectively. t -is the counting live time (s).

4.6.8 Detector Resolution

Detector resolution is a measure of the ability of a detector to resolve distinctively two energy peaks of close energies. Resolution measures Full-Width at Half Maximum (FWHM) of a single energy peak at a specific energy. It is expressed in absolute keV or as a percentage. The detector crystal is made of semiconductor (germanium) which usually have small band gap and can register small energies from ionizing radiation are registered as different peaks thus termed to have a good resolution. High detector resolution avoids unambiguous radionuclide identification. Germanium detectors have a high resolution because, besides small energy gap of 0.7 eV, their process of converting incident gamma ray energy to pulse is short and efficient compared to scintillators.

To maintain the high resolution of the detector during its operation, the germanium crystal is maintained at 77°K (-196°C), this reduces electronic noises due to thermally generated electrons owing to the small band gap of germanium. Electronic noises in the spectrum is also be minimized by setting up small reverse bias voltage across the crystal so that current flows only when the interaction occurs (Reguigui *et al.*, 2006).

4.7 Specifications of the Gamma-ray Spectrometer

The identity and quantification of the radioisotopes present in the various geological samples and their corresponding abundance was done using HPGe spectrometer of the specifications presented by Table (4.1) available at Institute of Nuclear Science and Technology of The University of Nairobi.

Table 4.1 Technical specifications of the gamma-ray spectrometer used for this work

DETECTOR MODEL	CPVDS30-30185
Serial no:	2489
Crystal characteristics	<ul style="list-style-type: none"> ❖ DIAMETER 57.4 MM ❖ LENGTH 56.9 MM ❖ ACTIVE VOLUME 144 CC ❖ GERMANIUM DEAD LAYER 600 MICRONS

	❖ DETECTOR WINDOW DISTANCE < 5 MM
End cap characteristics	❖ OUTSIDE DIAMETER 76 MM ❖ FRONT WINDOW 1 MM THICK Al
Performance specifications	❖ OPERATIONAL BIAS (3200 V) USED BETWEEN 800 V-1000 V)
Efficiency	❖ GUARANTEED 30% ❖ MEASURED 31.6%
Resolution	IT'S ORIGINAL RESOLUTION WAS 1.85 keV (FWHM) AT 1.33 MeV PEAK OF Co-60 (Vary with weather)
Software	MCA RUNS ON MAESTRO ORTEC
Spectrum acquisition time	30,000 SECONDS

4.8 Samples Analysis

4.8.1 Activity Concentration in Bqkg⁻¹

After running separately all the prepared rock and sand samples in the spectrometer, spectra with multiple peaks were recorded, analyzed and radionuclides from ²³⁸U and ²³²Th series identified from the gamma lines of their short-lived decay products i.e. (²¹⁴Bi & ²¹⁴Pb) and (²¹²Pb & ²²⁸Ac) respectively. ⁴⁰K was identified from its single photo-peak at 1460 keV. The relative abundance of the radioactive species of interest in all the samples was calculated from the spectrum after background correction. The specific activity concentration of ²³⁸U, ²³²Th, and ⁴⁰K in the sand and rock samples were calculated from the measurements of net counts (Bq), sample mass (Kg), counting live time (s) and efficiency response of the detector using equation 4.2 suggested by Ebaid (2010).

Activity concentration defined as the activity per unit mass of an element or compound containing a radionuclide (Gilmore, 2008). The equation (4.2) shows an analytical equation used in the calculation of the radionuclide activity concentrations in Bqkg⁻¹ (Ebaid, 2010).

$$A_c = \frac{N_D}{p \cdot \eta \cdot m} \dots \dots \dots (4.2)$$

Where N_D is the net count rate (cps) at energy E_γ , p is the gamma-ray emission probability (gamma ray yield) for a transition at energy E , $\eta(E)$ is the photo-peak efficiency of the detector system at energy E_γ , m is the mass of the measured environmental sample (kg).

4.8.2 Radium Equivalent (Ra_{eq})

The distribution of ^{238}U , ^{232}Th and, ^{40}K in the environmental mediums is not uniform and thus the concept of radium equivalent allows the use of the single index to represent the gamma emissions by ^{238}U , ^{232}Th and, ^{40}K from different mixtures. Radium equivalent was calculated based on the assumption that 1 Bq/Kg of ^{226}Ra , 1.428 Bq/Kg of ^{232}Th and 0.077 Bq/Kg of ^{40}K deliver the same gamma dose rate (Beretka and Matthew, 1985).

The equation (4.3) shows the empirical relation used for calculating the radium equivalent.

$$Ra_{eq} = C_{Ra} + 1.423C_{Th} + 0.077C_K \dots \dots \dots (4.3)$$

Where C_{Ra} , C_{Th} , and C_K are the specific activity concentrations of ^{226}Ra , ^{232}Th and ^{40}K in samples (sand & rock) respectively expressed in Bqkg^{-1} . For human safety, any construction material with $Ra_{eq} > 370 \text{ Bq/kg}$ should not be used as it will risk exposing the involved population to harmful radiations (UNSCEAR, 1988).

4.8.3 Estimation of Absorbed Dose (D)

Using the activity concentration-dose conversion factors (nGy^{-1} per Bq/Kg) of 0.427, 0.662 and 0.043 as provided by UNSCEAR 2000, the absorbed gamma dose was computed from the mean activity concentration of ^{226}Ra , ^{232}Th and ^{40}K .

Therefore, with knowledge of the activity concentrations of the primordial radioisotopes, equation 4.4 was used in the calculation of the dose rate.

$$D (\text{nGyh}^{-1}) = 0.427C_{Ra} + 0.662C_{Th} + 0.043C_K \dots \dots \dots (4.4)$$

Where: C_{Ra} , C_{Th} , and C_K are the average activity concentration of ^{238}U , ^{232}Th , and ^{40}K in Bqkg^{-1} , respectively in the homogeneous sample of rock and sand samples.

4.8.4 Annual Effective Dose Rate (AEDR)

It's a measure of an individual's total radiation risks. It's calculated based on assumption that most adults in Kenya spend about 60% of their time indoors, while the remaining 40% of the time is spent outdoors and must be taken into account (Mustapha *et al.*,1999). The global mean outdoor and indoor occupancy factors are 0.2 and 0.8 respectively (UNSCEAR, 2008). The constants 0.6 and 0.4 are the indoor and outdoor occupancy factors used to calculate internal and external Annual Effective Doses in Kenya and are denoted by E_{in} and E_{out} respectively. The AED denoted by E was computed using the equation (4.5) (UNSCEAR, 2000).

$$E = D \times T \times Q \times 10^{-6} \dots \dots \dots (4.5)$$

Where; D, T, and Q are the absorbed dose, occupancy time (indoor or indoor) and dose conversion factors (converts absorbed dose in the air to human effective dose) respectively. Since the occupancy factors for indoor and outdoor are different i.e. 0.6 for indoor and 0.4 for outdoor, the resulting two equations for calculating the AEDR were used.

$$E_{in} (mSv y^{-1}) = D (nGyh^{-1}) \times 8760(h y^{-1}) \times 0.6 \times 0.7(SvGy^{-1}) \times 10^{-6} \dots \dots \dots (4.6)$$

$$E_{out} (mSv y^{-1}) = D (nGyh^{-1}) \times 8760(h y^{-1}) \times 0.4 \times 0.7(SvGy^{-1}) \times 10^{-6} \dots \dots \dots (4.7)$$

Where; E_{in} and E_{out} are the indoor and outdoor Annual Effective Doses respectively, D is the absorbed dose, 8760 hy^{-1} is the time expressed in hours for one year, 0.7 ($SvGy^{-1}$) is the dose conversion factor and 0.6 and 0.4 are the indoor and outdoor occupancy factors respectively (UNSCEAR, 2000).

4.8.5 External Hazard Index (H_{ex})

It is a measure of external exposure to excess gamma radiation from ^{238}U (^{226}Ra), ^{232}Th and ^{40}K in building materials. For radiation to be considered to have negligible hazardous effects to the public, the external hazard index should be less than 1 which corresponds to the maximum radium-equivalent activity of 370 Bq/kg (Al-zahrani *et al.*, 2017). The external hazard index denoted by (H_{ex}) was calculated using the model suggested by Krieger (1981) and Orgun *et al* (2007) as shown by equation (4.8).

$$H_{Ex} = \frac{C_{Ra}}{370} + \frac{C_{Th}}{259} + \frac{C_K}{4810} \dots \dots \dots (4.8)$$

Where; C_{Ra} , C_{Th} , and C_K represent the specific mean activity concentrations of radionuclides in ($Bqkg^{-1}$).

4.8.6 Internal Hazard Index (H_{in})

This index gives internal exposure to carcinogenic radon and its accompanying short-lived progenies. Internal exposure emanates from inhalation of terrestrial radionuclides particularly from ^{40}K , ^{238}U and ^{232}Th series radionuclides present in soil and rocks (Tsai *et al.*, 2008). The internal hazard index (H_{in}) was evaluated using equation 4.9 (Beretka & Mathew, 1985).

$$H_{in} = \frac{C_{Ra}}{185} + \frac{C_{Th}}{259} + \frac{C_K}{4810} \dots \dots \dots (4.9)$$

Where: C_{Ra} , C_{Th} , and C_K are the mean activity concentrations for ^{226}Ra , ^{232}Th and ^{40}K in Bq/Kg respectively.

CHAPTER FIVE

RESULTS AND DISCUSSIONS

5.1 Introduction

Gamma-ray spectrometric analyses of representative rocks and sand from the riverine of a seasonal Tyaa river in Kitui County has been done. The identity and quantity of radioisotopes present in geogenic samples has been made. The dose rates; absorbed dose and the effective annual dose have been evaluated from the mean activity concentration of ^{238}U , ^{232}Th and ^{40}K . Radiation hazard indices (radium equivalent, internal and external hazard indices) have been calculated using the respective conversion factors suggested by UNSCEAR and ICRP reports.

The findings from this research have been compared with data reported by similar surveys done in various regions. The evaluation of the potential radiological harm due to the use of sand and rocks from this river has been done by calculating the range and the mean values for the relevant radiological indices. The data from this work has been compared with the global permissible thresholds suggested by various regulatory bodies as discussed below.

5.2 Preliminary Analysis

5.2.1 Energy Calibration

The energy calibration is responsible for determination of energies of unknown peaks in the spectrum which is useful for qualitative analysis.

A plot of photon energy (Y-axis) against channel numbers (X-axis) was used to obtain the calibration fit as shown in Figure 5.1

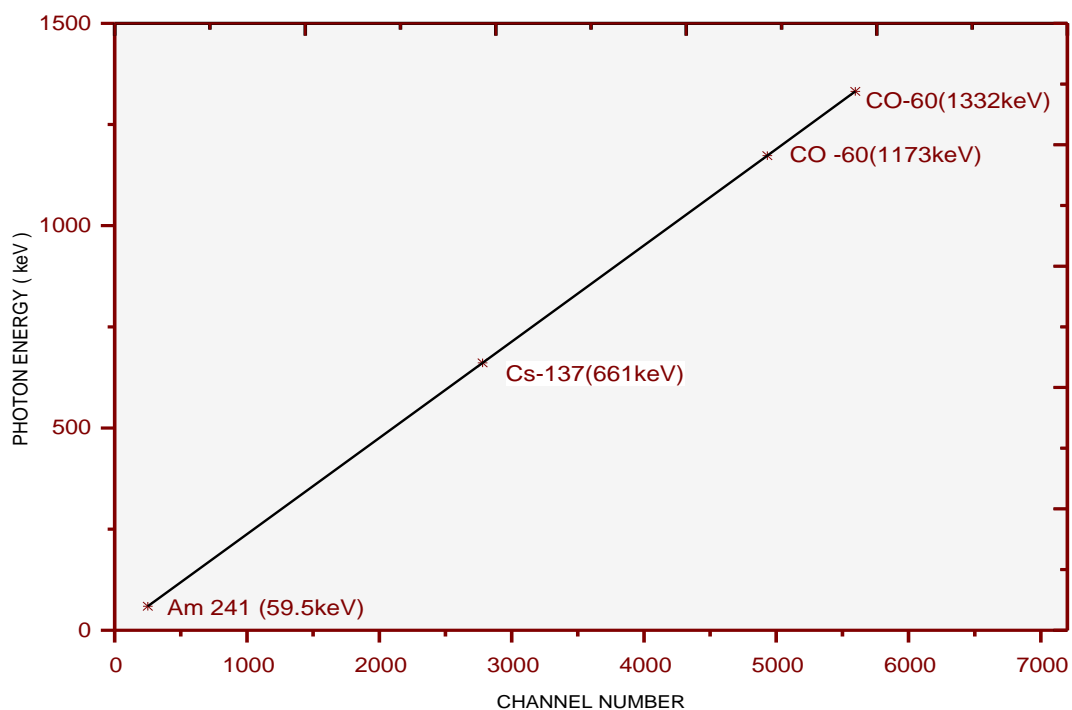


Figure 5.1: Energy calibration fit used in this work. Energy calibration was done using four standard sources. The line represents the second-order polynomial fit to the data.

The polynomial fit is in a general quadratic form $y(x) = A + Bx + Cx^2$ whose fit parameters are given in Table 5.1 (Shikali *et al.*, 2014)

Table 5.1: The polynomial and fit parameters used during energy calibration

Second order polynomial		$y(x) = A + Bx + Cx^2$	
Fit Parameter		Value	Standard Error
A	(Y-Intercept)	-0.12569	± 0.31138

B	0.23763	$\pm 2.74561 \times 10^{-4}$
C	5.5892×10^{-8}	$\pm 4.58458 \times 10^{-8}$

From the polynomial $y(x) = A + Bx + Cx^2$, y is the value of the resulting photon energy, x is the channel number and A, B, and C are the fit parameters. This means that for any channel number (x) of the MCA, if we put the channel contents into equation $y(x)$, we will output the channel energy owing to the linearity of the MCA.

5.2.2 Detector Counting Efficiency

Maintaining the same geometry for the standard and the geological sample source, the full-energy peak efficiency of the detector was calculated using equation 4.1 discussed earlier. The standard sources used for the efficiency calibration were; IAEA-RGK-1, IAEA-RGU-, and IAEA-RGTh-1. A plot of efficiency response of detector at different gamma-ray energies was done as shown in Figure 5.2

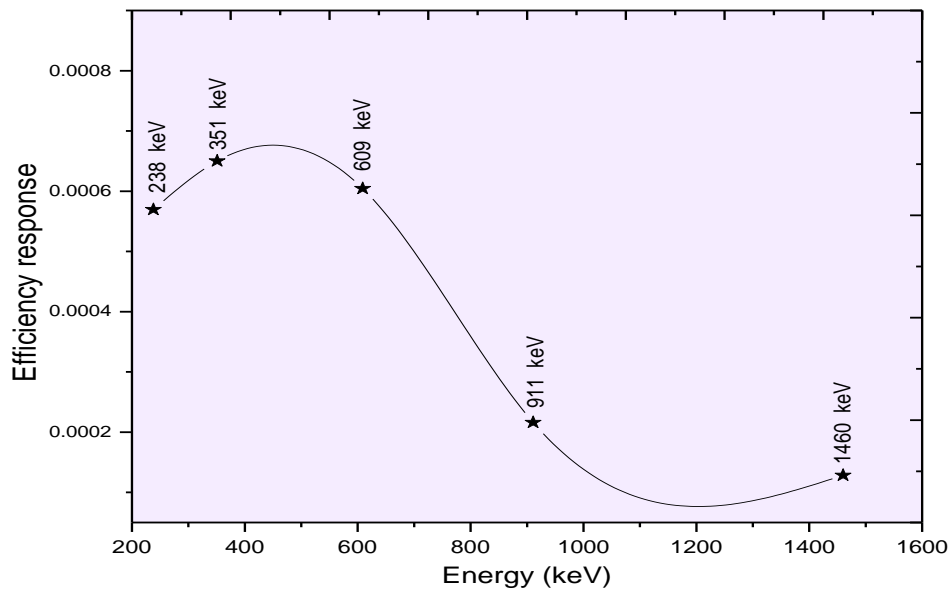


Fig 5.2: Efficiency response of the detector at different gamma-ray energies using standard sources.

From the plot of efficiency response of a detector at various gamma-ray energies, it is observed that the detection efficiency at low energies is high due to full absorption of photon energy through photoelectric absorption which is the dominant mechanism at

energies ranging between 0 - 100 keV (Debertin and Helmer, 1988). As the energy increases (100 keV-1 MeV), the Compton scattering dominates causing scattering of gamma-ray photons where some escape from the detector without interaction contributing to low energy peaks thus decrease in efficiency at these energies. Above 1 MeV, pair production becomes a dominant and large percentage of incident gamma ray photons pass through the detector without interaction thus a sharp decline of full energy peak efficiency is noted as shown in Figure (5.2). The curve may be extrapolated to cover a large range of energies.

5.2.3 Detector Energy Resolution

The resolution of the detector at the time of supply was 1.85 keV (FWHM) at 1.33 MeV peak of Co-60 (varies with weather). The detector resolution for this study was determined by fitting the ^{137}Cs spectral peak at 661.5 keV as shown in Figure (5.3).

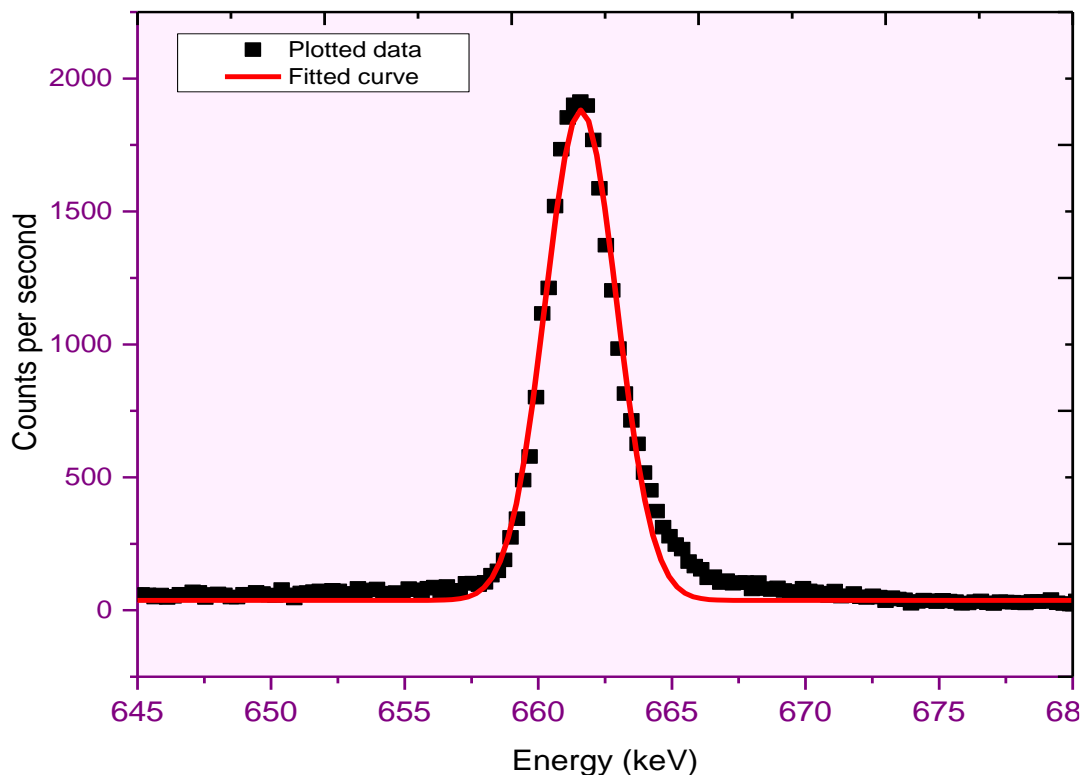


Figure 5.3: ^{137}Cs spectral peak at 661.5 keV with Gaussian fit used to derive fit parameters used for calculation of the energy resolution for this study.

The fit was generated using the Gaussian equation (5.1), whose fit parameters are presented in the Table (5.2)

$$y = y_0 + \frac{A}{w\sqrt{\frac{\pi}{2}}} \exp\left\{\frac{-2(x-x_0)^2}{w^2}\right\} \quad 5.1$$

Where; y_0 represents the baseline offset of the peak (above the x-axis), x_0 is the peak centroid number, A is the net area under the peak, and W is the width of the peak at half maximum

Table 5.2: The Gaussian fit and fit parameters used to calculate detector resolution. The chi-square for the fitting was 0.97278

Equation (Gaussian)	$y = y_0 + \frac{A}{w\sqrt{\frac{\pi}{2}}} \exp\left\{\frac{-2(x-x_0)^2}{w^2}\right\}$	
Parameter	Value	Standard error
y_0	3.1587	± 0.20940
x_0	661.5943	± 0.00886
A	6201.6482	± 35.8950
W	37.2986	± 0.77501

The percentage resolution (R) of the detector was calculated by substituting the values of W and x_0 in the formula shown by the equation (5.2)

$$R = \frac{W}{x_0} \times 100\% \quad (5.2)$$

Where; W is the full width of the peak at half maximum given as 37 ± 0.775 and x_0 is the centroid peak (energy) whose fit parameter is 661 ± 0.008 (Table 5.2). For this study, the resolution of the detector was determined to be 5.63% at 661 keV photopeak of ^{137}Cs which is in the reasonable range of practical detector resolution.

5.2.4 Background Spectrum

In the absence of geological sample in the detector window, detector registers counts from sources outside the detector like; cosmic radiations from ^7Be and ^{14}C in the Earth's space, emissions from terrestrial radionuclides like ^{40}K and ^{238}U within the detector site or from artificial radionuclides like ^{137}Cs (half-life; 30 years) and ^{90}Sr (half-life 28.1 years) whose spread in the environment depends on technology level and population

distribution on the universe. Such counts registered in detector without a sample in the detector window are known as background counts. To maintain the quality of the data in this radiometric survey, the ambient radiation count was subtracted from gross count registered to obtain the net activity of the sample under the study.

Background spectrum for this work was collected for a live time of 30,000 seconds using de-ionized water in the identical container to the one with samples under study and under the same counting geometry.

Use of de-ionized water was preferred over the use of a similar empty container of same geometry because the water drives out all the air in the container and this reduces the radon effects. Standard plastic container with de-ionized water and same dimensions as the one holding geological samples ensures counting geometry of the sample above detector window is maintained. Background counts for each channel were obtained from background spectrum and were used to correct the spectra for all the samples under study. Figure (5.4) shows a typical background spectrum taken from the Institute of Nuclear Science and Technology of the University of Nairobi laboratory site.

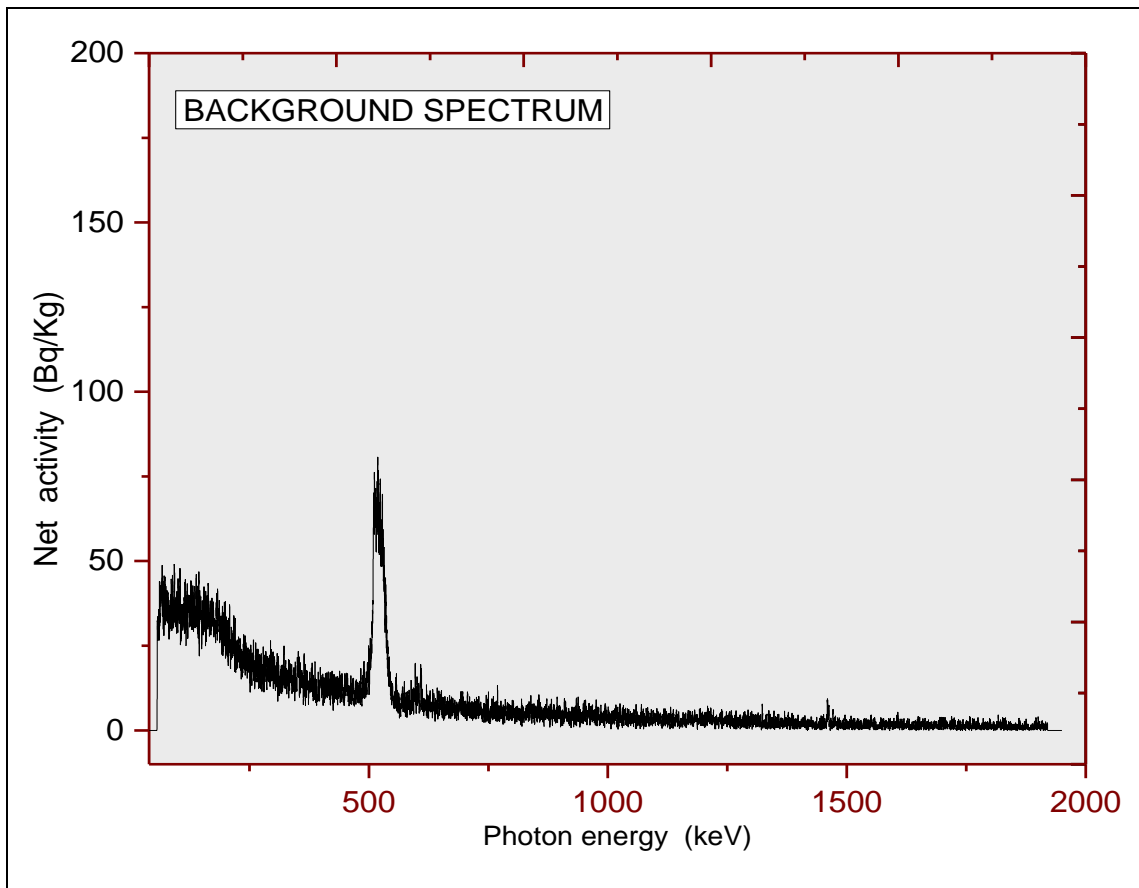


Figure 5.4: Background spectrum from the detector site collected using deionized water sample in the same counting geometry as the geogenic samples.

Figure 5.4 show most channels reported low activity suggesting the lead shield has significantly shielded the detector from non-intended sources. The area could also be a low background radiation area besides adequate shielding.

Figure (5.5) shows a typical spectrum for a sand sample before and after correction. The sample was collected during the rainy season.

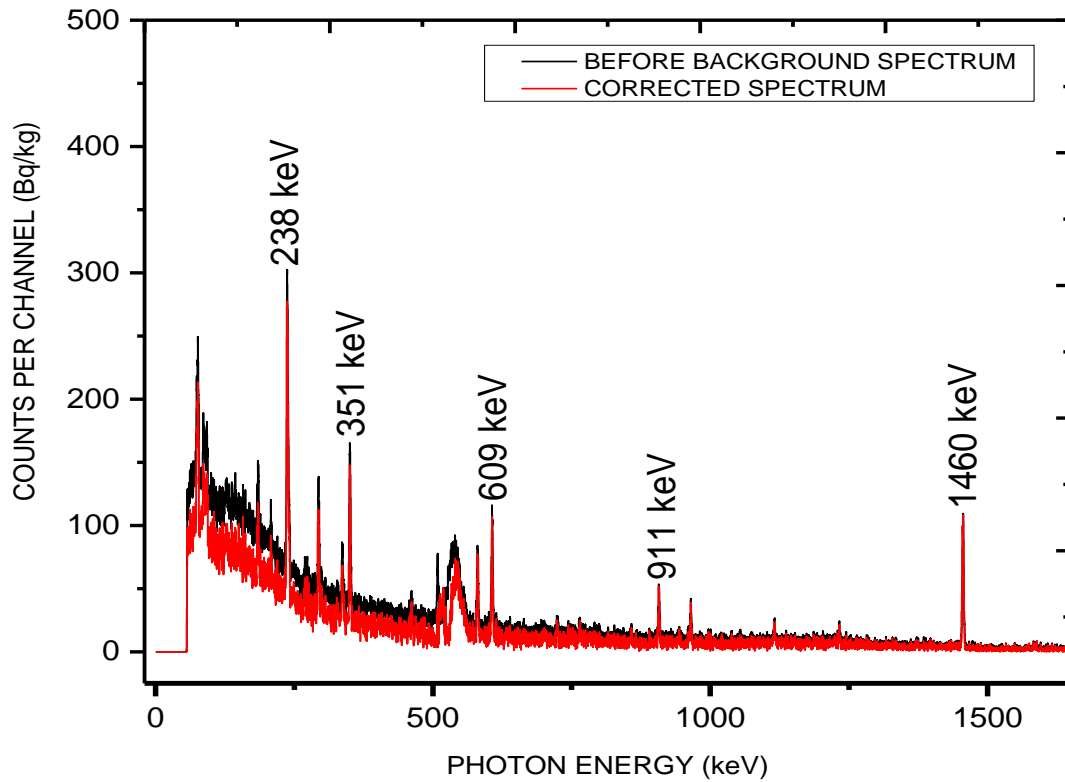


Figure 5.5: Typical gamma spectra from a sand sample collected along Tyaa River course during the rainy season, before and after background subtraction. The counting live time was 30,000 seconds.

Figure 5.5 shows a plot of a gross and corrected spectrum for a sand sample collected during the rainy season. The equation 5.3 was used to correct the counts used in this plot.

$$C_n = C_g - C_b \quad (5.3)$$

Where; C_n is the net count rate of the sample, C_g is the gross count from geological and non-geological sources. C_b , denotes the background count around the detector site.

Figure 5.5 shows the intensity of the background count detected is low which could be due to 10 cm thick passive lead shield surrounding the detector crystal.

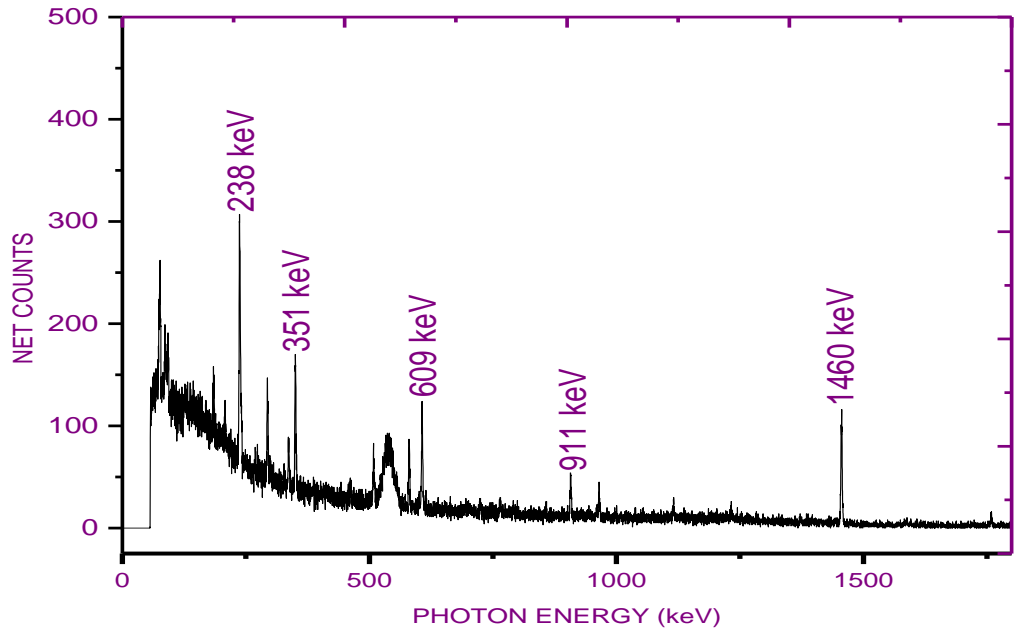


Figure 5.6: A typical gamma-ray spectrum analyzed from a sand sampled during the rainy season, from Tyaa River upstream. The spectral data acquisition live time was 30,000 seconds.

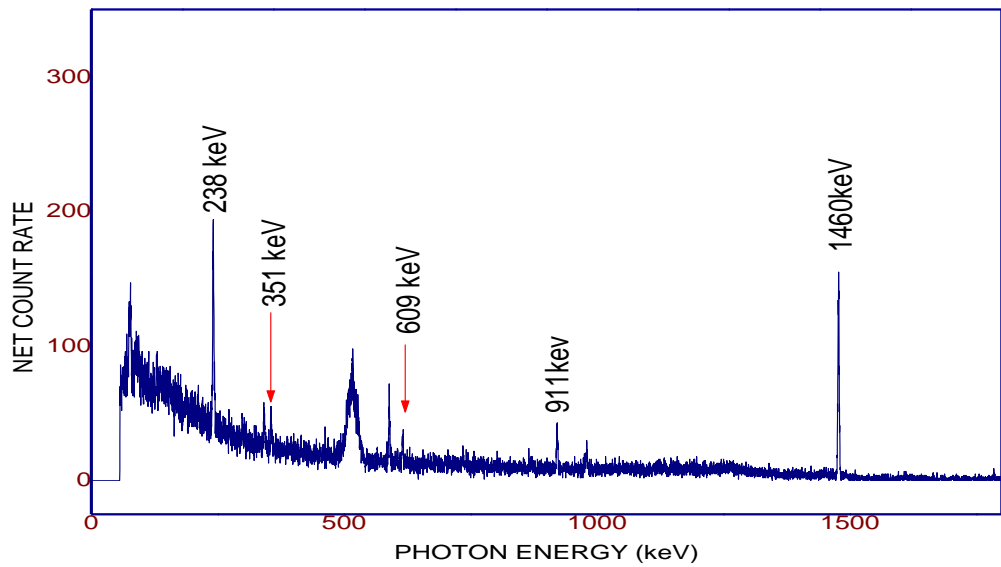


Figure 5.7: A typical gamma-ray spectrum analyzed from rock (Granitoid Gneisses) sample 01 collected from (0°56'21.5 S, 38°02'34.8 E) during the dry season, from Tyaa River upstream. The spectral data acquisition live time was 30,000 seconds.

5.3 Sample Dosimetric Analysis

5.3.1 Activity Concentration from the Representative Sand Samples

The activity concentration in the sand from lower (Kyanika location) and upper (Kavuwani location) river profile were evaluated. The average activity for the sampled length of the river for the consecutive rainy and dry season was evaluated and presented. Table 5.3 shows mean activity concentration of ^{238}U , ^{232}Th , and ^{40}K in sand sampled during the rain season.

Table 5.3: Activity concentration of ^{238}U , ^{232}Th , and ^{40}K in 20 sand samples collected during the rainy season

SAMPLE NUMBER	Activity concentration in sand samples (Bq/kg)					
	Upper stream			Lower stream		
	Ra-226	Th-232	K-40	Ra-226	Th-232	K-40
SS01	7±0.35	38±1	822±41	44±2.	70±3	1068±53
SS02	15±0.78	46±2	626±31	20±1	43±2	913±45
SS03	13±0.66	34±1	895±44	87±4	65±3	287±14
SS04	9±0.5	36±2	811±40	16±0.8	34±2	717±36
SS05	7±0.4	36±2	675±34	29±1.5	65±3.3	882±44
SS06	112±5	94±4	730±36	22±1.1	57±2.8	935±46
SS07	15±0.8	36±1.8	853±42	35±1.8	76±3.8	524±26
SS08	26±1.4	55±2.8	645±32	18±0.9	45±2.3	942±47
SS09	11±0.6	30±1.5	924±46	80±4.0	134±6	913±45
SS10	118±5	72±3.6	714±35	20±1.0	52±3	999±49
MIN	7±0.4	30±1.5	626±31	16±0.8	34±1.7	287±14
MAX	118±5.9	94±4.7	924±46	87±4.4	134±6.7	1068±53
MEAN	33±1.7	48±2.4	769±38	37±1.9	64±3.2	818±40

The activity concentration varied for each sample showing the non-uniform distribution of the natural crustal radionuclides in the studied area. Weathering to a greater degree facilitates the redistribution of radionuclides while the geological contents of the parent

rock vary depending on the type of rock. Therefore, sand a product of weathering consists of different mineral accessories.

The mean activity concentration for the sand sampled upper stream from the highway bridge during the rainy season was 33 ± 1.7 Bq/kg for ^{226}Ra , 48 ± 2.4 Bq/kg for ^{232}Th , and 769 ± 38 Bq/kg for ^{40}K .

Similar analyses for the sand collected lower stream (Kyanika Location) reports an average activity concentration of 37 ± 1.8 Bq/kg, 64 ± 3.2 Bq/kg, 818 ± 40 Bq/kg for ^{226}Ra , ^{232}Th and ^{40}K respectively which is higher than those collected upper stream. Higher activity concentration of ^{238}U , ^{232}Th , and ^{40}K in the sand lower stream was inferred to the presence of minerals from granitic and silic igneous rocks (Harenayama *et al.*, 2006).

Tributaries contribution could be another possible cause of variation in activity levels along the river profile as they feed river course with sand from different backgrounds at different river lengths. If a tributary traces its source from a background whose parent rock mineral accessories (terrestrial radionuclides) are elevated, then soils (sand) the products of disintegration are expected to reflect higher radioactivity levels.

The overall mean of sand for the two seasons was 33 ± 1 BqKg⁻¹, 55 ± 2 BqKg⁻¹ and 812 ± 40 BqKg⁻¹ for ^{226}Ra , ^{232}Th , and ^{40}K which is higher than the world's average of 33 Bq/kg, 45 Bq/kg and 400 Bq/kg for ^{238}U , ^{232}Th , and ^{40}K respectively (UNSCEAR, 2008). ^{40}K revealed higher abundance as its mean was twice the world's mean of 400 Bq/Kg (UNSCEAR, 2000).

The mean activity of ^{40}K was generally higher than ^{238}U and ^{232}Th for all the samples which is a common occurrence in the crustal contents. High potassium levels were inferred to the presence of minerals like potash feldspar e.g. Orthoclase, Microcline or Micas like Muscovite and Biotite in sand originating from rocks rich in such mineralogy (Abedel-Monem *et al.*, 1996). Graphical representation comparing the specific activities of ^{238}U , ^{232}Th , and ^{40}K for the 10 sand samples collected lower stream is shown by Figure 5.8

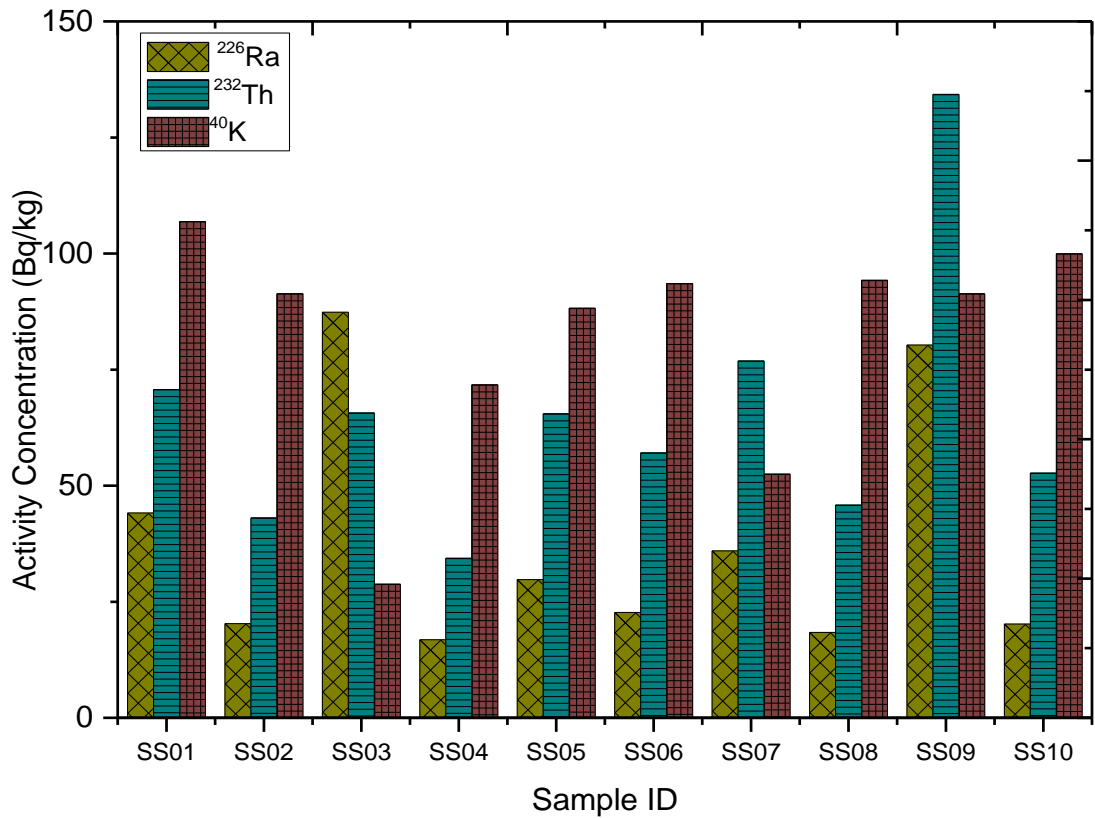


Figure 5.8: A Comparative bar graph showing activity concentration of ^{238}U , ^{232}Th , and ^{40}K in sand samples collected lower stream during the rainy season. The activity of ^{40}K has been reduced by order of 1 to zoom out the statistical bars of ^{238}U and ^{232}Th for clear comparison.

A repeat of a similar study using sand samples resampled during dry season showed variation of radionuclides level for each sample suggesting their non-uniform distribution in each sample which suggests geological make-up of the constituents collected is different. The analyses during dry season reported mean activity concentration of 34 ± 1.7 Bq/kg, 58 ± 2.9 Bq/kg and 830 ± 41 Bq/kg for samples collected lower stream and 25 ± 1.3 Bq/kg, 49 ± 2.5 Bq/kg and 870 ± 44 Bq/kg for ^{238}U , ^{232}Th and ^{40}K respectively for samples collected upper stream (Table 5.4). The overall mean activity concentration for the sand during the entire dry season was 39 ± 2.0 Bq/kg, 54 ± 2.7 Bq/kg and 850 ± 42 Bq/kg for ^{238}U , ^{232}Th and ^{40}K respectively.

Table 5.4: Activity concentration of ^{238}U , ^{232}Th and ^{40}K in sand samples, collected during the dry season

Activity concentration in the sand (Bq/kg)						
SAMPLE ID	Upper stream			Lower stream		
	Ra-226	Th-232	K-40	Ra-226	Th-232	K-40
SS02	9±0.5	41±2.0	841±42	50±2.5	68±3.4	831±41
SS04	12±0.6	40±2.0	750±37	34±1.7	57±2.9	811±40
SS06	52±2.6	71±3.5	850±42	30±1.5	65±3.3	800±40
SS08	18±0.9	36±1.8	955±47	28±1.4	61±3.1	1050±52
SS10	36±1.8	56±2.8	952±47	27±1.4	40±2.0	658±32
MIN	9±0.5	36±1.8	750±37	27±1.4	57±2.9	658±32
MAX	52±2.6	71±3.5	955±47	50±2.5	68±3.4	1050±52
MEAN	25±1.3	49±2.46	870±43	34±1.72	58±2.9	830±41

5.3.2 Activity Concentration of ^{238}U , ^{232}Th , and ^{40}K in Rock Samples

The activity of ^{238}U , ^{232}Th and ^{40}K in rocks averaged 21 ± 1.1 Bq/kg, 46 ± 2.3 Bq/kg and 724 ± 36 Bq/kg respectively for all the rock samples analyzed during the rainy season. The lower riverine reported higher activity averages compared to the upper river profile as the rock samples collected upstream revealed mean activity concentration of 20 ± 1 Bq/kg, 34 ± 1.7 Bq/kg and 689 ± 34 Bq/kg for ^{226}Ra , ^{232}Th , and ^{40}K respectively, while lower stream revealed averaged 23 ± 1 Bq/kg for ^{238}U , 59 ± 1.7 Bq/kg for ^{232}Th and 760 ± 34 Bq/kg for ^{40}K .

A repeat of a similar study for the entire sampled length during dry season reported a mean activity concentration of 21 ± 1.1 Bq/kg, 58 ± 2.9 Bq/kg and 975 ± 48 Bq/kg for ^{238}U , ^{232}Th , and ^{40}K respectively. Among the sampled rocks, Granitoid Gneiss collected from point ($0^\circ 56' 21.5$ S; $38^\circ 02' 34.8$ E) registered highest activity concentration of 1389 ± 69 Bq/kg for ^{40}K which is thought to concentrate in metamorphic rocks and also in granitic rocks during the formation of Si_2O as the rock of igneous origin cool and solidifies (Adel, 2005). Other sampled rocks like quartzite, limestone, and conglomerate reflected lower activity concentration and the present trends are in considerable agreement with findings reported by similar surveys done in other regions of the world. Generally, the average levels of ^{232}Th , ^{238}U , and ^{40}K were far below the

exemption level of 1000 Bqkg^{-1} for ^{238}U and ^{232}Th , and $100,000 \text{ Bqkg}^{-1}$ for ^{40}K and (IAEA, 1996).

5.3.3 Absorbed Dose Rate in Sand and Rocks sampled during the Rainy Season

The absorbed dose rate for all the samples varied due to the non-uniform spread of primordial radionuclides in soils and rocks of the earth crust (Fig. 5.9). The mean absorbed dose rate in sand samples varied from $79 \pm 3.9 \text{ nGy/h}$ to $94 \pm 4.7 \text{ nGy/h}$ for sand samples collected during the rainy season. The mean absorbed dose rate reported by the current research for the two seasons was $86 \pm 4.3 \text{ nGy/h}$ which is higher than the world's average of 60 nGy/h (UNSCEAR, 2000).

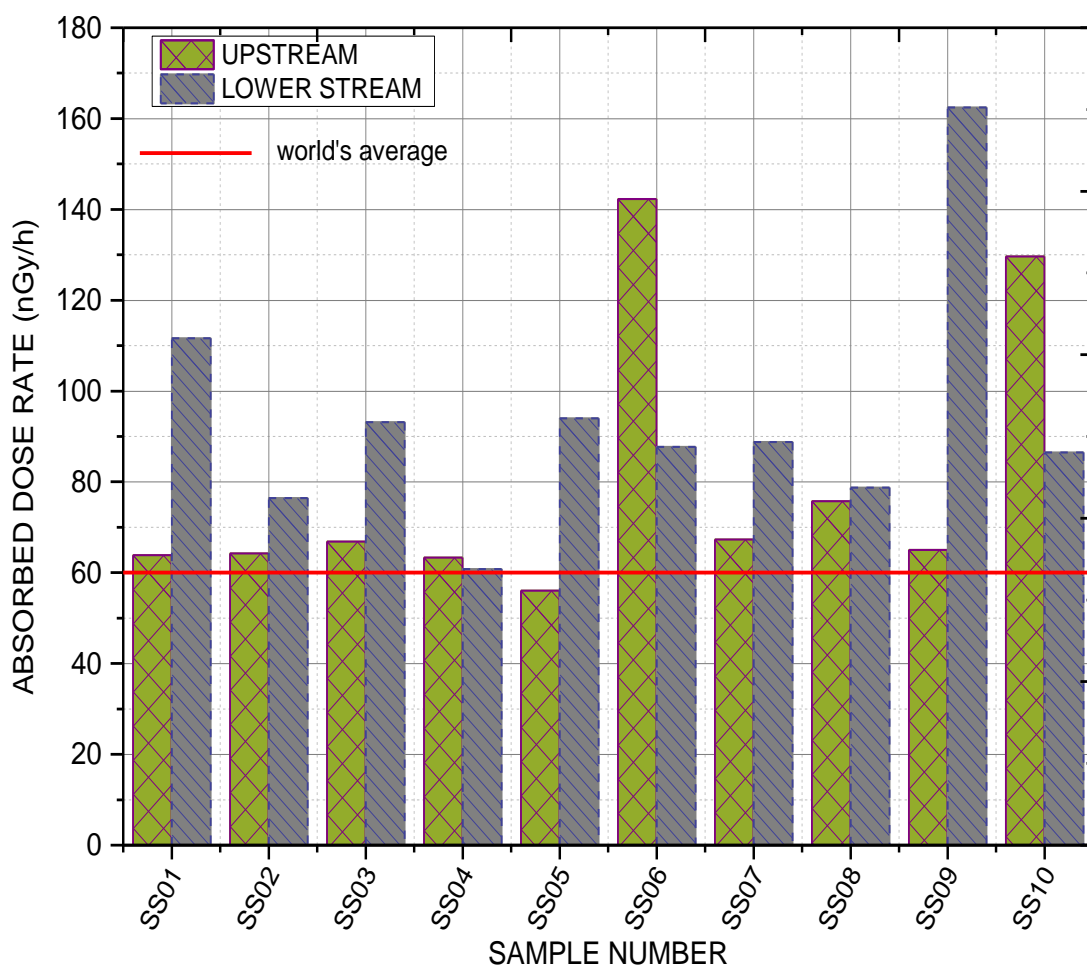
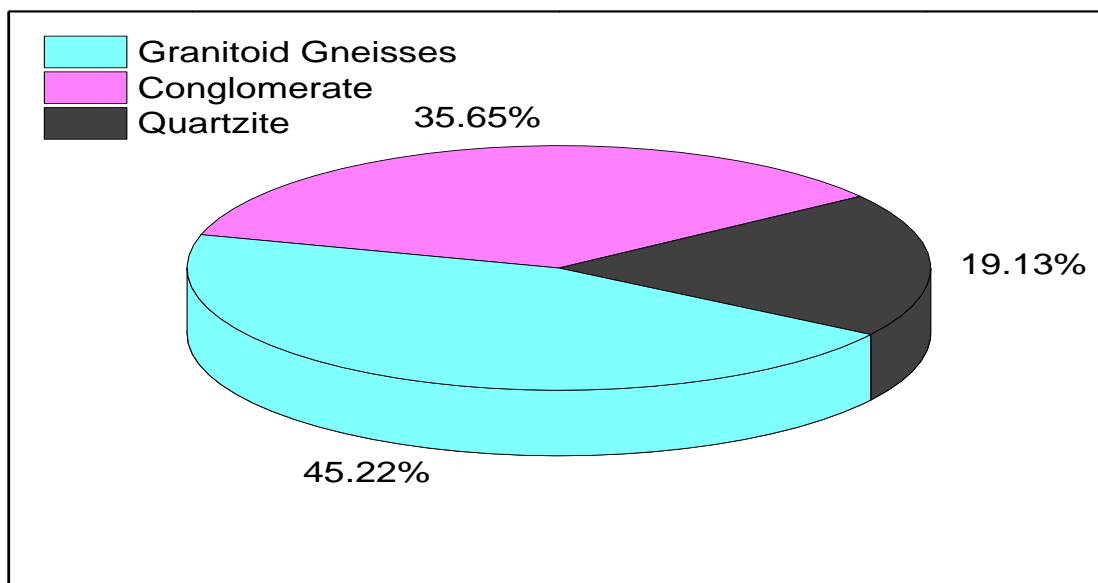


Figure 5.9: A comparative bar graph showing absorbed rate for sand samples collected lower and upper stream during the rainy season. The red strike shows the world's average level of absorbed dose rate.

The highest absorbed dose was reported from the sand sample 09 collected lower stream and the lowest dose was reported from the sand sample 05 collected upstream. Except for one sand sample i.e. SS05 collected upstream, the absorbed dose rate for the rest of the samples plotted was above the world's average. An average value of 60 ± 3.0 nGy/h



and 82 ± 4.1 nGy/h were reported from rocks sampled upper stream and lower stream during the rainy season, while rock samples analyzed for the two seasons reported an average of 75 ± 3.7 nGy/h which is above the world's mean reported in UNSCEAR reports (Appendix 2). The rocks had the least contribution to the absorbed dose compared to the sand. However, some rocks contributed significantly to radiation doses compared to others. The contributions of the absorbed dose from major rocks species found in the area were analyzed and expressed as a percentage as presented by Figure 10.

Figure 5.10: A pie chart showing an absorbed dose rate due to rock samples collected upper stream during the dry season.

Granitoid gneisses reported the highest contribution to the absorbed dose followed by the conglomerate. The average and the individual's absorbed dose rate for the rocks and sand samples collected for the two seasons are presented in the Appendix (2).

5.3.4 Annual Effective Dose Rate (AEDR)

To evaluate the radiological risks per individual exposure, modification factors suggested by UNSCEAR (2000) were used to convert absorbed dose rate to an annual

effective dose which is an adequate representation of the likely harm to the health of the population. Generally, the annual effective dose rate due to indoor exposure was greater than outdoor annual effective dose rates for all the samples analyzed in this work. Lower stream reported higher effective doses compared to analyses upper stream. The varying level of the annual effective dose for different samples was due to the corresponding variation in activity concentration for individual samples (Figure 5.11). The values for indoor AEDR from sand and rock samples collected during the rainy season are presented in Table 5.5

Table 5.5: Annual Effective Dose Rate in rock and sand samples collected during the rainy season

Sample number	Indoor Annual Effective Dose Rate (mSv/y)			
	Sand samples		Rocks samples	
	Upper stream	Lower stream	Upper stream	Lower stream
01	0.23±0.01	0.41±0.02	0.17±0.00	0.49±0.02
02	0.23±0.01	0.28±0.01	0.17±0.00	0.09±0.00
03	0.24±0.01	0.34±0.01	0.34±0.01	0.43±0.02
04	0.23±0.01	0.22±0.01	0.08±0.00	0.35±0.01
05	0.20±0.01	0.34±0.01	0.24±0.01	0.21±0.01
06	0.52±0.02	0.32±0.01	0.21±0.01	0.31±0.01
07	0.24±0.01	0.32±0.01	0.12±0.00	0.28±0.01
08	0.27±0.01	0.28±0.01	0.33±0.01	0.23±0.01
09	0.23±0.01	0.59±0.02	0.34±0.01	0.38±0.01
10	0.47±0.02	0.31±0.01	0.19±0.00	0.20±0.01
MIN	0.20±0.01	0.22±0.01	0.08±0.00	0.09±0.00
MAX	0.47±0.02	0.59±0.02	0.34±0.01	0.49±0.02
MEAN	0.29±0.01	0.34±0.01	0.22±0.01	0.30±0.01

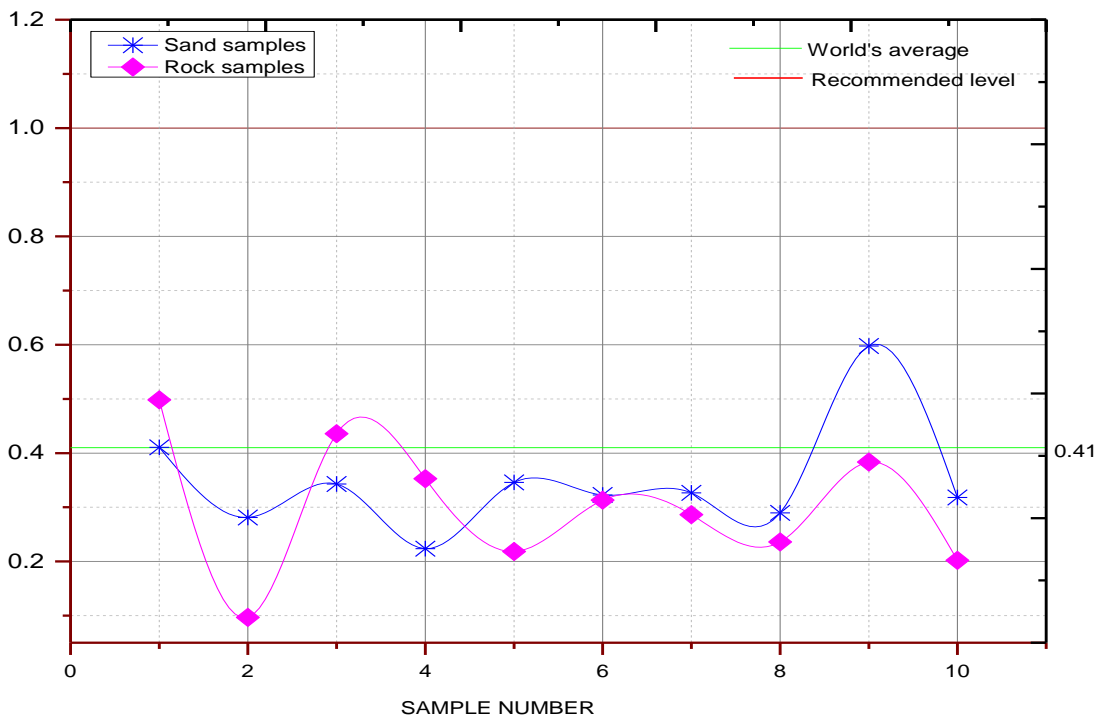


Figure 5.11: A comparative line graph showing indoor Annual effective dose rate for sand and rock samples collected lower stream during the rainy season.

The mean indoor AEDR for the two seasons was 0.31 ± 0.01 mSv y^{-1} and 0.27 ± 0.01 mSv y^{-1} for the sand and rock samples respectively, while the outdoor AEDR was 0.2 ± 0.01 and 0.18 ± 0 mSv y^{-1} for the sand and rock samples respectively. The average value for outdoor AEDR reported for two seasons was higher than the world's average of 0.07 mSv y^{-1} (UNSCEAR, 2008), while the mean level of indoor AEDR reported for the two seasons was below the global average of 0.41 mSv/y indoor AEDR. However, a few samples surpassed the world's average.

Based on values of annual effective dose rate from this study, use of the sand and rocks from this river for the construction of dwellings poses no radiological hazard due to indoor and outdoor radiation doses from radon, thoron and radioactive potassium species to the occupants of these dwellings. External gamma irradiation to human population interacting with sediments from this studied area can be termed insignificant. However, regular monitoring of the future trends is necessary as the river rejuvenation upstream may alter the river elemental composition in the context of radioactivity. The range and mean indoor AEDR for sand and rock samples collected during the dry season were computed and presented in Table (5.8). The mean values

for indoor annual effective dose rate in sand samples varied from (0.29 ± 0.01) to (0.34 ± 0.01) mSv/y for samples collected during the rainy season (Table 5.8) and outdoor AEDR in representative sand samples varied from (0.19 ± 0) to (0.23 ± 0.011) mSv/y (Appendix 3).

5.3.5 Radiation Hazard Indices

The potential harmful radiobiological effects due to interactions with high energy emissions from ^{238}U , ^{232}Th , and ^{40}K in the rocks and sand for both seasons were evaluated by calculating the three radiological parameters; radium equivalent, external and internal hazard indices. These parameters caters for the non-uniform distribution of ^{238}U , ^{232}Th , and ^{40}K in the geogenic sediments used as raw building materials.

Radium equivalent (R_{aeq}) was evaluated using equation 4.3 suggested by Beretka, (1985) and the results tabulated in the Table (5.10). The mean radium equivalent for the rock and sand samples upstream were higher during the dry season with a mean of 206 ± 10 and 181.4 ± 9 Bq/Kg respectively.

Sand samples collected during rainy season registered a mean radium equivalent of 161 ± 8.1 and 192 ± 9.6 Bq/Kg for upper and lower streams respectively (see appendix 4). The overall average radium equivalent for the entire survey was 175 ± 8.8 Bq/Kg and 152 ± 7.6 Bq/Kg for the sand and rock samples respectively.

Granitoid Gneiss collected from point $(0^\circ 56' 21.5)$ S; $(38^\circ 02' 34.8)$ E registered the highest radium equivalent of 277 ± 13 Bq/kg which is below 370 Bq/Kg the recommended world's limit for a material to have negligible hazardous effects when used as a construction material.

Table 5.6: Radium equivalent for rock and sand samples collected upper and lower stream during the rainy and dry seasons

Radium Equivalent upstream (Bq/Kg)					
Sand samples			Rock samples		
Sample ID	Rainy season	Dry season	Sample ID	Rainy season	Dry season
SS02	129±6	133±6	RS02	93±5	208±10
SS04	124±6	126±6			
SS06	303±15	219±10	RS06	118±6	92±5
SS08	155±8	144±7			
SS10	277±13	190±10	RS10	102±5	160±8
MEAN	197±10	162±8	MEAN	104±5	153±8
Radium equivalent lower stream (Bq/Kg)					
SS02	151±8	212±10	RS02	55±3	273±13
SS04	120±6	179±9			
SS06	175±9	185±9	RS06	170±8	218±10
SS08	156±7	196±10			
SS10	172±9	135±7	RS10	112±6	127±6
MEAN	154±8	181±9		112±6	206±10

External hazard indices in sand and rock samples collected during the rainy season were computed using equation 4.8 (Krieger, 1981). Sand samples reported higher external hazard indices compared to rocks during the rainy season (Fig.5.12). The overall mean H_{ex} in sand and rocks analyzed was 0.47 ± 0.02 and 0.41 ± 0.02 respectively, both below the admissible level set by ICRP reports.

A bar graph representing the external hazard indices for some rocks and sand samples collected during the rain season is shown by the Figure (5.12)

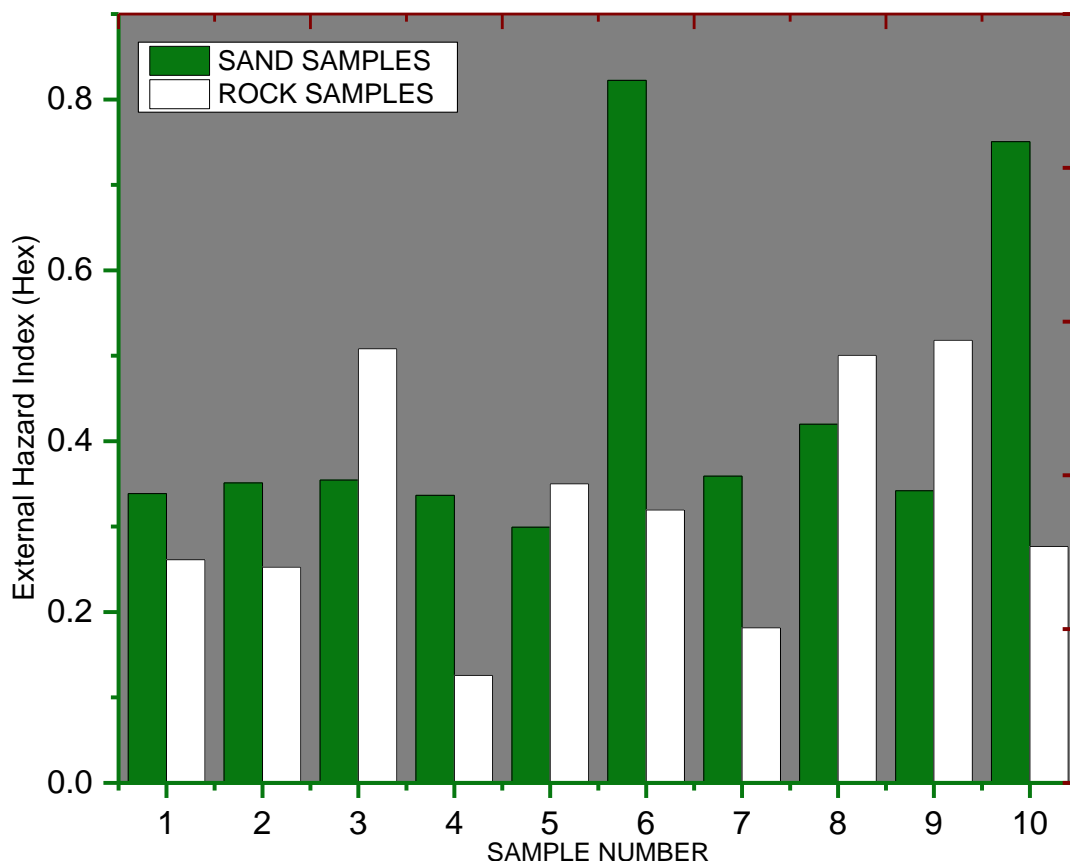


Figure 5.12: A bar graph showing external hazard indices the sand and rock samples collected upper stream during the rainy season.

Figure (5.12) shows that the external hazard indices for the rocks and sand samples were different. The indices level for the plotted samples were below the recommended limit of a unit and based on this radiological parameter, use of sand and rocks from this river for construction purposes poses no health hazard due to external gamma irradiation to those interacting with the latter.

Sand samples 06 and 10 show high indices over the other samples which were inferred to the corresponding high ^{226}Ra concentration reported by the two samples. High ^{226}Ra in the two samples collected upstream could probably be due to the traces of uranium-rich ore present in sampled sediments. High levels of radium in particular samples can

also be associated with high silt and organic matter contents in the samples (Valkovic, 2000).

The evaluation of internal radiation hazard indices in sand and rock samples during the rainy season was done using equation 4.9 (Matthew, 1985). The similar analyses were repeated during the dry season using samples collected from the same points with the help of GPS. This research reports an overall internal hazard index of 0.56 ± 0.02 and 0.47 ± 0.02 for the sand and rock samples respectively analyzed for the two seasons. The mean level for internal hazard index for the sand and rock samples were below the safety level of the unit although 3 sand samples collected during rainy season exceeded this limit (Appendix 4).

Based on the sample's individual hazard indices, the use of sand and rocks from this river for construction purposes may pose a health hazard to the immediate population. However, the mean index for all samples studied was below the set limits of 1 (ICRP, 2000). The scatter plot shown by Figure 5.13 shows internal hazard indices of rock and sand samples collected during the rainy season (Appendix 4)

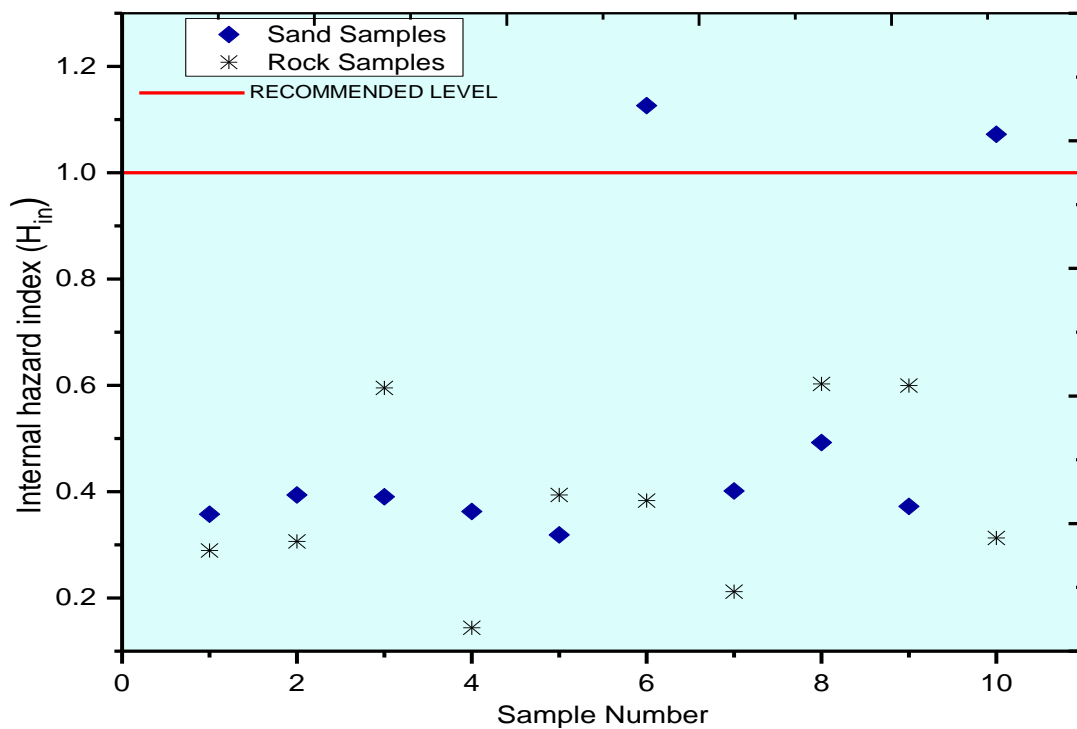


Figure 5.13: Scatter plot showing internal hazard indices for the rock and sand samples collected upper stream during the rainy season. The red line shows the level beyond which the material is termed to pose a significant radiation hazard.

5.4 Seasonal Effect on Natural Radiation Level of ^{238}U , ^{232}Th , and ^{40}K

The possible fluctuation in trends of levels of radionuclides with the season was evaluated by comparing the activity concentration, dose rates, and radiation hazard indices using data from samples collected during the consecutive rainy and dry seasons. The statistical parameters for various dosimetric quantities reported during the two seasons are explained in details below.

5.4.1 Activity Concentration of ^{238}U , ^{232}Th , and ^{40}K in Sand for the Two Seasons

Potassium (^{40}K) revealed high activity concentration for both seasons compared to uranium and thorium species which was inferred to the formation of Si_2O which favours the lithological concentration of potassium element and not thorium and uranium species. Generally, most samples reported higher activities of ^{226}Ra , ^{232}Th , and ^{40}K during the dry season. This shows variation in water contents in the rocks and sand due to change in the season affected the levels of radionuclides since other factors which might have affected the levels of radionuclides for this research were maintained constant.

The solubility of radioactive elements like potassium and uranium facilitates their lateral and horizontal migration within the soil profile. The migration pattern depends on hydrology and porosity of soils and rocks as this facilitates leaching, chemical and biochemical interactions (Karakelle, 2002). The deposition and re-distribution of sand after the samples for the rainy season had been collected might have led to new minerals along the sampled cross-section.

High organic contents in the sand during dry season might also be a reason for the upward trend noted as the season changed. Research shows that crustal contents with high organic composition have elevated levels of primordial radionuclides particularly ^{238}U (Valkovic, 2000). Trapping of silt and other minerals in the grains of the rock could be a reason for the rise in radioactivity levels during a repeat study as silt is associated

with high levels of terrestrial radionuclides particularly ^{226}Ra , ^{232}Th , and ^{40}K (Baeza, Rio and Paniagua, 1995).

The bar graph showing ^{226}Ra concentration in sand samples collected during rainy and dry seasons is shown in Figure 5.14. ^{226}Ra concentration was higher for most samples collected during the dry season.

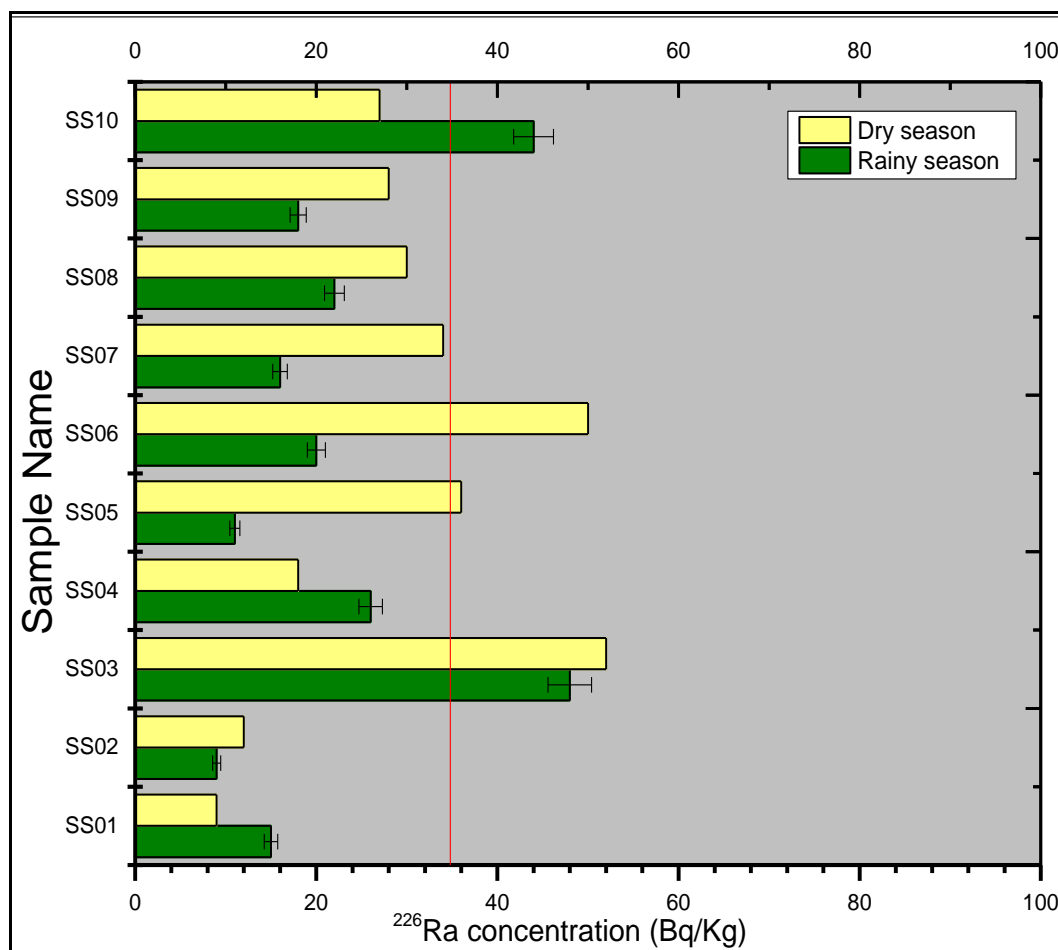


Figure 5.14: A bar graph showing the concentration of ^{226}Ra in sand samples collected during the rainy and dry seasons.

5.4.2 Absorbed Dose Rate

The absorbed dose rate evaluated from the activity concentration of ^{238}U , ^{232}Th , and ^{40}K was higher for most samples collected during the dry season. The higher absorbed dose rate reported during the dry season was due to the corresponding higher activities reported during the dry season which was attributed to the change of geological

composition, silt and organic contents of sand samples due to new deposits from the upper riverine.

Table 5.7: Absorbed dose rate in rocks and sand sampled from lower riverine during the rainy and dry season

Sample number	Absorbed Dose rate (nGy/h)			
	Sand lower stream		Rocks lower stream	
	Rainy season	Dry season	Rainy season	Dry season
02	76±3.8	103±5.2	26±1.3	136±6.8
04	60±3.0	87±4.4		
06	87±4.4	90±4.5	59±3.0	108±5.4
08	78±3.9	98±4.9		
10	86±4.3	66±3.3	54±2.7	63±3.2
MIN	60±3.0	66±3.3	26±1.3	63±3.2
MAX	87±4.3	103±5.2	59±2.9	108±5.4
MEAN	77±3.8	88±4.4	46±2.3	102±5.1

Figure 5.15 shows the seasonal comparison of absorbed dose rate for sand collected lower stream for both seasons. Four out of five sand samples collected during dry season presented a higher dose than corresponding samples collected during the rainy season. This was attributed to the fact that the sand remained undisturbed during the dry season and radionuclides in the river sediments attained secular equilibrium unlike during the rainy season when the water in the river is flowing.

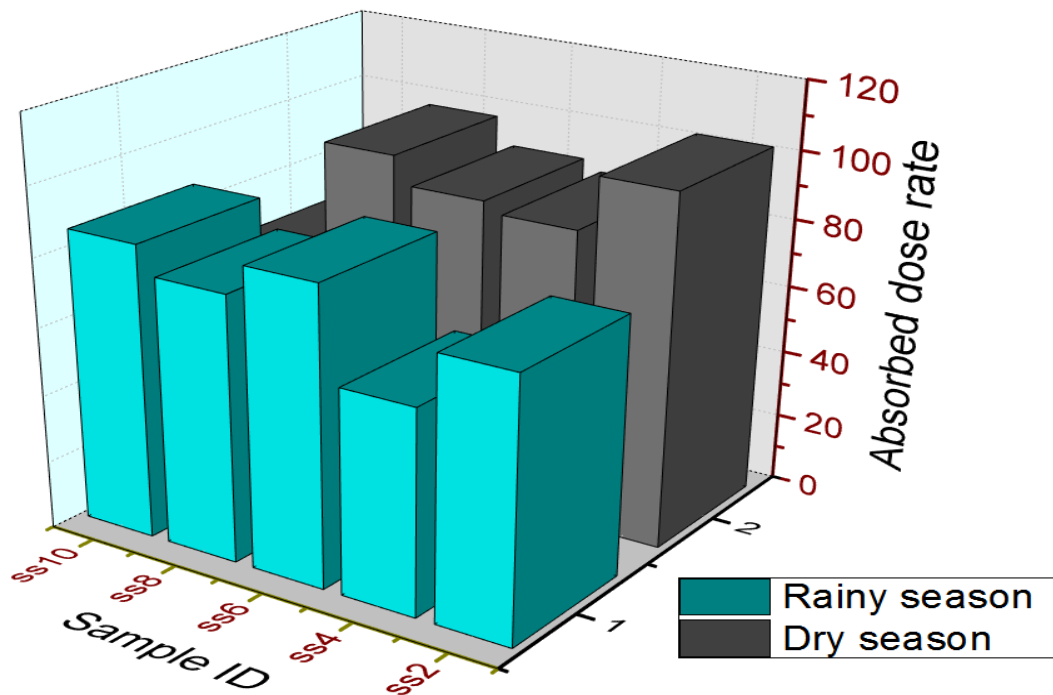


Figure 15: Evaluation of the seasonal effect on absorbed dose rate in sand samples collected lower stream during the rainy and dry season

5.4.3 Radiological Hazard Indices

The average radium equivalent, internal hazard indices and external hazard indices for sand and rock samples collected lower stream during the dry season were generally higher than for samples collected during the rainy season from the same points

Radium equivalent generally ranged from 120 ± 6.0 to 175 ± 8.8 Bq/Kg in sand samples collected lower stream during the rainy season and 135 ± 6.8 to 212 ± 10 Bq/Kg for samples collected during the dry season. The range of radium equivalent reported by the rock samples was 55 ± 2.8 to 170 ± 8.5 Bq/Kg and 127 ± 6.4 to 273 ± 13 Bq/Kg for the rainy and dry seasons respectively.

The seasonal change revealed a significant rise in radium equivalent during the dry season which was attributed to changes in some physical and chemical factors of the samples. For both seasons, the radium equivalent was below the safety level of 370 Bq/Kg.

The graphical representation of radium equivalent for some sand samples for the two consecutive seasons is shown by Figure 5.16

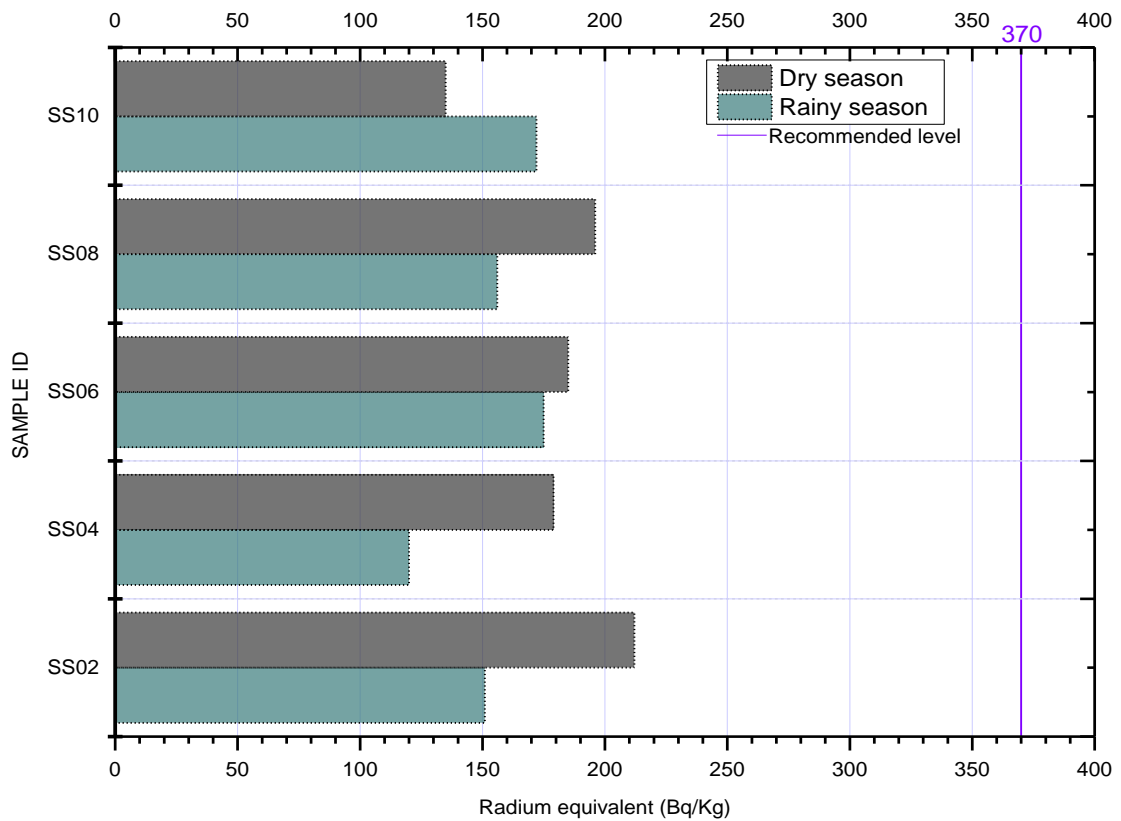


Figure 5.16: Comparison of Radium Equivalent for Sand sampled lower stream

The findings from this radiogenic survey show the significant fluctuation in levels of natural radioactivity with the seasonal change. The radium equivalent was slightly higher for all rock and sand samples collected during the dry season. The mean radium equivalent for the samples collected lower stream is higher than for samples collected upstream. The mean radium equivalent varied from (166 ± 8.3) to (206 ± 10) Bq/Kg and (121 ± 8.1) to (162 ± 8.1) Bq/Kg for lower and upstream respectively. The mean internal hazard index for the rainy and dry season was 0.35 ± 0.02 and 0.52 ± 0.03 respectively for rock samples. Sand samples reported a mean index of 0.42 ± 0.02 and 0.49 ± 0.02 for rainy and dry season respectively.

The values for all the radiological hazard parameters for sand and rock samples done for two seasons are presented in Table 5.16

Table 5.8: Mean values for radiological parameters for sand and rock samples subjected to analysis for the two seasons.

Mean radiological hazard indices for samples collected lower stream				
	Sand		Rock	
	Rainy Season	Dry season	Rainy Season	Dry season
$R_{a_{eq}}(\text{Bq/Kg})$	154±7.7	181±9.05	112±5.6	206±10
H_{in}	0.47±0.02	0.58±0.03	0.35±0.02	0.52±0.03
H_{ex}	0.42±0.02	0.49±0.02	0.3±0.02	0.55±0.03

5.5 Statistical Evaluation

5.5.1 Descriptive Statistics for Activity Concentration of ^{238}U , ^{232}Th , and ^{40}K in Sand and Rocks Sampled

The data on specific activity concentration of ^{238}U , ^{232}Th , and ^{40}K in rocks and sand samples were organized and summarized further for easy and quick statistical comparison and understanding.

Measures of central tendency and dispersion were calculated and presented in Table 5.9. The values for the range and mean activity concentration obtained for this work were compared with findings similar radiometric surveys done by other scholars in Kitui County, other regions of Kenya and in other parts of the world and the data tabulated in Table 5.10.

The mean values for dose rates and radiological indices were within the reported ranges and the use of construction materials from this river has no significant radiological implication on health as the findings are within the allowed limit by the relevant bodies.

Table 5.9: Descriptive statistics for activity concentration in sand and rock samples used for this work

Variable	Sample					
	Sand			Rocks		
	²²⁶ Ra	²³² Th	²³⁸ U	²²⁶ Ra	²³² Th	²³⁸ U
Minimum	7	30	287	6	14	94
Maximum	118	134	1068	42	119	1389
Median	25	53	836	20	39	899
Mean	33	55	812	21	49	782
Standard deviation	29	21	163	7	28	351
Sum	1015	1667	24389	567	1288	20350

5.5.2 Correlational Analysis

Sand is a product of rock mass after it has been subjected to biological, mechanical or chemical agents of weathering, there was a need to test whether the trends of mineralogy in sand and rocks had any relationship more so their extent in radioactivity level. Radium equivalent was used to evaluate this relationship. Figure 17 shows the scatter plot showing the association between the radium equivalent in the sand and the rocks.

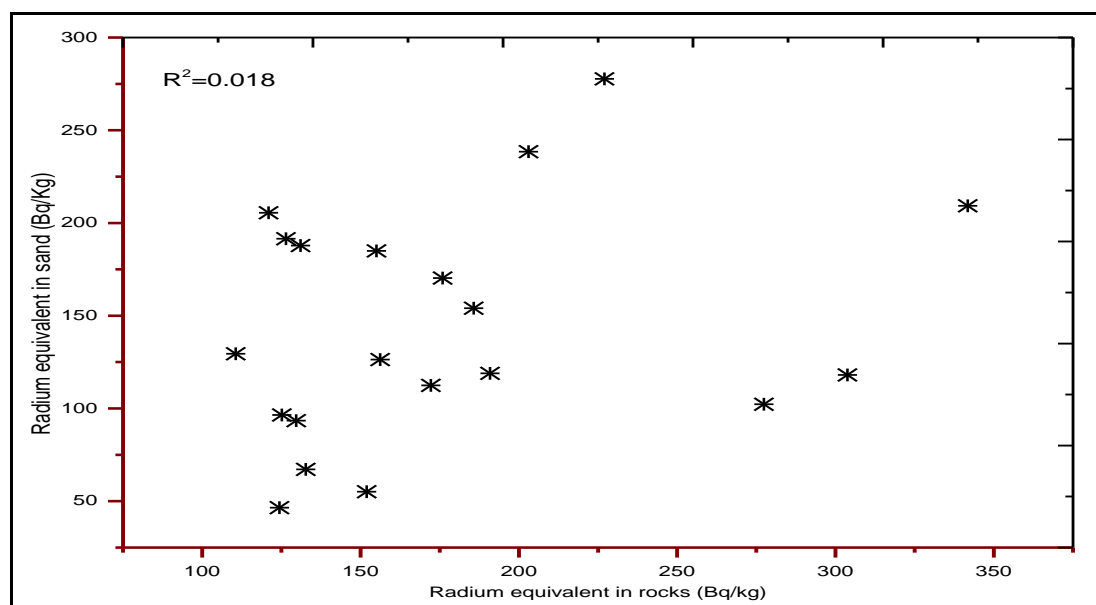


Figure 17: A scatter plot showing a correlation between radium equivalent of sand and rocks sampled from the basement of Tyaa River.

The R² (R- squared) value show a small positive non-linear trend between the radium equivalent in sand and rocks. However, the degree of co-relationship is insignificant and was attributed to differences in the mineral composition of their parent rocks.

Most lithological surveys show that rocks of similar origin have relatively same minerals trends. Correlational analysis for the rocks and sand samples analyzed in this work suggests that they might have different geological origins and thus differences in concentrations of similar mineral accessories.

5.5.3 Comparison of the Findings of the Current Study with Data from Similar Studies

The findings of this research have been compared with results from similar radiometric surveys done in different parts of Kenya and other countries. The cumulative mean concentration of ²³⁸U (²²⁶Ra), ²³²Th, and ⁴⁰K was 33±1.7 Bq/Kg, 55±2.8 Bq/Kg and 812±40 Bq/Kg respectively which was higher than the national average of 28.7 Bq/Kg, 73.3 Bq/Kg and 255.7 Bq/Kg (Mustapha *et al.* ,1999).

The mean activity concentration of ⁴⁰K was over 3 times the national average of 255.7 Bq/Kg and twice the world's mean of 400 Bq/Kg. This was attributed to the abundance of minerals like potash feldspar in sand and rock samples (Abdel-Monem *et al.*, 1996). The mean activity concentration for this work and for other similar radiometric surveys are summarized in Table 5.10 and Table 5.11.

Table 5.10: Comparison of mean activity concentration of ²²⁶Ra, ²³²Th, and ⁴⁰K in sand reported by this work and other similar studies

Region	Activity concentration in Sand (Bq/Kg)			Reference
	²²⁶ Ra	²³² Th	⁴⁰ K	
Kenya	33	55	812	This work (Tyaa river)
Kenya	8.8	199	329	Koech (2017) (Tiva river)
Kenya	39	68	973	Ochieng' (2016) (Mwingi)
Kenya	207	500	805	Kebwaro (2010)(Mrima hill)
Saudi Arabia	29	158	139	Kinsara (2014)

Table 5.11: Comparison of mean activity concentration of ^{226}Ra , ^{232}Th , and ^{40}K in rocks reported by this work and other similar studies

Region	Activity concentration in rocks (Bq/Kg)			Reference
	^{226}Ra	^{232}Th	^{40}K	
Kenya	21	49	782	This work (Tyaa river)
Kenya	94	64	1004	Agora <i>et al.</i> , 2012
Egypt	51	46	1213	Shaban <i>et al.</i> , 2011
Nigeria	69	63	487	Joshua <i>et al.</i> , 2009
Kenya (National average)	28	73	255	Mustapha <i>et al.</i> , 1999
World's average	35	30	400	UNSCEAR 2000

CHAPTER SIX

CONCLUSIONS AND RECOMMENDATIONS

6.1 Conclusions

Measurements of natural radioactivity levels in sand and rock samples from Tyaa river of Mwingi, Kitui County has been done using a lead shielded high-resolution gamma-ray spectrometer. The research has further determined the seasonal effect on levels of natural radioactivity of rock and sand in Tyaa River using samples collected during the dry and rainy season. Correlational analysis between the radioactivity levels of rocks and that of sand samples from the same river has been also done.

The overall mean activity of the sand for the entire study (two seasons) was $33.84 \pm 1.55 \pm 2.8$ BqKg⁻¹ and 812 ± 40.46 BqKg⁻¹ for ²²⁶Ra, ²³²Th, and ⁴⁰K respectively, while similar analysis of rock samples reports average activity concentration of 21 ± 2.47 BqKg⁻¹, 49 ± 2.47 BqKg⁻¹ and 782 ± 39.13 BqKg⁻¹ for ²²⁶Ra, ²³²Th and ⁴⁰K respectively. The mean activity concentration for the sand sample from this river was higher than the reported world's average of 33 Bq/kg, 45 Bq/kg and 400 Bq/kg for ²³⁸U, ²³²Th, and ⁴⁰K respectively (UNSCEAR, 2008). Except for the mean of sand samples upstream during the rainy season the average concentration of ⁴⁰K upper stream was twice the reported global mean of 400 Bq/kg (UNSCEAR, 2008). High potassium contents were inferred to the presence of silica in the sand since potassium is trapped in silicate bond during cooling and solidification of igneous rocks.

The radium equivalent for rock samples collected lower stream during the dry season was higher than for samples collected during rainy season with a mean of 206 ± 10.3 Bq/kg and 112 ± 5.61 Bq/kg respectively (Table 5.16) while for the sand samples the mean radium equivalent was 154 ± 7.74 Bq/kg and 181 ± 9.05 Bq/kg for dry and rainy seasons respectively. Based on this parameter, sand and rocks (building materials) from this river is safe to both the mining and consuming population.

Samples collected from Kyanika location (lower stream) registered higher absorbed dose rate relative to those sampled from Kavuwani location (upper stream). The mean

absorbed dose varied from (60 ± 3.04) nGy/h for rock samples collected upstream to (102 ± 5.13) nGy/h for rocks samples collected lower stream and (79 ± 3.97) nGy/h to (94 ± 4.7) nGy/h for sand collected upstream and lower stream respectively (Appendix 2). The absorbed dose rate was generally higher than the world average of 60 nGy/h.

Calculations on mean AEDR based on the indoor and outdoor occupancy conversion factors of 0.6 and 0.4 (Mustapha, 1997) reported a mean annual indoor dose varying from (0.27 ± 0.01) mSv/y to (0.79 ± 0.03) mSv/y with a mean of 0.46 ± 0.02 mSv/y in sand and 0.1 ± 0 mSv/y to 0.66 ± 0.03 mSv/y with a mean of 0.5 ± 0.02 mSv/y in rock samples collected during dry season lower stream. The reported mean indoor AEDR is higher than the world's average annual effective dose equivalent from indoor terrestrial gamma radiation of 0.460 mSv/y (UNSCEAR, 2000). The mean outdoor AEDR ranged from 0.06 ± 0 mSv/y to 0.19 ± 0 mSv/y for sand samples and 0.02 ± 0 mSv/y to 0.07 ± 0.003 mSv/y for rock samples which is within the world's average of 0.07 mSv/y. For all the geological samples subjected for spectrometric analysis, none exceeded the recommended dose constraint of 1mSv/y as set by ICRP, 2000.

The external hazard indices for all the sand and rock samples were below the recommended level of a unit. Internal hazard indices for 27 out of 30 samples which translate to 90% of the total sand samples analyzed were below a unit. However, three sand samples surpassed this level. Based on mean radiological indices, use of sand and rocks from this river for construction purposes poses no significant radiological hazard to occupants of the latter dwellings (ICRP, 2000)

Generally, the dry season reported higher mean radiological hazard indices (radium equivalent, internal and external hazard indices) and radiation doses (absorbed dose and annual effective dose rate) because during dry season the sand remained undisturbed for quite some time and had attained secular equilibrium (Appendix 1, 2, 3 and 4).

The correlational analysis of the radioactivity levels in rock and sand reveal a weak non-linear trend suggesting differences in mineralogy contents thus the sand and rock samples are from different bedrocks.

6.2 Recommendations

Based on the research findings, the use of sand and rocks from Tyaa River for construction purposes, along the studied length poses no significant radiological risks to users of such houses.

However, more radiometric studies are needed to ascertain the levels of natural radioactivity since with time the current trends in radioactivity may change due to intruding contaminants from bed rock. Studies on radon levels in water are necessary as the local residents' use water from this river for various domestic uses; drinking and watering domestic animals respectively (Appendix 6 and 7). Further evaluation of indoor radon indices and associated exposures in dwellings build with materials (rocks and sand) from this river are necessary as radon accumulates faster in enclosed dwellings.

Thoron gas accumulates faster in structures whose ventilation is compromised more so if the material used to erect the structure are drawn from background with elevated levels of radio nuclides.

Similar studies need to be repeated for several seasons to obtain consistent results on the seasonal effects on levels of radioactivity of this river. There is a need to stretch sampled length beyond 2 km for proper statistical representation of the area. Carrying out elemental analysis of heavy elements in rocks, sand, and soils from this area and more so lower stream which reported higher radioactivity levels for sand and rocks samples compared to upstream is highly recommended.

REFERENCES

- Ajithra, A., and Shanthi, G. (2016). Assessment of Beach sand using Gamma Ray Spectrometer in Thiruvananthapuram District, Kerala of South India. *IRA-International Journal of Technology & Engineering* (ISSN 2455-4480), 5(3), 56-69.
- Al-Zahrani, J. H. (2017). Estimation of natural radioactivity in local and imported polished granite used as building materials in Saudi Arabia. *Journal of radiation research and applied sciences*, 10(3), 241-245.
- A.O. Mustapha, J.P. Patel, I.V.S. Rathore (1999). Assessment of Human Exposures to Natural Sources of Radiation in Kenya, *Radiation Protection Dosimetry*, Volume 82, Issue 4, Pages 285–292,
- Abbadly, A., El-Arabi, A. M., Abbadly, A. G. E., and Taha, S. (2008). Gamma-ray measurements of natural radioactivity in cultivated and reclaimed soil, Upper Egypt. *International Conference on Radioecology and Environmental Radioactivity 15-20 Norway*.
- Abdel-Monem, A. A., Hussein, H. A., Abdel Kader, Z. M., Abu, Z. H. and Ammar, S. E. (1996). Radioactivity and distribution of U and Th in some granitic masses, Wadi El-Saqia area, central eastern desert, Egypt. *Journal of Radiation Physics and Chemistry*, 45(5): 775-778.
- Abd El-mageed, A.I. (2011). Assessment of natural and anthropogenic radioactivity levels in rocks and soils in the environments of Juban town in Yemen. *Radiat. Phys. Chem.* 80 (6), 710–715.
- Abhishek & Singh, Divya and Dubey, Kavita & Maurya, Renuka & Pandey, Alok. (2017). Chromosomal Aberrations. 10.1016/B978-0-12-809252-1.00004-3.
- Achola, S., Patel, J., Mustapha, A., and Angeyo, H. (2012). Natural radioactivity and external dose in the high background radiation area of Lambwe East, Southwestern Kenya. *Radiation Protection Dosimetry*, 152(4), 423-428.
- Achola S. O. (2009). Radioactivity and elemental analysis of carbonatite rocks from parts of Gwasi area, South Western Kenya. *M.Sc Thesis (Physics)* University of Nairobi, Kenya.

- Adel G. E. A and E-Taler, M. A. M. (2005). Natural Radioactivity and dose assessment for phosphate rocks from Wadi EL-Mashash and El-Mahamid mines in Egypt. *Journal of Radiation and Isotopes*. 84: 65-78.
- Agora J. O. (2012). Assessment of Natural Radioactivity Levels and Radiation risk due to the Different Rock-type in the Kerio Valley Region of Kenya. *M.sc Thesis (Physics)*. Kenyatta University, Kenya.
- Akiba, S., Jayalekshmi, P., Nair, R. K., Rajan, B., Nair, M. K., Gangadharan, P., and Sugahara, T. (2009). Background radiation and cancer incidence in Kerala, India—Karanagappally cohort study. *Health Physics*, 96(1), 55-66.
- Atambo V. O. (2011). Determination of naturally occurring radioactive elements and radiation exposure levels in the soapstone quarries of Tabaka region of Kisii district, Kenya. *M.Sc Thesis (physics)*. Jomo Kenyatta University of Agriculture and Technology, Kenya.
- Baeza, A., Del Río, M., Jiménez, A., Miró, C., Paniagua. J., (1995). Influence of geology and soil particle size on the surface-area/volume activity ratio for natural radionuclides. *Journal of Radio analytical and Nuclear Chemistry*. 189, 289-299.
- Bavarnegin E., Moghaddam M.V., and Fathabadi, N (2013). Natural radionuclide and radiological assessment of building materials in high background areas of Ramsar, Iran. *Journal of Med Physics*.2013;38(2):93-97. Doi: 10.4103/0971-6203.111325
- Bavarnegin, E., Fathabadi, N., Moghaddam, M. V., Farahani, M. V., Moradi, M., and Babakhni, A. (2013). Radon exhalation rate and natural radionuclide content in building materials of high background areas of Ramsar, Iran. *Journal of environmental radioactivity*, 117, 36-40.
- Bastos, R. O., & Appoloni, C. R. (2009). Radioactivity of rocks from the geological formations belonging to the Tibagi River hydrographic Basin.
- Bendibbie M. M., David M. M. and Jayanti P. P.(2013) Radiological analysis for suitability of Kitui south limestone for use as a building material. *International Journal of Fundamental Physical Sciences*, 3:32-35.

- Benke, R. R., and Kearfott, K. J., (1999). Soil Sample Moisture Content as a Function of Time during Oven Drying For Gamma-Ray Spectroscopic Measurements. *Nuclear Instruments and Methods in Physics Research Section A, Accelerators, Spectrometers, Detectors, and Associated Equipment*, 422(1-3), 817-819.
- Beretka, J., and Matthew, P. (1985). Natural radioactivity of Australian building materials, industrial wastes, and by-products. *Health Physics*, 48(1), 87.
- Bharatwal, D.S. and G.H. Vaze., (1959). Radiation dose measurements in the monazite areas of Kerala state in India, Volume 23. Proceedings of the Second International Conference on the Peaceful Uses of Atomic Energy. United Nations, New York,
- Debertin K., and Herlmer R. G. (1988). *Gamma and X-Ray Spectrometry with Semiconductor Detectors*. North Holland, Amsterdam.
- Desouky O. and Nan Din (2015). Targeted and non-targeted effects of ionizing radiation. *Journal of radiation research and applied sciences-pp3*
- Dodson, R. G (1953). A Geology of South-East Machakos area. *Geol. Surv. Kenya. Report No. 25: pp.3*
- Debertin K. and Herlmer R. G. (1988). *Gamma and X-Ray Spectrometry with Semiconductor Detectors*. North Holland, Amsterdam.
- Eappen, K. P., Chougankar, M. P., Ramachandran, T. V., Shetty, P. G., Mayya, Y. S., Sadasivan, S., & Raj, V. V. (2004). Profiles of doses to the population living in the high background radiation areas in Kerala, India. *Journal of Environmental Radioactivity*, 71(3), 275-297.
- Ebaid YY (2010) Use of gamma-ray spectrometry for uranium isotopic analysis of environmental samples. *Rom J Phys* 55(1-2):69-74
- Furusawa, Y., Nagai, S., Hirano, A., Ippommatsu, M., Aosaki, K., Yamada, K., & Akasaki, I. (2014). Development of under filling and encapsulation for deep-ultraviolet LEDs. *Applied Physics Express*, 8(1), 012101.
- Ghiassi-Nejad, M. (2002) very high background radiation areas of Ramsar, Iran: preliminary biological studies
- Gilmore, G. (2008). *Practical gamma-ray spectroscopy*. John Wiley & Sons.

- Gilmore, G. (2011). *Practical gamma-ray spectroscopy*. 2nd ed., England, John Wiley & Sons.
- Gruppen C. (1996). Particle detectors, *Cambridge University Press*. pp 30-35.
- Hall, E. J., and Giaccia, A. J. (2011). *Radiobiology for the radiologist* (7th ed.). Philadelphia: Lippincott Williams & Wilkins.
- Halliday, D. and Krane, K. S. (1987). *Introductory nuclear physics*.
- Halime Kayakökü, Şule Karatepe, Mahmut Doğru (2016). "Measurements of radioactivity and dose assessments in some building materials in Bitlis, Turkey", *Applied Radiation and Isotopes*.
- Harenyama, M., N. Tsuchiya, M. Takeba and T. Chida, 2006. Two-dimensional measurement of radioactivity of Granite rocks by Photostimulated Luminescence Technique. *Geochem.J* 34: 1-9
- Hossain, I., Sharip, N., and Viswanathan, K. K. (2012). Efficiency and resolution of HPGe and NaI (Tl) detectors using gamma-ray spectroscopy. *Scientific Research and Essays*, 7(1), 86-89.
- IAEA. (2005). *Radiation Oncology Physics textbook. A Handbook for teachers and students*. IAEA. Vienna Austria.
- International Atomic Energy Agency (IAEA) (1987) Preparation and certification of IAEA gamma spectrometry reference materials, RGU-1, RGTh-1, and RGK1. Report-IAEA/RL/148. International Atomic Energy Agency, Vienna: *International Journal of the Physical Sciences* Vol. 6(13), pp. 3105–3110, 4 July 2011.
- IAEA Yearbook (1996). Vienna: International Atomic Energy Agency.
- IAEA. (2005). *Radiation Oncology Physics text book. A Handbook for teachers and students*. IAEA. Vienna Austria.
- International Nuclear Atlantic Conference - INAC 2009 Rio de Janeiro, RJ, Brazil, September 27 to October 2, 2009.
- International Commission on Radiological Protection (ICRP), (2007). *Radiation protection dosimetry*. ICRP 2007 recommendations. Oxford: Pentagon press.

International Commission on Radiological Protection (ICRP), (2005). Low-dose Extrapolation of Radiation-related cancer risks. ICRP 2005. Oxford: Pentagon press.

International Commission on Radiation Protection (ICRP), (2000). Protection of the public in situations of prolonged radiation exposure ICRP Publication 82; Ann. ICRP 29 (1–2), Pergamon Press, Oxford.

International Commission on Radiation Protection ICRP, (1992). Principles for Intervention for Protection of the Public in a Radiological Emergency. ICRP Publication 63. Ann. ICRP 22 (4).

ICRP (1991). Annual limits on the intake of radionuclides by workers based on 1990 recommendations. International Commission of Radiological Protection, 66: Annals of the ICRP 21 (4).

Jaikrishan, G., Andrews, V. J., Thampi, M. V., Koya, P. K. M., Rajan, V. K., and Chauhan, P. S. (1999). Genetic monitoring of the human population from high-level natural radiation areas of Kerala on the southwest coast of India. I. Prevalence of congenital malformations in newborns. *Radiation Research*, 152(6s), S149-S153.

Jain, A. K., Singh, D., Dubey, K., Maurya, R., and Pandey, A. K. (2017). Chromosomal Aberrations. In *Mutagenicity: Assays and Applications* (pp. 69-92). Academic Press.

James E. P. (2014). Compton Scattering and Gamma-Ray Spectrometry. *Department of Physics and Astronomy*. The University of Tennessee.

Joshua, E. O., Ademola, J. A., Apanowo, M. A. and Oloronde, D. O. (2009). Natural Radionuclides and hazard of rock samples collected from South Eastern Nigeria. *Journal of Radiation Measurement*. 44: 401-404.

Karakelle, B., Ozturk, N., Kose, A., Varinlioglu, A., Erkol, A. Y and Yilmaz, F (2002). Natural radioactivity in soil samples of Kocaeli basin, Turkey. *J. Radioanal. Nucl. Chem.* 254. 649-651.

Kebwaro, M. J. (2011). Gamma-ray spectrometry analysis of the surface soil around Mrima hill, Kenya Using NaI (TI) detector and decomposition technique. *M.Sc. thesis at Kenyatta University, Kenya*.

- Kinsara A. A., Shabana E.I. and Qutub M.M.T. (2014). Natural Radioactivity in Some Building Materials Originating from a High Background Radiation Area. *International Journal for Innovation Education and Research*, 2 (6): 70-78.
- Kinyua R., Atambo V. O. and Ongeri R. M. (2011). Activity concentrations of ^{40}K , ^{232}Th and ^{228}Ra and radiation exposure of Tabaka soapstone quarries of the Kisii region, Kenya. *African Journal of Environmental Science and Technology*, 5:682-688.
- Knipp J.K., G.E. Uhlenbeck. (1936) Emission of gamma radiation during the beta decay of nuclei, *Physica*, Volume 3, Issue 6, Pages 425-439,
- Knoll G.F. (1999). *Radiation Detection and Measurement* (Third edition) John Wiley & Sons, inc. New York USA, (Chapter 18-19).
- Knoll G.F. (2010). *Radiation Detection and Measurement* (Fourth edition) John Wiley & Sons, inc. New York USA, (Chapter 18-19).
- Koech Nehemiah Kipkirui (2017). Analysis of heavy metals, minerals and radionuclides in heavy sands from Tiva and Mwitwa Syano rivers, Kitui County. *M.Sc Thesis*
- Kurnaz, A., Kucukomeroglu, B., Damla, N., and Çevik, U. (2011). Radiological maps for Trabzon, Turkey. *Journal of environmental radioactivity*, 102(4), 393-399.
- Krane, Kenneth S., and Chichester W. (1988). *Introductory nuclear physics*, New York. ISBN: 047180553X.
- Krane, S. Kenneth., (1987). *Introductory nuclear physics*. 2nd Edition.
- Krieger, R., (1981). Radioactivity of construction materials. *Betonwerkfertigteile Tech.*, 47:468.
- Lakshmi, K. S., Selvasekarapandian, S., Khanna, D., and Meenakshisundaram, V. (2005). Primordial radionuclides concentrations in the beach sands of East Coast region of Tamilnadu, India. In *International Congress Series* (Vol. 1276, pp. 323-324). Elsevier.

- Mansour, N. A., Hassan, N. M., Fayez-Hassan, M., & Sedqy, E. (2016). Assessment of natural radioactivity in fertilizers and phosphate ores in Egypt. *Journal of Taibah University for Science*, 10(2), 296-306.
- Mohanty, A.K. S. D., Vijan, S. K. and Saha, S. K. (2004). Natural radioactivity in the newly discovered high background radiation area on the eastern coast of Orissa, India. *Radiation Measurements*, 38(2): 153-165.
- Mudd G. Gavin (2008): Radon sources and impacts: A review of mining and non-mining issues. *Journal of Environmental Scientific Biotechnology*, 7: 325-353.
- Mulwa, B., Maina, D., and Patel, J. (2012). Multi elemental Analysis of Limestone and Soil Samples of Kitui South (Kenya) Limestone Deposits. *International Journal of Fundament Physical Sciences (IJFPS)*, 2(4), 48-51.
- Mustapha A. O. (1999). Assessment of human exposures to natural sources of radiation in Kenya. *Ph.D. Thesis (Physics)*. The University of Nairobi. Kenya.
- Mustapha, A. O., Patel, J. P. and Rathore, I. V. S (1999). Assessment of human exposure to natural sources of radiation in Kenya. *Radiation Protection Dosimetry*. 82, 285–292.
- Nyamai, C. M., Mathu, E. M., Opiyo-Akech, N., and Wallbrecher, E. (2003). A reappraisal of the geology, geochemistry, structures and tectonics of the Mozambique belt in Kenya, east of the rift system. *African Journal of Science and Technology*, 4(2), 51-71.
- Ochieng Stephen Kabasa., (2016). “Environmental Radiation Exposure Hazard Associated With Coal Deposits Of Mui Basin Block C, Kitui County”- *M.Sc. Thesis*- Institute Of Nuclear Science And Technology, University of Nairobi.
- Odumo, B. O. (2009). Radiological survey and elemental analysis in the gold mining belt, southern Nyanza, Kenya, *M.Sc Thesis, University of Nairobi, Unpublished*.
- OECD. (1979). Exposure to radiation from the natural radioactivity in building materials. Report by a group of experts of the OECD Nuclear Energy Agency. Paris, France: Organization for Economic Cooperation and Development

- Orgun, Y.N., Altinsoy, S.Y. Sahin, Y. Gungor, A.H. Gultekin. (2007). Natural and anthropogenic radionuclides in rocks and beach sands from Ezine region (Canakkale), Western Anatolia, Turkey. *Applied Radiation and Isotopes*. 65, 739–747
- Otwoma D., Patel J. P., Bartilol S., and Mustapha A. O. (2013). Estimation of annual effective dose and radiation hazard due to natural radionuclides in Mount Homa South-western Kenya. *Radiation Protection Dosimetry*. pp 1-8.
- Ramachandran, E. N., Karuppasamy, C. V., Cheriyan, V. D., Soren, D. C., Das, B., Anilkumar, V., ... and Seshadri, M. (2013). Cytogenetic studies on newborns from high and normal level natural radiation areas of Kerala in southwest coast of India. *International journal of radiation biology*, 89(4), 259-267.
- Rittersdorf, I. (2007). Gamma ray spectroscopy. *Nuclear Engineering & Radiological Sciences*, 18-20.
- Patel J. P. (1991). An environmental radiation survey of the area of high natural radioactivity of Mrima hill of Kenya. *Discovery and Innovation*, 3: 31-35.
- Rittersdorf I., (2007). Gamma Ray Spectroscopy, Nuclear Engineering & Radiological Sciences
- Reguigui, N. (2006). Gamma Ray Spectrometry. *Practical Information*.
- Ouko Samuel. (2015). Radiometric Survey and estimation of radiation from Archean rocks: A case study of the Migori Gold belt complex, Kenya –*M.Sc, Physics KU*.
- Saha G.B, (2013) *Physics and Radiobiology of Nuclear Medicine*, DOI 10.1007/978-1-4614-4012-3. Media New York.
- Senthilkumar, B., *et al.*, 2010. Measurement of gamma radiation levels in soil samples from Thanjavur using γ -ray spectrometry and estimation of population exposure. *J. Med. Phys.* 35 (1), 48.
- Shaban, H., Abd, E. A., Abd, E., Imran, I. S., and Abdallah, I. A. (2011). Natural Radioactivity and their radiological effect for different types of rocks from Egypt. *Journal of Radiation and Physics*. Elsevier. 60: 201-231.

- Shikali C. Munji M. Ambusso W. (2014). Radionuclide content of sands used for construction in Kakamega County, Kenya, and associated indoor radiation diffusion fluxes. *Journal of Environmental and Earth sciences*, 4 (15): 157-164.
- Sohrabi M. (1990). Recent radiological studies of high-level natural radiation areas of Ramsar, Iran. *International conference of high levels of natural radiation, Ramsar 3-7 Nov 1990*. IAEA, Vienna 71-86.
- Sohrabi, M. (1998). The state-of-the-art on worldwide studies in some environments with elevated naturally occurring radioactive materials (NORM). *Applied Radiation and Isotopes*, 49(3), 169-188.
- Susman, M. and Therman, E., (2012). *Human chromosomes: structure, behavior, and effects*. Springer Science & Business Media.
- Szymanska, K., Achenbach, P., Agnello, M., Botta, E., Bracco, A., Bressanid, T. & Wieland, O. (2008). The Resolution, efficiency, and stability of HPGe detector operating in a magnetic field at various gamma-ray energies. *Nuclear Instruments and Methods in Physics Research*, 592, 486–492.
- The government of Kenya (GOK) (2016). Kenya national cancer control strategy 2011-2016. *Ministry of Public Health and Sanitation and Ministry of Medical Services Report*. Pg. 5-8.
- Tao, Z., Akiba, S., Zha, Y., Sun, Q., Zou, J., Li, J., and Koga, T. (2012). Cancer and non-cancer mortality among inhabitants in the high background radiation area of Yangjiang, China (1979–1998). *Health physics*, 102(2), 173-181.
- Tsai, T., Lin, C., Wang, T. & Chu, T. (2008). Radioactivity concentrations and dose assessment for soil samples around nuclear power plant IV in Taiwan. *Journal of Radiological Protection*, 347, 347–360.
- Tzortzis, M., Tsertos, H., Christofides, S., & Christodoulides, G. (2003). Gamma-ray measurements of naturally occurring radioactive samples from Cyprus characteristic geological rocks. *Radiation Measurements*, 37(3), 221-229.
- UNSCEAR. (2017). *Sources and Effects of Ionizing Radiation*. Report to General Assembly, with Scientific Annexes, United Nations, New York.

UNSCEAR. (2010). Sources and effects of ionizing radiation. Report to the General Assembly, with scientific annexes. New York: United Nations.

UNSCEAR, (2008). United Nations Scientific Committee on the effects of atomic radiation, sources, and effects of ionizing radiation. Report to General Assembly, with Scientific Annexes United Nations. United Nations, New York.

UNSCEAR (2000) Sources, effects, and risks of ionizing radiation. United Nations Scientific Committee on the Effects of Atomic Radiation. Exposures from natural sources. Report to General Assembly, Annex B, New York

UNSCEAR (1993). United Nations Committee on Effects of Atomic Radiation. Exposure from natural sources of radiation. United Nations, New York.

UNSCEAR, (1988).Sources of ionizing radiation. United Nations Scientific Committee on Effects of Atomic Radiation 2000 report, United Nations, New York.

Valkovic, V., (2000). Radioactive nuclides in nature. Radioactivity in the environment. Amsterdam: *Elsevier*, pp. 5-31 (Chapter 2).

Varley, N. R. and Flowers, A. G (1998). Indoor radon prediction from soil gas measurements. *Health Physics*. 74: 714-718.

Vasconcelos, D. C., Reis, P. A., Pereira, C., Oliveira, A. H., Santos, T. O., and Rocha, Z. (2013). Modelling natural radioactivity in sand beaches of Guarapari, Espírito Santo State, Brazil. *World Journal of Nuclear Science and Technology*, 3(02), 65.

WHO. (2014) World Health Organization. Global status report on non-communicable diseases 2014. Geneva, Switzerland:

APPENDIX 1

Table: The rocks sample's individual activity and the overall average activity concentration of ^{226}Ra , ^{232}Th and ^{40}K in rocks sampled during the entire work

	Activity concentration for the rock samples (Bq/Kg)
--	---

	RAINY SEASON					
	UPPER STREAM			LOWER STREAM		
Sample ID	Ra-226	Th-232	K-40	Ra-226	Th-232	K-40
RS01	10±0.5	35±1.8	456±22	42±2.1	106±5.3	1097±54
RS02	20±1.0	14±0.7	688±34	14±0.7	19±0.95	174±8.8
RS03	32±1.6	57±2.8	963±48	19±1.0	91±4.5	1151±57
RS04	6±0.33	22±1.1	94±4.7	23±1.2	119±5.9	164±8.2
RS05	16±0.8	23±1.1	1037±51	20±1.0	33±1.6	663±33
RS06	23±1.1	33±1.6	604±30	25±1.2	49±2.4	962±48
RS07	11±0.5	15±0.7	440±22	23±1.1	38±1.9	983±49
RS08	37±1.8	50±2.5	972±48	17±0.8	31±1.5	836±41
RS09	30±1.5	60±3.0	984±49	28±1.4	66±3.3	1112±55
RS10	13±0.6	27±1.3	648±32	19±0.9	40±2.0	458±22
MIN	6±0.34	14±0.7	94±4.74	14±0.72	19±0.9	164±8.2
MAX	37±1.9	60±3.0	1037±51	42±2.11	119±5.9	1151±57
MEAN	20±1.0	34±1.74	689±34	23±1.0	59±1.74	760±34
	UPPER STREAM			LOWER STREAM		
SAMPLE ID	Ra-226	Th-232	K-40	Ra-226	Th-232	K-40
RS01	23±1.2	65±3.3	1189±59	25±1.2	98±4.9	1389±69
RS05	21±1.1	30±1.5	368±18	21±1.0	79±3.9	1106±55
RS010	18±0.9	36±1.8	1174±58	20±1.0	41±2.0	626±31
MIN	18±0.9	30±1.5	368±18	20±1.0	41±2.0	626±31
MAX	23±1.2	65±3.2	1189±59	25±1.2	98±4.9	1389±69
MEAN	21±1.1	43±2.1	911±45	22±1.0	73±2.1	1040±45
WORLD'S AVERAGE	33 Bq/Kg	45 Bq/Kg	400 Bq/Kg	33 Bq/Kg	45 Bq/Kg	400 Bq/Kg
OVERALL MEAN	21±2.4 BqKg⁻¹, 49 ±2.4 BqKg⁻¹, 782 ±39 BqKg⁻¹ for ²²⁶Ra, ²³²Th and ⁴⁰K respectively					

APPENDIX 2

Table A 3: The absorbed dose rate from geogenic samples analyzed.

SAMPLE NUMBER	ABSORBED DOSE RATE (nGy/h)			
	SAND SAMPLES			
	RAINY SEASON		DRY SEASON	
	Upper stream	Lower stream	Upper stream	Lower stream
SS01	63±3.1	111±5.5	67±3.3	103±5.1
SS02	64±3.2	76±3.8		
SS03	66±3.3	93±4.6	63±3.1	87±4.3
SS04	63±3.1	60±3.0		
SS05	56±2.8	94±4.7		
SS06	142±7.1	87±4.3	106±5.3	90±4.5
SS07	67±3.3	88±4.4		
SS08	75±3.7	78±3.9	73±3.6	98±4.9
SS09	65±3.2	162±8.1		
SS10	129±6.4	86±4.3	93±4.6	66±3.3
MIN	56±2.8	60±3.0	63±3.1	66±3.3
MAX	142±7.1	162±8.1	106±5.3	103±5.1
MEAN	79±3.9	94±4.7	81±4.0	89±4.4
OVERALL MEAN	86±4.3 nGyh⁻¹			

APPENDIX 3

Table A 4: The ranges and mean annual dose rate for both sand and rock samples analyzed during the entire radiometric survey

	OUTDOOR ANNUAL EFFECTIVE DOSE RATE (mSv/y)
--	---

SAMPLE NUMBER	Sand samples			
	RAINY SEASON		DRY SEASON	
	Upper stream	Lower stream	Upper stream	Lower stream
SS01	0.15±0.01	0.27±0.01		
SS02	0.15±0.01	0.18±0.01	0.16±0.005	0.25±0.01
SS03	0.16±0.01	0.22±0.01		
SS04	0.15±0.01	0.14±0.01	0.15±0.011	0.21±0.01
SS05	0.13±0.01	0.23±0.01		
SS06	0.34±0.02	0.21±0.01	0.26±0.002	0.22±0.01
SS07	0.16±0.01	0.21±0.01		
SS08	0.18±0.01	0.19±0.01	0.18±0.008	0.24±0.01
SS09	0.15±0.01	0.39±0.01		
SS10	0.31±0.02	0.21±0.01	0.23±0.007	0.16±0.008
MIN	0.13±0.01	0.14±0.01	0.15±0.011	0.16±0.008
MAX	0.34±0.02	0.39±0.02	0.26±0.002	0.25±0.012
MEAN	0.19±0.01	0.23±0.01	0.19±0.009	0.21±0.01
MEAN FOR BOTH SEASONS	0.2±0.01 mSv/y			

APPENDIX 4

Table A 5: The Radium equivalent (R_{eq}), internal hazard index (H_{in}) and external hazard indices reported from sand sampled for this work.

	RADIATION HAZARD INDICES IN SAND SAMPLES		
	RAINY SEASON		
	R_{eq}	H_{in}	H_{ex}

SAMPLE NUMBER	Upper stream	Lower stream	Upper stream	Lower stream	Upper stream	Lower stream
SS01	125±6.2	227±11	0.35±0.01	0.73±0.03	0.33±0.01	0.61±0.03
SS02	129±6.4	151±7.5	0.39±0.01	0.46±0.02	0.35±0.01	0.41±0.02
SS03	131±6.5	203±10	0.39±0.01	0.78±0.03	0.35±0.01	0.54±0.02
SS04	124±6.2	120±6.0	0.36±0.01	0.37±0.01	0.33±0.01	0.32±0.01
SS05	110±5.5	190±9.5	0.31±0.01	0.59±0.02	0.29±0.01	0.51±0.02
SS06	303±15	175±8.7	1.12±0.05	0.53±0.02	0.82±0.04	0.47±0.02
SS07	132±6.6	185±9.2	0.4±0.02	0.6±0.03	0.35±0.01	0.5±0.02
SS08	155±7.7	156±7.8	0.49±0.02	0.47±0.02	0.41±0.02	0.42±0.02
SS09	126±6.3	341±17	0.37±0.01	1.14±0.05	0.34±0.01	0.92±0.04
SS10	277±13	172±8.6	1.07±0.05	0.52±0.02	0.75±0.03	0.46±0.02
MIN	110±5.5	120±6.0	0.31±0.01	0.37±0.01	0.29±0.01	0.32±0.01
MAX	303±15	341±17	1.12±0.05	1.14±0.05	0.82±0.04	0.92±0.04
MEAN	161±8.0	192±9.6	0.52±0.01	0.62±0.06	0.43±0.02	0.52±0.02
DRY SEASON						
SS02	133±6.6	212±10	0.38±0.01	0.71±0.03	0.36±0.01	0.57±0.02
SS04	126±6.3	179±8.9	0.37±0.01	0.57±0.02	0.34±0.01	0.48±0.02
SS06	219±10	185±9.2	0.73±0.03	0.58±0.02	0.59±0.02	0.5±0.02
SS08	144±7.2	196±9.8	0.44±0.02	0.6±0.03	0.39±0.01	0.53±0.02
SS10	190±9.5	135±6.7	0.61±0.03	0.44±0.02	0.51±0.02	0.36±0.01
MIN	219±10	135±6.7	0.37±0.01	0.44±0.02	0.34±0.01	0.36±0.01
MAX	190±9.5	212±10	0.73±0.03	0.71±0.03	0.59±0.02	0.57±0.02
MEAN	162±8.0	181±9.0	0.51±0.51	0.58±0.01	0.44±0.02	0.49±0.02
OVERALL MEAN	175±8.7 Bq/Kg		0.56±0.02		0.47±0.02	
PERMISSIBLE LIMIT	370 Bq/Kg		1 (ICRP, 2005)			

Table A 6: Radiological hazard indices for the rock reported by this work.

SAMPLE NUMBER	RADIATION HAZARD INDICES FOR THE ROCKS					
	RAINY SEASON					
	R_{eq}		H_{in}		H_{ex}	
	Upper stream	Lower stream	Upper stream	Lower stream	Upper stream	Lower stream

RS01	96±4.8	277±13	0.28±0.01	0.86±0.04	0.26±0.01	0.75±0.03
RS02	93±4.6	55±2.7	0.3±0.01	0.18±0.0	0.25±0.01	0.14±0.0
RS03	187±9.3	238±11	0.59±0.0	0.69±0.03	0.5±0.02	0.64±0.03
RS04	46±2.3	205±10	0.14±0.0	0.62±0.03	0.12±0	0.55±0.02
RS05	129±6.4	118±5.9	0.39±0.01	0.37±0.01	0.35±0.01	0.32±0.01
RS06	118±5.9	170±8.5	0.38±0.01	0.52±0.02	0.31±0.01	0.46±0.02
RS07	67±3.3	154±7.7	0.21±0.01	0.48±0.02	0.18±0	0.41±0.02
RS08	184±9.2	126±6.3	0.6±0.03	0.38±0.01	0.5±0.02	0.34±0.01
RS09	191±9.5	209±10	0.59±0.02	0.64±0.03	0.51±0.02	0.56±0.02
RS10	102±5.1	112±5.6	0.31±0.01	0.35±0.01	0.27±0.01	0.3±0.01
MIN	46±2.3	55±2.7	0.14±0.0	0.18±0.0	0.18±0.0	0.14±0.0
MAX	191±9.5	238±11	0.6±0.03	0.86±0.04	0.51±0.02	0.75±0.03
MEAN	121±8.1	166±8.3	0.38±0.3	0.51±0.01	0.32±0.01	0.45±0.02
	DRY SEASON					
RS1	208±10	273±13	0.62±0.03	0.8±0.04	0.56±0.02	0.73±0.03
RS2	92±4.6	218±10	0.3±0.01	0.64±0.03	0.25±0.01	0.59±0.02
RS3	160±8.0	127±6.3	0.48±0.02	0.4±0.02	0.43±0.02	0.34±0.01
MIN	92±4.6	218±10	0.3±0.01	0.4±0.02	0.25±0.01	0.34±0.01
MAX	208±10	273±13	0.62±0.03	0.8±0.04	0.56±0.02	0.73±0.03
MEAN	153±7.6	206±10	0.47±0.47	0.52±0.61	0.41±0.02	0.55±0.02
OVERALL MEAN	152±7.62 Bq/Kg		0.47±0.02		0.41±0.02	
PERMISSIBLE LIMIT	370 Bq/Kg		1 (ICRP,1999)			

APPENDIX 5



UNIVERSITY OF NAIROBI

Institute of Nuclear Science & Technology

College of Architecture & Engineering
P.O. Box 30197
Nairobi, KENYA.
Fax: 254-2-245566

Telephone: 318262
Exts. 28483/28545/28536
Telegram: Varsity
Telex: 22095 VARSITY KE

REF: UON/CAE/INST/5/7

23rd August, 2018

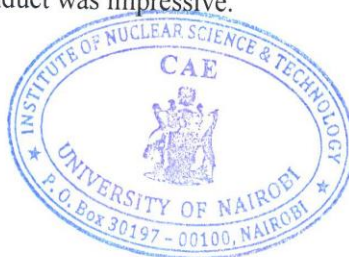
RE: MUTHAMA MATSITSI - REG No. I64/KIT/20647/2015

This is to confirm that the above named student from South Eastern University of Kenya (SEKU) used our laboratory facility – Gamma Spectrometry - for his sample preparation and analysis between February and May, 2018. During his stay at our laboratory, he used our facilities appropriately, and his conduct was impressive.

Yours faithfully,

A handwritten signature in black ink, appearing to be 'Michael J. Mangala', written over a blue circular stamp.

Michael J. Mangala
For Director
Institute of Nuclear Science and Technology



Recommendation letter from The University of Nairobi (Institute of Nuclear Science and Technology Laboratory) where the sample's preparation and analyses were carried out.

APPENDIX 6



Figure A 6 (a) Large-scale sand mining during the rainy season



Figure A6 (b) Local resident quenching thirst using water from a shallow well in the river course (Taken on 18th, Dec 2017)

APPENDIX 8



Figure A8 (a) Local resident watering his domestic animals from shallow wells along the river course (Taken on 18th, Dec 2017)



Figure A8 (b): Sand sample 08 being collected upper stream with help of research assistant. The surveyor's tape shows the inter-sampling length of 50 M used.



Figure A8 (c): Collection of Sand Sample One (SS01-Upper Stream) during the rainy season at GPS (0° 56' 17.3) S (38° 02' 36.3) E (Taken on 18th, Dec 2017)



Figure A8 (d): Collecting a rock sample from Gneiss basement at Kyanika Location. (Taken on 18th, Dec 2017)

APPENDIX 9

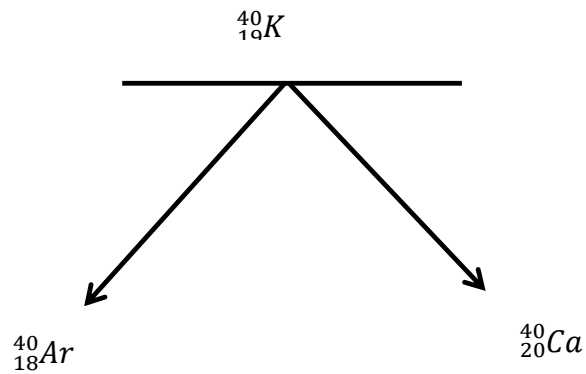


Figure A9 (a): Decay of radiogenic ${}^{40}\text{K}$

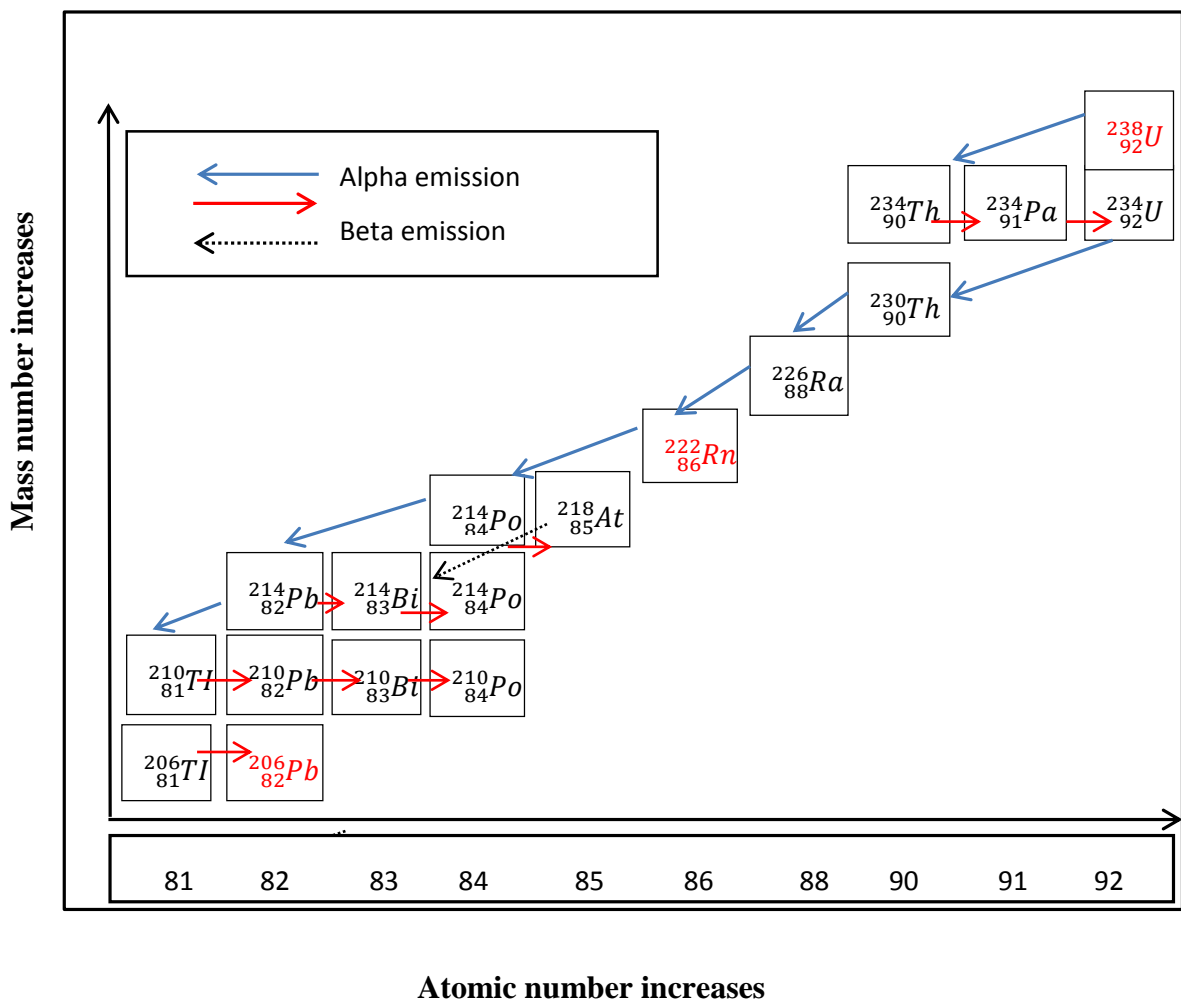


Figure A9 (b): Decay series of ${}^{238}_{92}\text{U}$ to final stable nuclide ${}^{206}_{82}\text{Pb}$. The solid arrows shows the decay path and dotted arrows represents the alternative decay routes.

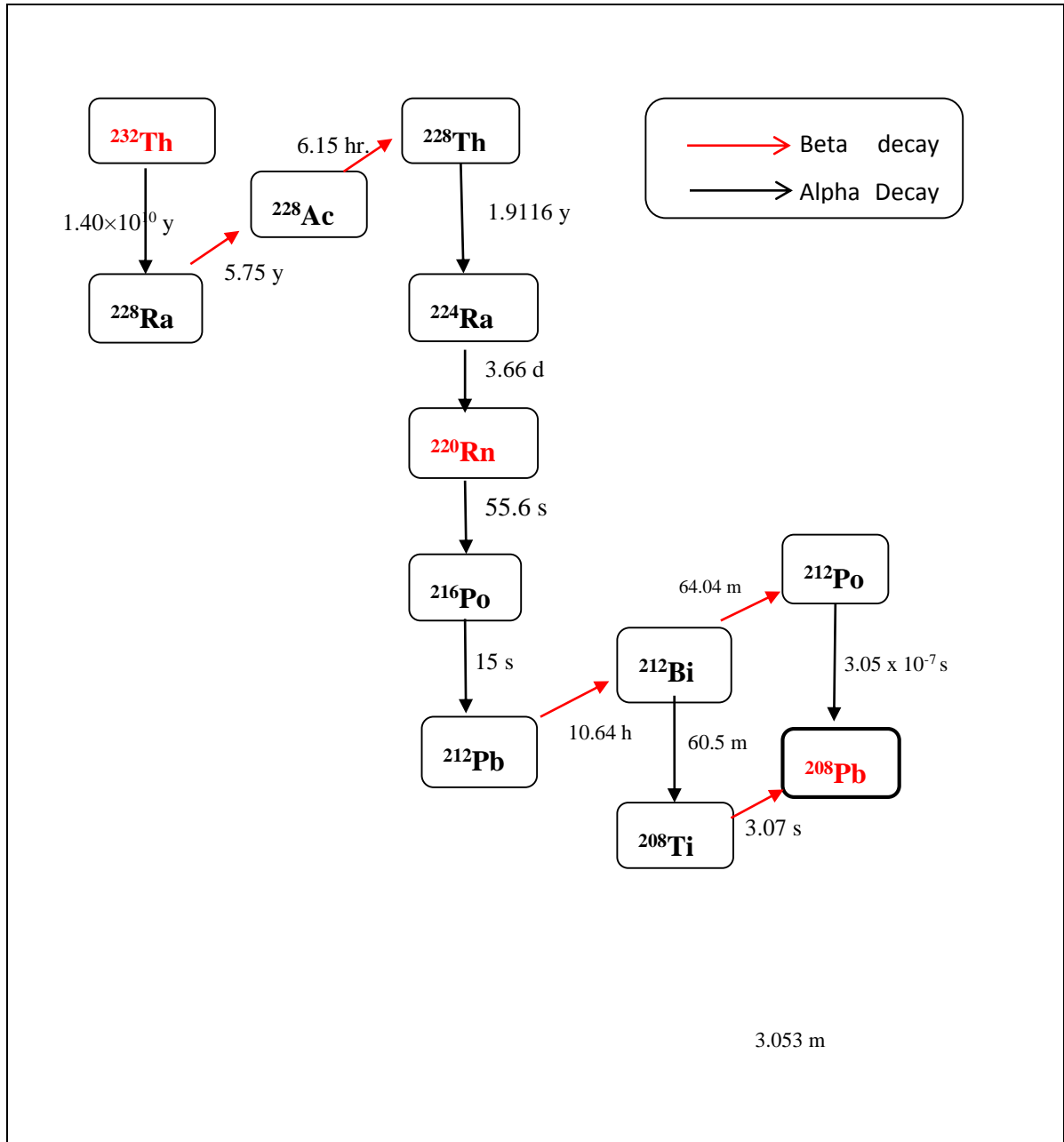


Figure A9 (c): Decay chain of ^{232}Th to ^{208}Pb

APPENDIX 10

List of Presentations and Publications

Presentation(s)

- *Preliminary findings on Natural radioactivity levels in rock and sand from Tyaa River in Mwingi, Kitui County.* International Conference on Science, Technology, and Innovation for Sustainable Development in Dry Land Environments held at UMMA University in Kajiado County from 21st -23rd November, 2018.

Publications include

- Matsitsi, S. M., Linturi, J. M., Kebwaro, J. M., & Maweu, O. M. (2019). Effects of Seasonal Change on the Levels of Geogenic Radionuclides in Sand and Rocks from Tyaa River deposit in Kitui County. *International Journal of Fundamental Physical Sciences (IJFPS)*, 9(1), 14-19.
- Matsitsi, S. M., Linturi, J. M., Kebwaro, J. M., & Kirago, L. M. (2020). RADIOMETRIC SURVEY OF THE TYAA RIVER SAND MINE IN KITUI, KENYA. *Radiation Protection Dosimetry*.